Technische Universität München
Institut für Organische Chemie und Biochemie

Max-Planck-Institut für Biochemie
Abteilung Strukturforschung (NMR-Arbeitsgruppe)

Functional and structural studies on the signal transduction proteins involved in tumorigenesis: insulin-like growth factor binding proteins (IGFBPs), integrin linked kinase (ILK), and 14-3-3σ

Joma K. Joy

Vollständiger Abdruck der von der Fakultät für Chemie der Technischen Universität München zur Erlangung des akademischen Grades eines

Doktors der Naturwissenschaften

genehmigten Dissertation.

Vorsitzender:	Univ.-Prof. Dr. St. J Glaser
Prüfer der Dissertation:	1. apl. Prof. Dr. Dr. h. c. R. Huber
	2. Univ.-Prof. Dr. J. Buchner

Die Dissertation wurde am 01.12.2005 bei der Technischen Universität München eingereicht und durch die Fakultät für Chemie am 09.01.2006 angenommen.

Acknowledgements

I would like to express my gratitude to all those who gave me the possibility to complete this thesis.

My foremost thanks goes to Prof. Dr. Robert Huber for giving me the opportunity to work in his department.

I am deeply grateful to my supervisor Dr. Tad A. Holak. I thank him for his suggestions, constructive criticism, patience, and steadfast encouragement throughout my thesis work. All these together helped me shape my research skills.

I thank all my NMR group members- Ola, Sudipta, Mahavir, Grzegorz, Tomek, Kinga, Marcin, Przemek, and the former members especially- Igor, Dorota, Madhu, Narasimha, Pawel, Chrystelle, Michael, and Till for their support and providing a friendly atmosphere. I owe Ulli a special thanks for all the German translations. I wish to thank members of the Roche lab- Magda, Yuri, and Sreejesh for their help.

During this work I have collaborated with colleagues outside the department and I wish to extend my warmest thanks to Anne and Carsten for their cooperation.

I would also like to acknowledge Shruti, Bhumi, Satish, and the rest of the gang for their friendship.

I am very grateful for the love, support and constant encouragement from my parents, my sister- Jemy, her husband Kanna, in-laws, and family.

Last, but not least, I would like to thank my husband Loy. Without his love, care, and understanding this thesis could not have been accomplished.

Publications

Parts of this thesis have already been published or will be published in due course:

Anne Benzinger, Grzegorz M. Popowicz, **Joma K. Joy**, Sudipta Majumdar, Tad A. Holak, and Heiko Hermeking. *The crystal structure of the non-liganded 14-3-3sigma protein: insights into determinants of isoform specific ligand binding and dimerization*. Cell Res. 15(4), 219-27, 2005.

Pawel Smialowski, Mahavir Singh, Aleksandra Mikolajka, Sudipta Majumdar, **Joma K. Joy**, Narasimharao Nalabothula, Marcin Krajewski, Roland Degenkolbe, Hans-Ulrich Bernard, and Tad A. Holak. *NMR and mass spectrometry studies of putative interactions of cell cycle proteins pRb and CDK6 with cell differentiation proteins MyoD and ID-2*. Biochim. Biophys. Acta (BBA)- Proteins and Proteomics 1750(1), 48-60, 2005.

Igor R. Siwanowicz, Grzegorz M. Popowicz, Loyola D'Silva, **Joma K. Joy**, Sudipta Majumdar, Magdalene Wisniewska, Louis Moroder, Sue M. Firth, Robert Huber, Robert C. Baxter, and Tad A. Holak. *Molecular architecture of the insulin-like growth factor binding proteins.* J. Biol. Chem., submitted, 2005.

Joma K. Joy, Sudipta Majumdar, Grzegorz M. Popowicz, Igor R. Siwanowicz, and Tad A. Holak. *Structural insights into the interaction between insulin-like growth factor and its bindng protein* – a short review. (manuscript in preparation).

Joma K. Joy, Narasimharao Nalabothula, Madhumita Ghosh, Oliver Popp, Marianne Jochum, Werner Machleidt, Shirley Gil-Parrado, and Tad A. Holak. *Identification of calpain cleavage sites in the G1 cyclin- dependent kinase inhibitor p19.*^{INK4d} Biol. Chem., in press, 2006.

Contents

1 Structural insights into the interaction between insulin-like growth factor and its binding proteins

1.1 Introduction

The insulin-like growth factor system is an evolutionarily conserved pathway consisting of a network of two ligands insulin-like growth factors (IGF-I and IGF-II), several transmembrane receptors (IGF-IR, IR), and six IGF-binding proteins (IGFBP 1-6) (reviewed in Bach and Rechler, 1995; Baxter, 2000). The molecular era for IGFs began in 1978 with the purification and amino acid sequencing of human IGF-I and IGF-II (Rinderknecht and Humble, 1978). IGF-I and -II are ubiquitously expressed growth factors that have profound effects on the growth and differentiation of many cell types and tissues. These potent mitogens act through their receptors to promote cell proliferation and differentiation (reviewed in Jones and Clemmons, 1995). Despite the high sequence similarity between IGFs and insulin, distinct functional differences exist between both. IGF-I is a pleiotropic cytokine that is involved in a wide variety of both developmental and metabolic processes, whereas, insulin is a metabolic hormone that regulates glucose homeostasis and acts systemically. IGFs on the other hand act in both systemic and paracrine/autocrine signaling pathways (Isaksson et al., 1987; Daughaday and Rotwein, 1989).

The cellular effects of IGFs are tightly controlled by IGFBPs. Because IGFBPs have higher affinities for IGFs than does the type-I IGF receptor, it is believed that IGFBPs achieve their regulation of IGFs through high affinity binding (Hwa et al., 1999).

IGFBPs function as carrier proteins for circulating IGFs and regulate IGF turnover, transport and tissue distribution, thus determining physiological concentrations of IGFs. At least 99% of the IGF in circulation are associated with one of the six IGFBPs. Among these IGFBP-3 and IGFBP-5 have the ability to form ternary complexes with IGFs and a 85 kDa glycoprotein, the acid labile subunit (ALS). The ternary complex serves as a reservoir for IGF release and increases the half life of IGFs (Baxter et al., 1992).

In tissues IGFBPs can both inhibit and potentiate IGF action either by sequestering IGF from IGF-I receptor or by releasing IGFs to bind to IGF-I receptors. IGF is released from the complex by either proteolysis of IGFBPs or binding of IGFBPs to the extracellular matrix. IGFBP phosphorylation can also alter their activity (reviewed in Firth and Baxter, 2002). Molecules that bind to IGFBPs might potentiate some of the effects of IGF-I, by liberating IGF-I from binding protein complexes either in the serum or at tissue-specific sites in the body. Hence, antagonism of a protein-protein binding event could potentially be used to produce net agonist activity (Loddick et al., 1998; Lowman et al., 1998).

IGFBPs have additional activities that are independent of their IGF binding; these include promoting apoptosis, cell growth inhibition, modulation of cell adhesion and migration (Mohan and Baylink, 2002). The carboxyl-terminal domain is most probably engaged in mediating IGF independent actions (Baxter, 2000).

IGFs have been implicated in many diseases including cancer and other disorders such as neurodegeneration and osteoporosis (Wetterau et al., 1999; Walsh, 1995; Rosen and Donahue 1998). A major constraint in defining the relationship between molecules that interact with IGFBPs has been a limited number of three dimensional structures of

IGFBPs. The knowledge of IGFBP intrinsic dynamic properties and their structure together can be incorporated in the development of therapeutic compounds.

1.1.1 Domain organization of IGFBPs

All IGFBPs share a common domain organization (Figure 1.1) with three distinct domains of approximately equal size. IGFBPs (1-6) each contain 216-289 amino acids, with an N-terminal domain containing 12 conserved cysteine residues (except in IGFBP-6 which has only 10 conserved cysteines), a C-terminal domain with six conserved cysteine residues, and a central (L) domain with no cysteine residues (except in IGFBP-4) (Duan, 2002). The highest conservation is found in the N- (residues 1 to ~100) and C- (from residue 170) terminal cysteine rich regions. The N- and C-domains are at least 50% homologous among the six IGFBPs in a given species (Rechler, 1993). The C-domains of IGFBPs enclose important subdomains; IGFBP-1 and IGFBP-2 contain Arg-Gly-Asp (RGD) integrin binding motifs, IGFBP-3 and IGFBP-5 have a 18-residue basic motif with heparin binding activity and additional residues that interact with the cell surface, matrix and the nuclear transporter importin-β proteins (Firth and Baxter, 2002).

The central, weakly conserved (L) domain shows little similarity between species. This domain is the site of specific proteolysis and ECM association (Kelly et al., 1998; Chernausek et al., 1995). Most of the post translational modifications occur in this L domain and it can be speculated that these modifications may participate in other diverse functions of IGFBPs (Hwa et al., 1999).

1.1.1.1 Architecture of the IGFBPs N-domain

The structure of N-terminal domain of IGFBP-5 (mini-IGFBP-5, residues Ala40-Ile92),

N-domains:

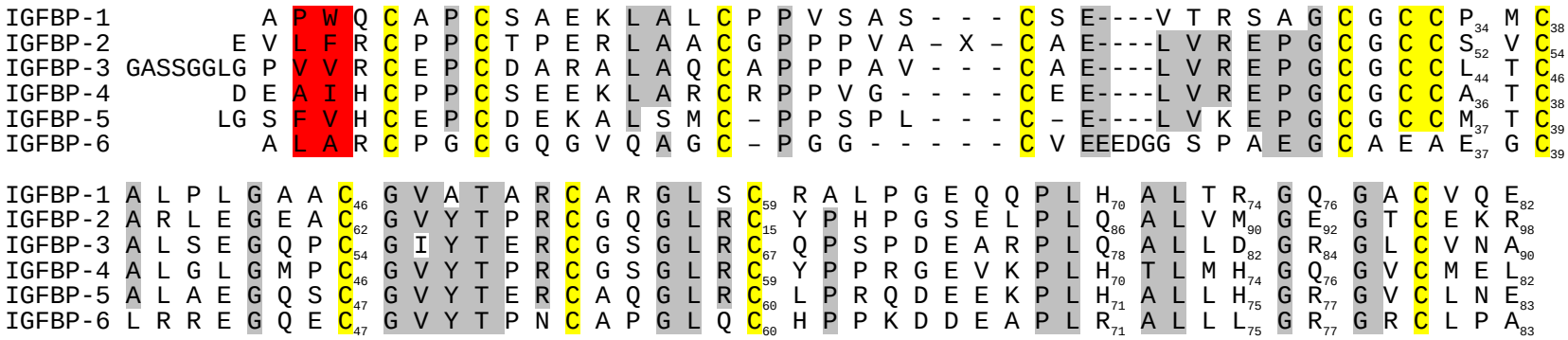

C-domains:

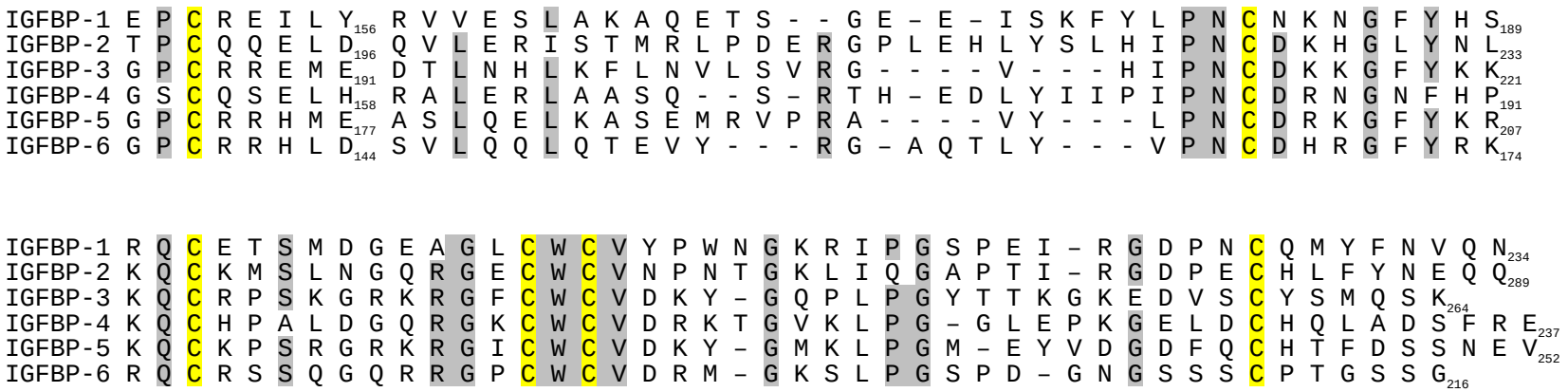

Figure 1.1: Sequence and structure alignments of human IGFBP-1 to -6.

The conserved residues are indicated by gray shading and cysteines are in yellow. The hydrophobic residues of the "thumb" domain of IGFBPs are shown in red.

determined by nuclear magnetic resonance spectroscopy gave us the first structural information about IGFBPs (Kalus et al., 1998). Mini-IGFBP-5 has a rigid, globular structure, whose scaffold is secured by an inside packing of two cysteine bridges, which are stabilized further by three short anti-parallel β strands. A single high affinity binding site for IGF-I was identified in mini-IGFBP-5 that comprises residues Val49, Tyr50, Pro62, and Lys68-Leu74. The hydrophobic residues (including Val49, Leu70, and Leu74) expose their side chain into solution to form a hydrophobic patch on the surface of mini-IGFBP-5.

Recently the crystal structure of the N-terminal domain of IGFBP-4 (residues 3-82) complexed with IGF-I was published by Siwanowicz et al. (2005). From the crystal structure it was evident, that the N-terminal domain can be divided into two subdomains: the fragment from residues Ala3 to Cys38, and the segment Ala39-Leu82. The latter corresponds approximately to the mini-IGFBP-5 (Klaus et al., 1998) that can fold autonomously and is also referred to as mini-NBP-4. The two subdomains are perpendicular are connected by short stretch of amino acids. The core of NBP-4 (residues 3-38) is referred as a "palm" of a hand because a short two-stranded β sheet and four disulphide bridges all are arranged in one plane, making the structure appear flat from one side. The palm is extended further with a "thumb" segment (Figure 1.2) consisting of the very N-terminal residues up to the equivalent of Cys6 in IGFBP-4 and also contains a consensus XhhyC motif, where h is a hydrophobic and y is a positively charged amino acid.

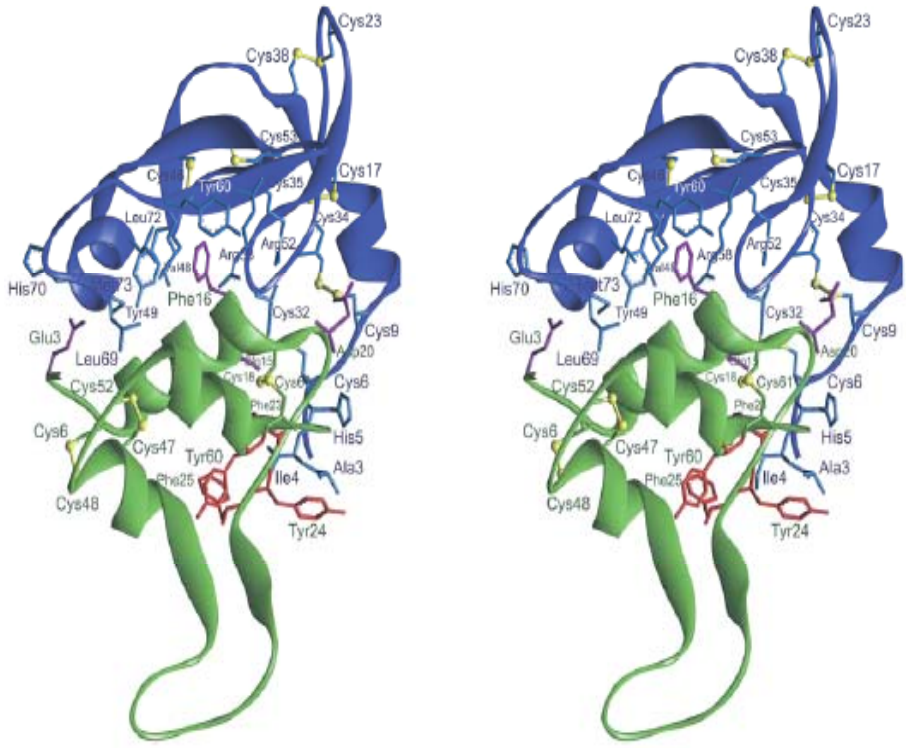

Figure 1.2: Structure of the NBP-4/IGF-I complex.

Ribbon plot of the binary complex. NBP-4 (residues 3-82) is shown in blue, and IGF-I is shown in green. Residues shown in violet constitute the binding site for interaction with NBP-4. Residues marked in red are determinants for binding to IGF-IR.

1.1.1.2 Architecture of IGFBPs C-domain

Our structural basis of understanding IGFBPs has grown with the 3D-structures of the C-terminal domain of IGFBP-6 (Headey et al., 2004a) and IGFBP-1 (Sala et al., 2005). The structure of C-BP-6 (Gly161-Gly240) solved using NMR spectroscopy shows a thyroglobulin type-I fold with an initial four-turn α-helix followed by a three stranded antiparallel β sheet, which are separated by a loop. It is evident from the structure that the anterior region is flexible. This flexibility is in agreement with ^{15}N NMR relaxation

measurements on the C-terminal domain of IGFBP-6 that had considerable mobility at time scales ranging from pico- to nanoseconds (Yao et al., 2004). A similar thyroglobulin type-I fold was detected from the X-ray structure of the C-terminal fragment of IGFBP-1 isolated from human amniotic fluid (Sala et al., 2005). The C-terminal domain of the IGFBP-6 (NMR structure) and IGFBP-1 (X-ray structure) were superimposed and the overall thyroglobulin type-I fold was found preserved in both the structures (Figure 1.3).

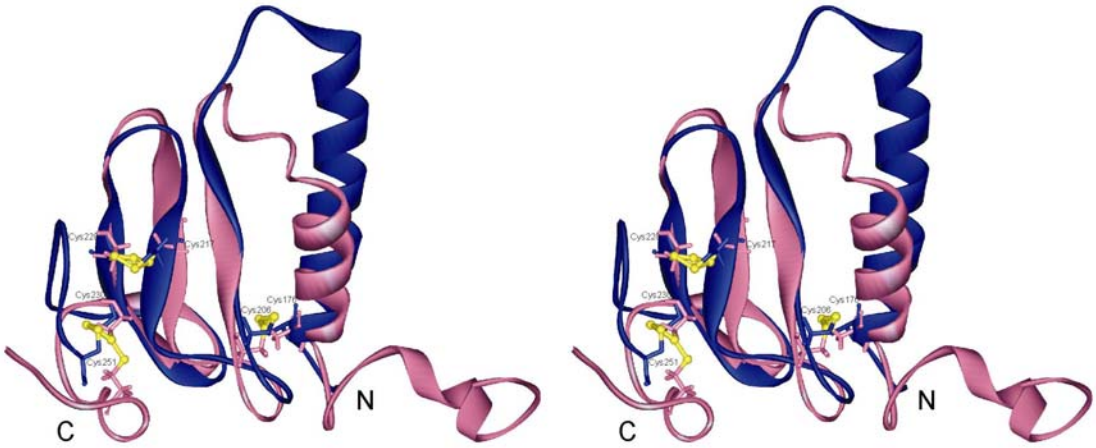

Figure 1.3: Comparative superposition of the C-terminal domains of IGFBP-1 (residues 172-251) and IGFBP-6 (residues 161-240).

This representation shows IGFBP-1 (pink) superimposed on IGFBP-6 (blue). The disulphide bridge connectivities in IGFBP-6 are represented in yellow.

1.1.3 Mutational studies on IGFBPs and their role in binding to IGF-I

IGF-I and IGF-II constitute a 70 and 67 residue single chain basic peptide, respectively, with a linear organization consisting of four domains, termed B, C, A, D. The IGF-I molecule has a high (45-52%) sequence similarity with the B and A chains of insulin (the

D domain is unique to the IGFs) and it also shares 67% sequence identity with IGF-II. (Baxter et al., 1992; Murray-Rust et al., 1992). The three dimensional structures of IGF–I have been described in low resolution by NMR spectroscopy (Cooke et al., 1991; Sato et al., 1993; Shaffer et al., 2003), X-ray (Vajdos et al., 2001; Brzozowski et al., 2002; Zeslawski et al., 2001), and recently a high resolution structure of IGF-I complexed with NBP-4 (residues 3-82) has been described (Siwanowicz et al., 2005).

For more than a decade, mutagenesis has been extensively used to study the structure and functional relationships of IGFBPs. A comprehensive review by Clemmons (2001) accounts for performing functional analysis with the mutants. The structure of N-terminal domain of IGFBP-5, with a hydrophobic patch (Val49, Tyr50, Pro62 and Lys68 to Leu74) determined by NMR studies was found to be critical in binding IGF-I (Kalus et al., 1998). Mutational studies in the hydrophobic patch resulted in a 1000-fold reduction in IGF-binding affinity compared to the wild type IGFBP-5 (Imai et al., 2000). Based on the IGFBP-5 N-terminal conservation, three residues in the hydrophobic patch of IGFBP-3 (Ile56, Leu 80, Leu81) were mutated. Substitution of Val for Ile56 had no affect on binding but when Gly was used instead of Val it produced marked reductions in binding. A greater reduction was seen when both Leu80 and Leu81were substituted with Gly, and complete loss of affinity for IGF-I and –II occurred when all three targeted amino acids were changed to glycine (Buckway et al., 2001). Evidence supporting the N-terminal domain as a site of IGF binding came from Hobba and co-workers (1998) who examined the binding of IGFBP-2 to IGF-I and –II. They observed that Tyr60 in the N-terminal region of bovine IGFBP-2 is an important residue in IGF binding.

Many groups have shown that apart from the N-terminal residues, the C-terminal residues are important determinants in binding IGFs especially IGF-II (Firth et al., 1998; Hashimoto et al., 1997) and mutations in the C-terminal domain of IGFBP-5 markedly reduce IGF binding (Bramani et al., 1999). The relative IGF-binding affinities of isolated N- and C-domains differ among IGFBPs. Carrick et al. (2001) and Galanis et al. (2001) showed that the C-domains of IGFBP-2 and IGFBP-3 had a higher affinity for IGF-I and –II and a slower dissociation constant when compared to N-domains of IGFBP-2 and -3. Contradicting results originated from Vorwerk et al. (2002), in which the dissociation kinetics and IGF binding affinity for N- and C-domains of IGFBP-3 were found to be similar. On the other hand, a low affinity binding of the C-domain of IGFBP-4 to IGF-I and -II and a high affinity of N-domain to IGF-I and -II was observed by Stander et al. (2000). Headey et al. (2004a) mapped the IGF-II surface involved in binding the C-terminal domain of IGFBP-6. The binding site for the C-BP-6 on IGF-II lies between and overlaps with the binding sites for the N-domains of IGFBPs and the IGF-I receptor. Recently, Carrick et al. (2005) monitored the chemical shift perturbations of IGF-I and -II upon complex formation with thioredoxin-tagged bovine IGFBP-2. The chemical shift perturbations were found to be significantly greater than that reported by Jansson et al. (1998) for binding of IGF-I to IGFBP-1. Significant perturbation in the Gly22-Phe25 (region essential for interaction with IGF-IR) was observed in both IGF-I and -II. They state the perturbations arose from interaction with the C-domain of IGFBP-2. Hence, the C-domain of IGFBPs may play a crucial role in blocking the interaction of IGF-I and IGF-II with the IGF-1R. Also the low resolution structure (Siwanowicz et al., 2005) of the ternary complex of NBP-4 (3-82)/IGF-I/CBP-4 (151-232) shows the binding site for

the C-terminal domain on IGF-I. It is seen that C-terminal domain of IGFBP-4 contacts the amino terminal part of both NBP-4 and IGF-I. This further strengthens Headey and groups (2004a) studies on the interaction of IGF-II with the C-terminal domain of IGFBP-6. Even though there exists incongruity between the binding properties of N- and C-domains of different IGFBPs, based on the X-ray and NMR complexes of IGF and IGFBPs, we can conclude that both N- and C-domains of IGFBPs contribute to the binding.

1.2 Materials and methods

1.2.1 Materials

1.2.1.1 *E. coli* strains

Cloning strains

XL1-Blue	Stratagene (USA)
One Shot® TOP10	Invitrogen (Holland)
DH5α	Novagen (Canada)

Protein expression strains

One Shot® BL21 Star™ (DE3)	Invitrogen (Holland)
One Shot® BL21 Star™ (DE3) pLysS	Invitrogen (Holland)

1.2.1.2 Plasmids

pET-28a (+)	Novagen (Canada)
pETDUET-1	Novagen (Canada)
pACYCDuet-1	Novagen (Canada)
pGEX 6P-1	Amersham
pAcG2T	Pharmingen

1.2.1.3 Antibiotics

Ampicillin, sodium salt	Sigma (USA)
Kanamycin, monosulfate	Sigma (USA)
Chloramphenicol	Sigma (USA)

1.2.1.4 Cell growth media and stocks

LB medium

Bacto tryptone	10 g/l
Bacto yeast extract	5 g/l
Sodium chloride	10 g/l

pH was adjusted to 7.0. For the preparation of agar plates the medium was supplemented with 15 g agar.

TB medium

Bacto tryptone	12 g/l
Bacto yeast extract	24 g/l
Sodium chloride	10 g/l
Glycerol	4 ml

The medium was autoclaved, cooled to 60°C. 100 ml sterile K phosphate and glucose was added. The final concentration of glucose was 1%.

K phosphate

$KH_2 PO_4$	23.1 g/l
K_2HPO_4	125.4 g/l

Stock solution of glucose

20 g glucose was dissolved in distilled water and the final volume was made to 100ml, autoclaved.

Stock solution of ampicillin

100 mg/ml of ampicillin was dissolved in distilled water. The stock solution was filtered

and stored in aliquots at -20°C until use.

Stock solution of kanamycin

50 mg/ml of kanamycin was dissolved in distilled water. The stock solution was filtered and stored in aliquots at -20°C until use.

Stock solution of IPTG

A sterile 1 M stock of IPTG in distilled water was prepared and stored in aliquots at -20°C until use.

1.2.1.5 Common buffers

Buffer P (0)	8 mM KH_2PO_4
	16 mM Na_2HPO_4
	0.05% NaN_3
	pH 7.0
Buffer P (1000)	8 mM KH_2PO_4
	16 mM Na_2HPO_4
	1 M NaCl
	0.05% NaN_3
	pH 7.0
Buffer T	60 mM NaCl (thrombin cleavage buffer)
	60 mM KCl
	2.5 mM $CaCl_2$
	50 mM Tris
	0.05% NaN_3

	pH 8.0
PBS	140 mM NaCl
	2.7 mM KCl
	10 mM Na_2HPO_4
	1.8 mM KH_2PO_4
	0.05% NaN_3
	pH 7.3

1.2.1.6 Buffers for purification of proteins under native conditions

Binding buffer	50 mM NaH_2PO_4
	300 mM NaCl
	10 mM imidazole
	pH 8.0
Wash buffer	50 mM NaH_2PO_4
	300 mM NaCl
	20 mM imidazole
	pH 8.0
Elution buffer	50 mM NaH_2PO_4
	300 mM NaCl
	250 mM imidazole
	pH 8.0
Modified buffer	50 mM Na_2HPO_4 x $2H_2O$
	250 mM NaCl

	pH 8.0
Lysis buffer (parvin)	50 mM TrisHCl
	10 mM imidazole
	1% Triton x-100
	pH 9.0
Wash buffer (parvin)	50 mM TrisHCl
	20 mM imidazole
	2% glycerol
	pH 9.0
Elution buffer (parvin)	50 mM TrisHCl
	175 mM imidazole
	2% glycerol
	pH 9.0

1.2.1.7 Buffers for purification of proteins under denaturing conditions

Buffer A	6 M guanidinium chloride
	100 mM NaH_2PO_4 x H_2O
	10 mM Tris
	10 mM β-mercaptoethanol
	pH 8.0
Buffer B	6 M guanidinium chloride
	100 mM NaH_2PO_4 x H_2O
	10 mM Tris

	10 mM β-mercaptoethanol
	pH 6.5
Buffer C	6 M guanidinium chloride
	100 mM NaAc x $3H_2O$
	10 mM β-mercaptoethanol
	pH 4.0
Buffer D	6 M guanidinium chloride
	pH 3.0
Buffer E (refolding buffer)	200 mM arginine
	1 mM EDTA
	100 mM Tris
	2 mM reduced GSH
	2 mM oxidized GSH
	0.05% NaN_3
	pH 8.4

1.2.1.8 Reagents for baculovirus expression

Spodoptera frugiperda (Sf9) cells (PharMingen)

Medium for Sf9 cells

Sf-900 II SFM	Gibco (UK)
Fetal Bovine Serum (FBS)	Gibco (UK)
Antimycotic (100X), liquid	Invitrogen (Germany)
Co-transfection kit	PharMingen

Easy-DNA kit	Invitrogen (Germany)

1.2.1.9 Enzymes and antibodies

BSA	New England BioLabs (USA)
P*fu* turbo DNA Polymerase	Stratagene (USA)
BamHI	New England BioLabs (USA)
EcoRI	New England BioLabs (USA)
Not I	New England BioLabs (USA)
Bgl II	New England BioLabs (USA)
Xa factor	Sigma (USA)
Thrombin	Sigma (USA)

1.2.1.10 Kits and reagents

Glutathione Sepharose beads	Amersham (USA)
Ni-NTA Agarose	Qiagen (Germany)
QIAquick PCR Purification Kit	Qiagen (Germany)
QIAprep Spin Miniprep Kit	Qiagen (Germany)
QIAGEN Plasmid Midi Kit	Qiagen (Germany)
QIAGEN Plasmid Maxi Kit	Qiagen (Germany)
Quick Change Site-Directed Mutagenesis Kit	Stratagene (USA)
Rapid Ligation Kit	Roche (Germany)
BM chemiluminescence Western Blotting Kit (Mouse/Rabbit)	Roche (Germany)
Complete Protease Inhibitor Cocktail	Roche (Germany)

1.2.1.11 Protein and nucleic acids markers

Prestained Protein Marker	New England BioLabs (USA)
1 kb DNA-Leiter	Peqlab (Germany)

1.2.1.12 Chromatography equipments, columns, and media

ÄKTA explorer10	Amersham Pharmacia
Peristaltic pump P-1	Amersham Pharmacia
Fraction collector RediFrac	Amersham Pharmacia
Recorder REC-1	Amersham Pharmacia
UV flow through detector UV-1	Amersham Pharmacia
BioloLogic LP System	Biorad
HiLoad 16/60 Superdex S30pg, S200pg	Amersham Pharmacia
HiLoad 26/60 Superdex S75pg	Amersham Pharmacia
HiLoad 10/30 Superdex S75pg	Amersham Pharmacia
Mono Q HR 5/5, 10/10	Amersham Pharmacia
Mono S HR 5/5, 10/10	Amersham Pharmacia

1.2.2 General laboratory methods

1.2.2.1 Transformation of *E. coli*

1.2.2.1.1 Transformation by heat shock

2 µl of a ligation mix or 1 µl of plasmid DNA were added to 50 µl of chemically compet-

ent cells. The mixture was incubated on ice for 30 min followed by a heat shock of 30 s at 42°C, short cooling on ice, and addition of 250 µl SOC medium. After 1 h of incubation at 37°C, 20-50 µl of the mixture were spread out on LB agar plates including selective antibiotic and incubated overnight at 37°C.

1.2.2.1.2 Transformation by electroporation

1 µl of plasmid DNA was added to 50 µl of electrocompetent cells, the mixture was pipetted into a 2 mm electroporation cuvette. The electroporation was performed in an electroporation vessel (Gene pulser) at 1650 V. Then the suspension was transferred into an Eppendorf tube and mixed with 1 ml LB medium. After 1 h of incubation at 37°C, 20-50 µl of the mixture were spread out on LB agar plates including selective antibiotic and incubated overnight at 37°C.

1.2.2.2 Preparation of plasmid DNA

The isolation of plasmid DNA from *E. coli* was done with assistance of plasmid kits offered by Qiagen company. The preparation of plasmid DNA in a small scale (up to 20 µg) was performed to check the successful cloning. Larger amounts of DNA (up to 500 µg) were needed for baculovirus transfection. Both types of preparation were carried out following the instructions of the manufacturer (Qiagen plasmid mini kit and plasmid maxi kit protocol, respectively).

1.2.2.3 Digestion with restriction enzymes

Usually, 1-2 units of restriction enzyme were employed per µg DNA to be digested. The

digestion was performed in the buffer specified by the manufacturer at the optimal temperature (37°C) overnight. The fragment ends that occurred after digestion were cohesive or blunt ends.

1.2.2.4 Purification of DNA fragments

DNA obtained from restriction digestion, phosphatase treatment or PCR was purified from primers, nucleotides, enzymes, mineral oil, salts, agarose, ethidium bromide, and other impurities using silica-gel column (QIAquick PCR purification kit, Qiagen). The QIAquick system uses a simple bindwash-elute procedure. Binding buffer was added directly to the PCR sample or other enzymatic reaction, and the mixture was applied to the spin column. Nucleic acids adsorbed to the silica-gel membrane in the high-salt conditions provided by the buffer. Impurities were washed away and pure DNA was eluted with a small volume of low-salt buffer provided or water, ready to use in all subsequent applications.

1.2.2.5 DNA agarose gel electrophoresis

To verify the DNA samples, agarose gel electrophoresis was performed. For this purpose 1% agarose in TBE buffer plus ethidium bromide was prepared. The solution was poured into a horizontal gel chamber to cool down. The DNA samples were mixed with sample buffer and loaded into the wells. Electrophoresis was carried out at 50-100 V. Results evaluation was done by UV illuminator.

1.2.2.6 Sonication

Sonication is a simple method used for the disruption cells by ultrasounds. The bacterial suspension was filled into the pre-cooled glass and the suitable pulse of ultrasounds was applied (output control 7.5, 50%). To avoid overheat of the sample sonication was carried out in two steps of 5 min each with 5 min intervals between steps and on ice.

1.2.2.7 SDS polyacrylamide gel electrophoresis (SDS PAGE)

To verify the protein samples, SDS polyacrylamide gel electrophoresis was done. Because small proteins were analyzed, tricine gels were chosen to use (Schagger and von Jagow, 1987).

Anode Buffer (+):	200 mM Tris pH 8.9
Cathode Buffer (-):	100 mM Tris pH 8.25
	100 mM tricine
	0.1% SDS
Separation Buffer:	1 M Tris pH 8.8
	0.3% SDS
Stacking Buffer:	1 M Tris pH 6.8
	0.3% SDS
Separation acrylamide:	48% acrylamide
	1.5% bis-acrylamide
Stacking acrylamide:	30% acrylamide
	0.8% bis-acrylamide

Pouring gels

Separation gel:	1.675 ml H_2O
	2.5 ml separation buffer
	2.5 ml separation acrylamide
	0.8 ml glycerol
	25 µl APS
	2.5 µl TEMED
Intermediate gel:	1.725 ml H_2O
	1.25 ml separation buffer
	0.75 ml separation acrylamide
	12.5 µl APS
	1.25 µl TEMED
Stacking gel:	2.575 ml H_2O
	0.475 ml stacking buffer
	0.625 ml stacking acrylamide
	12.5 µl 0.5 M EDTA, pH 8.0
	37.5 µl APS
	1.9 µl TEMED

The guanidinium HCl-free protein samples were prepared by mixing 20 µl of protein solution with 5 µl of sample buffer (SB) followed by 3 min incubation at 100°C. Due to the rapid precipitation of SDS in contact with guanidine, the samples to be

examined by PAGE after Ni-NTA chromatography under denaturing conditions had to be prepared in a following fashion: 20 µl of the protein solution in a denaturing buffer was diluted with 400 µl of 20% trichloroacetic acid (TCA). The sample was incubated for 5 min at room temperature followed by centrifugation for 5 min at 20 000 x g. Supernatant was discarded by suction, precipitated protein pellet was washed once by vortexing with 400 µl ethanol. After centrifugation and ethanol removal, protein pellet was resuspended in 20 µl of 2x SB and the sample was boiled for 3 min.

1.2.2.8 Staining of proteins

Staining of proteins with Coomassie-Blue solution was performed as described in Sambrook and Russell (2001).

Coomassie-Blue solution:	0.025% Coomassie Brillant Blue R250
	45% ethanol
	10% acetic acid
Destaining solution:	5% ethanol
	10% acetic acid

1.2.3 Establishment of insect cell lines

The *Sf9 (Spodoptera frugiperda)* cell lines which double every 18-24 h were grown in Sf-900 II SFM media along with 5% fetal bovine serum. The cells were maintained in an incubator at 27°C. When they reached confluency, healthy cultures of monolayer *Sf9* cells were maintained by sub culturing.

1.2.3.1 Generation of recombinant baculovirus by co-transfection method

A 60 mm tissue culture plate was seeded with 2 x 10^6 cells with an initial cell density of 50 –70% confluency and the cells were allowed to attach.

1.2.3.2 Experimental co-transfection

0.5 μg of BaculoGold DNA (pharMingen) was mixed with and 5 μg of recombinant baculovirus transfer vector containing the insert in a microcentrifuge tube. It was mixed by vortexing and the mixture was allowed to incubate for 5 min. 1 ml of transfection Buffer B was added to this.

1.2.3.3 Positive control co-transfection

- 0.5 μg of BaculoGold DNA (pharmingen) was mixed with 2 μg of pVL 1392-XylE (PharMingen) in a microcentrifuge tube. It was mixed by vortexing and the mixture was allowed to incubate for 5 min. 1 ml of transfection Buffer B was added to this.
- The old medium was aspirated from the cells on the experimental co-transfection plate and replaced with 1 ml of transfection buffer A.
- The old medium was aspirated from the cells on the positive control co-transfection plate and replaced with 1 ml of transfection buffer A. Along with this a negative control containing Sf9 monolayer cell was maintained.
- The previously prepared transfection buffer B / DNA mix was then added drop wise to the experimental co-transfection plate. After the addition of every three to five drops, the plate was gently rocked to mix the drops with the medium. A fine calcium phosphate DNA precipitate was formed. Similarily, 1 ml of transfection buffer

B/XylE positive control DNA solution was added drop by drop to the positive control co-transfection control plate. All plates were incubated at 27°C for 4 h.

- The medium was removed after 4 h from the experimental and positive control co-transfection plates and 3 ml fresh medium was added to the plate. All plates were incubated at 27°C for 4–5 days. After 4 days, the plates were checked for signs of infection.

Observation

Infected cells appeared much larger with an enlarged nuclei than uninfected cells. After 5 days, the supernatant from the positive control and experimental co-transfection plates were collected and assayed for co-transfection efficiencies by end-point dilution assay.

1.2.3.4 End point dilution assay (EPDA)

1 x 10^5 *Sf9* cells per well were seeded and allowed to attach firmly on a 12-well EPDA plate. 100, 10, 1, and 0 µl of the recombinant virus supernatant (obtained five days after the start of transfection) were added to separate wells. In a similar manner, it was repeated for the positive control. All plates were incubated at 27°C for three days and the cells were examined for signs of infection.

Observation

A successful transfection resulted with uniformly large infected cells in the 100, 10, and 1µl experimental wells. The cells in the 0 µl control well showed no infection.

1.2.3.5 Virus amplification

2 x 10^7 *Sf9* cells were seeded on a tissue culture plate and allowed to attach for 15 min. A 100 µl of low titer recombinant stock was added to the plate. The cells were incubated at 27°C for almost a week before collecting the supernatant. The supernatant was collected by spinning down the cellular debris in a table-top centrifuge. The virus supernatant obtained was stored at 4°C in a sterile tube and covered with foil to protect against light. Later, large scale virus amplication was carried out. The presence of the gene in the amplified virus titer was checked by isolating the DNA from baculovirus.

1.2.3.6 Isolation of DNA from baculovirus

Isolation of viral particles

750 µl of an occlusion negative cell suspension was transferred to a micro centrifuge tube and centrifuged at 5,000 rpm for 3 min at room temperature. 750 µl of ice cold 20% PEG in 1 M NaCl was added to the supernatant, mixed and incubated on ice for 30 min. The viral particles were pelleted by centrifuging at maximum speed for 10 min at 4°C. Re-centrifuged again at maximum speed for 2 min and the residual supernatant was removed and finally the viral particle was dissolved in 100 µl of TE buffer.

Isolation of DNA

To the viral particle, 143 µl of solution A was added, vortexed for 1 s and incubated at 65ºC for 6 min. 58 µl of solution B was added to this and vortexed vigorously for 5 s, followed by addition of 258 µl of chloroform. To separate the phases it was centrifuged

at maximum speed for 10 min. The upper aqueous phase was transferred into a fresh micro centrifuge tube.

DNA precipitation

To the DNA solution 500 µl of ice cold 100% ethanol was and centrifuged at maximum speed for 5 min at 4°C. The supernatant was discarded, to the pellet 500 µl of ice cold 70% ethanol was added and centrifuged at maximum speed for 5 min at 4°C. The supernatant was discarded and again spun to remove residual ethanol and the pellet was resuspended in 20 µl of sterile water.

1.3 Experimental procedures

1.3.1 Cloning

DNA fragment corresponding to the N-terminal domain of IGFBP-4 residues (residues 1-92) was generated by PCR amplification using human IGFBP-4 cDNA as a template. The carboxyl and amino-terminal domain of IGFBP-5 were also generated by PCR amplification. All the proteins were expressed and purified as described in section 1.3.2. Several deletion mutants of C-terminal domain of IGFBP-4 were generated: CBP-4Δ (Gln168-Asp174)), (CBP-4Δ (Ser167-Ile178)), (CBP-4Δ (Leu216-Lys223)), (CBP-4Δ (Gly213-Glu225)). The mutagenic PCR followed by parental DNA digestion with Dpn I and PCR product ligation was performed using ExSite site-directed mutagenesis kit (Stratagene) according to the supplier's instructions.

1.3.2 Purification

The *E. coli* BL21 cells containing the plasmid were grown at 37°C with the appropriate antibiotic. Cells were induced by 1 mM IPTG at a cell density of OD_{600} = 0.8 and cell pellet was resuspended in 30 ml of buffer A and stirred overnight to lyse the cells. The solution was then centrifuged for 1h at 60,000 g, the lysate was adjusted to pH 8.0 and kept for binding with a previously equlibriated Ni-NTA (Qiagen) column. The column was washed with 100 ml of buffer A, 100 ml of buffer B (buffer A at pH 6.0), and protein was eluted using buffer C. The fraction containing the protein was pooled and concentrated to 4 ml by 3 kDa membrane (Amicon). 10 mM β-mercaptoethanol was added to reduce every cysteine bridge. The protein was dialysed against buffer D to remove β-mercaptoethanol, followed by refolding in 50 ml of buffer E. After 50 h at 4ºC

the His-tagged protein was completely refolded. The CBP5 was dialyzed against a buffer containing 50 mM NaCl and 50 mM Tris, pH 8.0 and then loaded on a Mono S column (Figure 1.4). The fractions containing the protein was pooled, dialyzed against TAGZyme buffer, the His-tag was cleaved by incubating the protein for 24 h with DAPase. The CBP5 protein was finally purified (Figure 1.6) on a Supedex 75pg (Pharmacia) with PBS buffer. All the buffers used for purification are described in section 1.2.1.7.

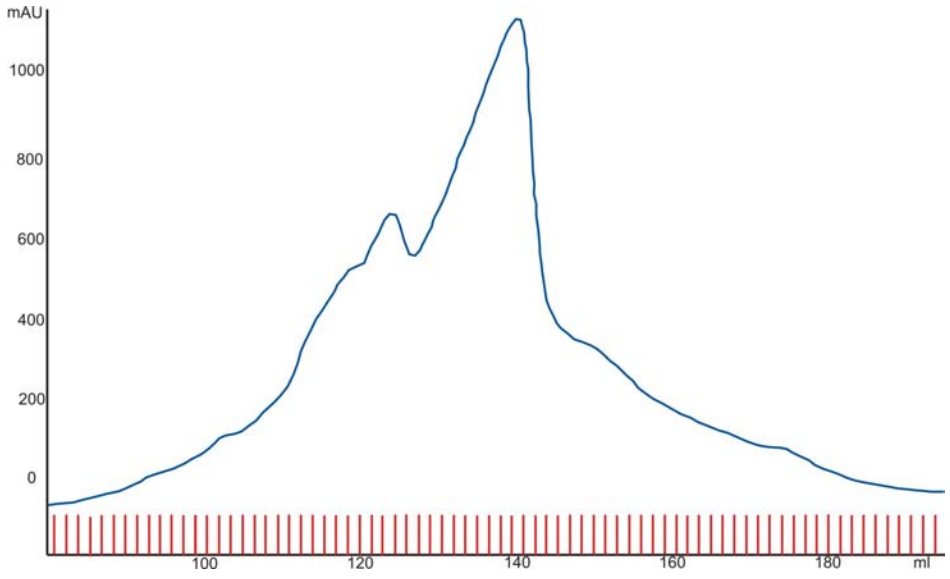

Figure 1.4: A chromatogram of the CBP-5 purified on the mono S column.
The CBP-5 protein was eluted with 250-800 mM NaCl gradient, the main peak corresponds to the protein.

1.3.3 Binary complex of NBP-4/IGF-I

The complex of NBP-4(residues 1-92) and IGF-I (GroPep, Australia) was prepared by mixing equimolar amounts of the components. The complex was separated from any excess of either protein by gel filtration chromatography on the Superdex S75pg column with a buffer containing 5 mM Tris, pH 8.0, 50 mM NaCl and 0.01% NaN_3.

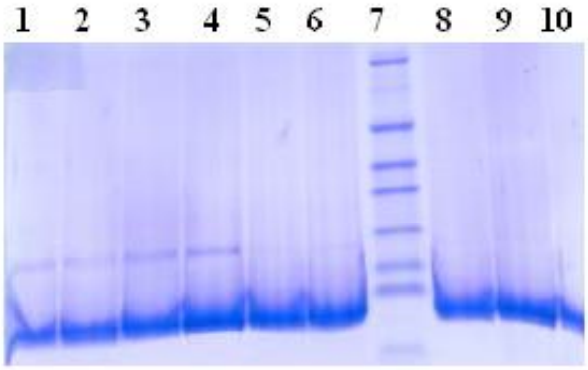

Figure 1.5: SDS-PAGE analysis of fractions of CBP-5 eluted from the mono S column.
Lanes 1-6 and lanes 8-10 correspond to the CBP5 protein.

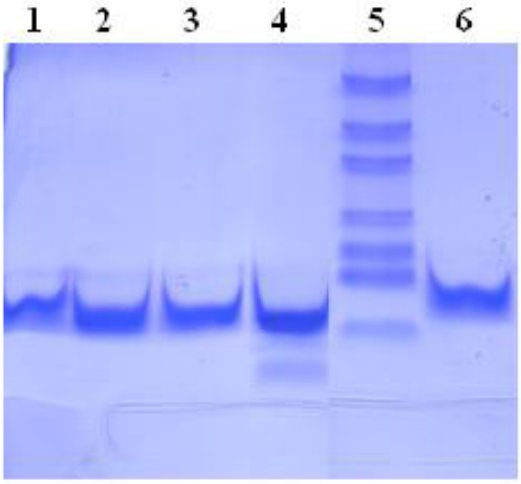

Figure 1.6: SDS-PAGE analysis of fractions of CBP-5 after removal of His-tag.
Lanes 1-4: CBP5 without His-tag; lane 6: CBP5 with His-tag.

1.3.4 Ternary complex of NBP-5/CBP-5/IGF-I

The complex of NBP-5, CBP-5, and IGF-I was prepared by mixing equimolar amounts of the components in 5 mM Tris pH 8.0, 100 mM NaCl and 0.01% NaN_3 (Figure 1.7).

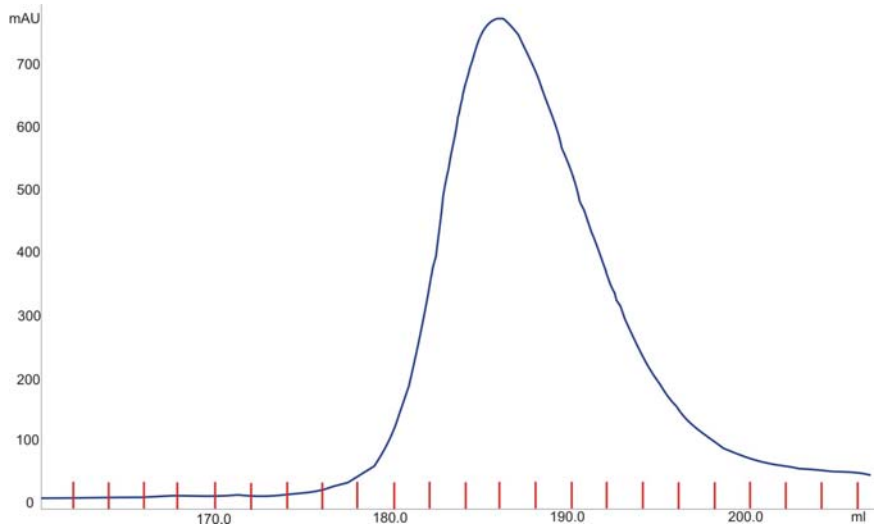

Figure 1.7: A chromatogram of the ternary complex of NBP-5/CBP-5/IGF-I.
The proteins were mixed in approximately equal molar ratios, and separated on the analytical Superdex 75 column.

1.3.5 Nuclear magnetic resonance and X-ray crystallography

All NMR experiments were carried out on a Bruker DRX 600 spectrometer equipped with a triple resonance, triple gradient 5 mm probehead, at 300 K. The samples contained typically 0.1-0.5 mM protein in PBS buffer supplemented with 10% D2O. All the 1D ^{1}H NMR spectra were recorded with a time domain of 32 K complex points and a sweep-width of 10,000 Hz. The 2D ^{1}H-^{15}N-HSQC spectra were recorded with a time domain of 1K complex data points in t_2, with 128 complex increments in t_1, and a sweep width of 8 kHz in the ^{1}H dimension and 2 kHz in the ^{15}N dimension. In order to assess the flexibility within the N-terminal domain of IGFBP-4, a ^{15}N-Gly and ^{15}N-Leu selectively labeled protein sample was prepared and a ^{1}H-^{15}N het-NOE experiment was performed with the amide proton being saturated with a 120 degree pulse for a time of 2.5 s before the

experiment. Crystallization of the binary and ternary complex was carried out with the sitting drop vapor diffusion method.

1.4 Results and Discussion

1.4.1 Domain organization of IGFBPs and the determination of exact domain boundaries

Amino acid sequence homology of distinct regions of IGFBPs suggests that all consist of three domains of approximately equal lengths. Figure 1.8 shows one dimensional ^{1}H NMR spectra of isolated N terminal domains of IGFBP-4 and –5. A typical intensity pattern of a folded protein can be observed in the spectra of the N-terminal domain of IGFBP-4 (residues 1-92) and IGFBP-5 (residues 1-83). Figure 1.9 shows the one dimensional ^{1}H NMR spectra of the C-terminal fragments of CBP-4 (residues 151-232) and CBP-5 (residues 170-247), respectively. The spectra indicated some unstructured regions located in the C-terminal fragments. The two subdomains of N-terminal domain of IGFBP-4 are connected by a short linker rich in Gly and Leu, i.e. Ala39, Leu40, Gly41, Leu42, and Gly43 (Siwanowicz et al., 2005). In order to check whether the linker is flexible, ^{1}H-^{15}N het-NOE was measured on a ^{15}N-Gly, ^{15}N-Leu labeled sample of NBP-4. The values of NOEs obtained for each of these residues is shown in Figure 1.10. Except for a single peak, the measured residues show hetNOEs above 0.6, indicating that the linker stretch is rigid. The single peak can be assigned with high probability to Gly56. Based on previous NMR studies on mini-NBP-5 (Kalus et al., 1998), this residue belongs to a loop that is flexible.

1.4.1 Optimization of the carboxyl-terminal construct of IGFBP-4

1D NMR experiments revealed that the COOH-terminal fragments of IGFBP-4 and -5 contained disordered polypeptide fragments. Assuming that disordered regions are most

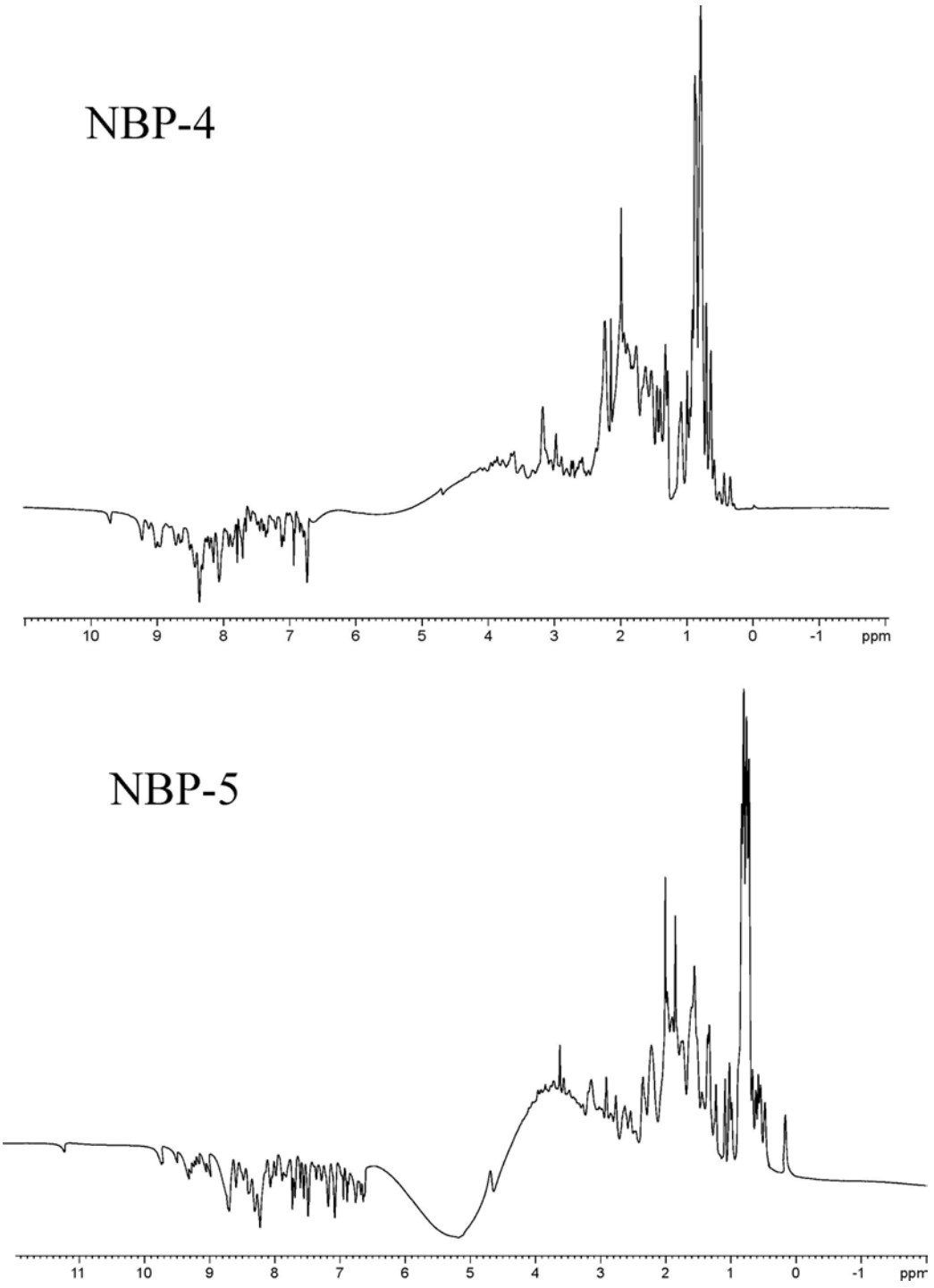

Figure 1.8: Characterization of the IGFBP folding by one-dimensional NMR spectroscopy.
The isolated N-terminal domains of IGFBP-4 (residues 1-92) and -5 (residues 1-83) are represented in the top and bottom spectra, respectively.

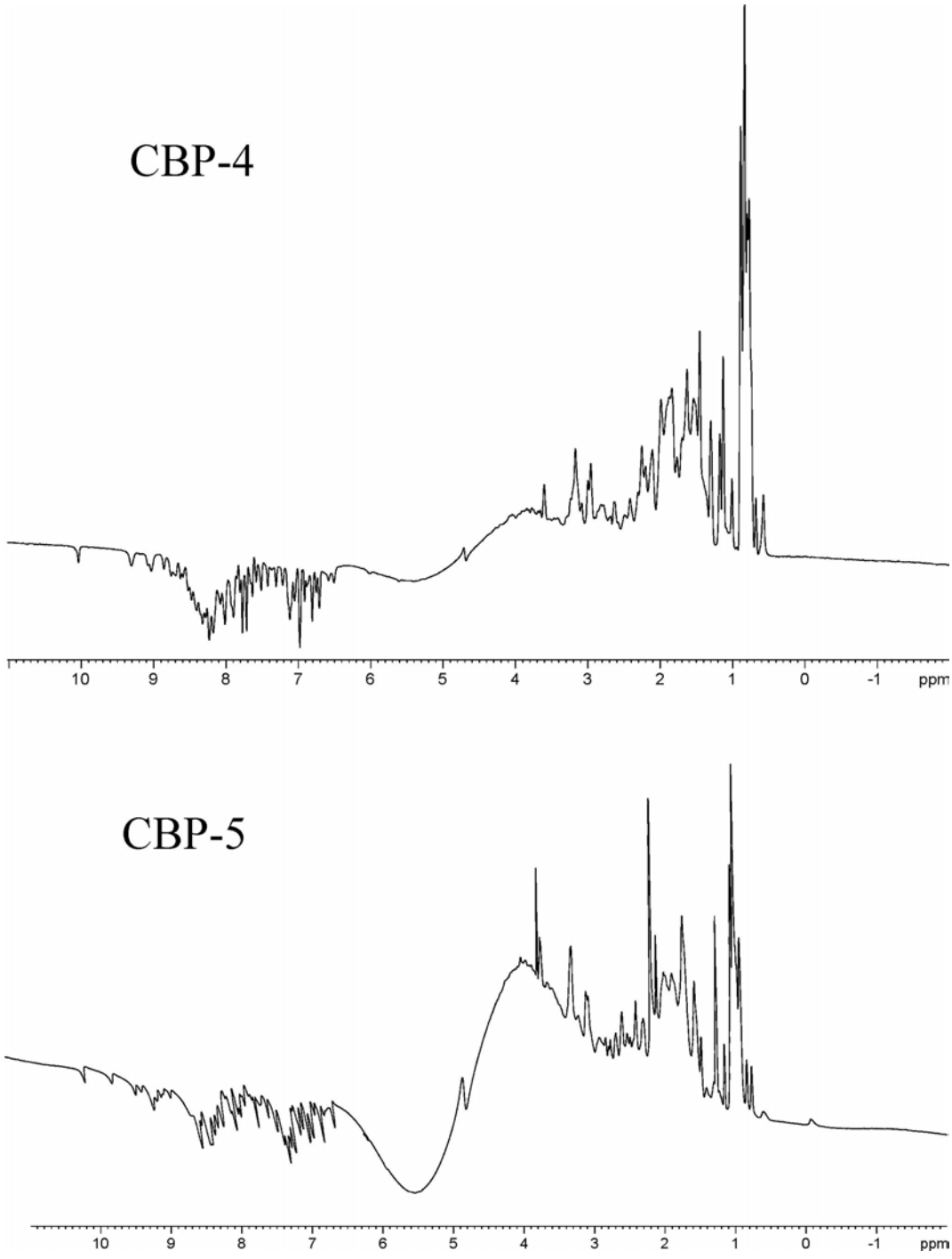

Figure 1.9: Characterization of the IGFBP folding by one-dimensional NMR spectroscopy. The isolated C-terminal domains of IGFBP-4 (residues 51-232) and CBP-5 (residues 170-247) are represented in the top and bottom spectra, respectively.

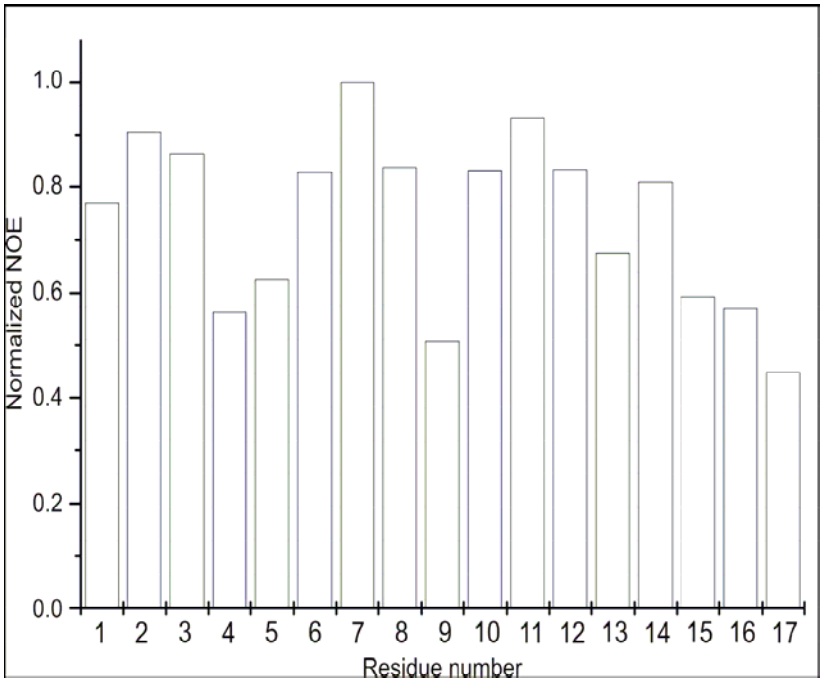

Figure 1.10: ^{1}H-^{15}N heteronuclear NOEs for all glycine and leucine residues of NBP-4 (residues 3-82).

The numbers of the residues have been assigned randomly.

likely to occur within the longest stretches of amino acids between cysteines of disulfide bridges, we designed four deletion mutants. The deletions spanned different lengths of polypeptide chains and were localized either between Cys153 and Cys183: CBP-4Δ(Gln168-Asp174) and CBP-4Δ(Ser167-Ile178), or Cys207 and Cys228: CBP-4Δ(Leu216-Lys223) and CBP-4Δ(Gly213- Glu225). The four mutants did not exhibit any improvement in the extent of folding over the wild type proteins, as determined by ^{15}N–HSQC spectra of the uniformly ^{15}N-labeled mutant proteins. On the contrary, determinants of unstructured regions were more pronounced, more so in the case of both longer deletion mutants (Figure 1.11).

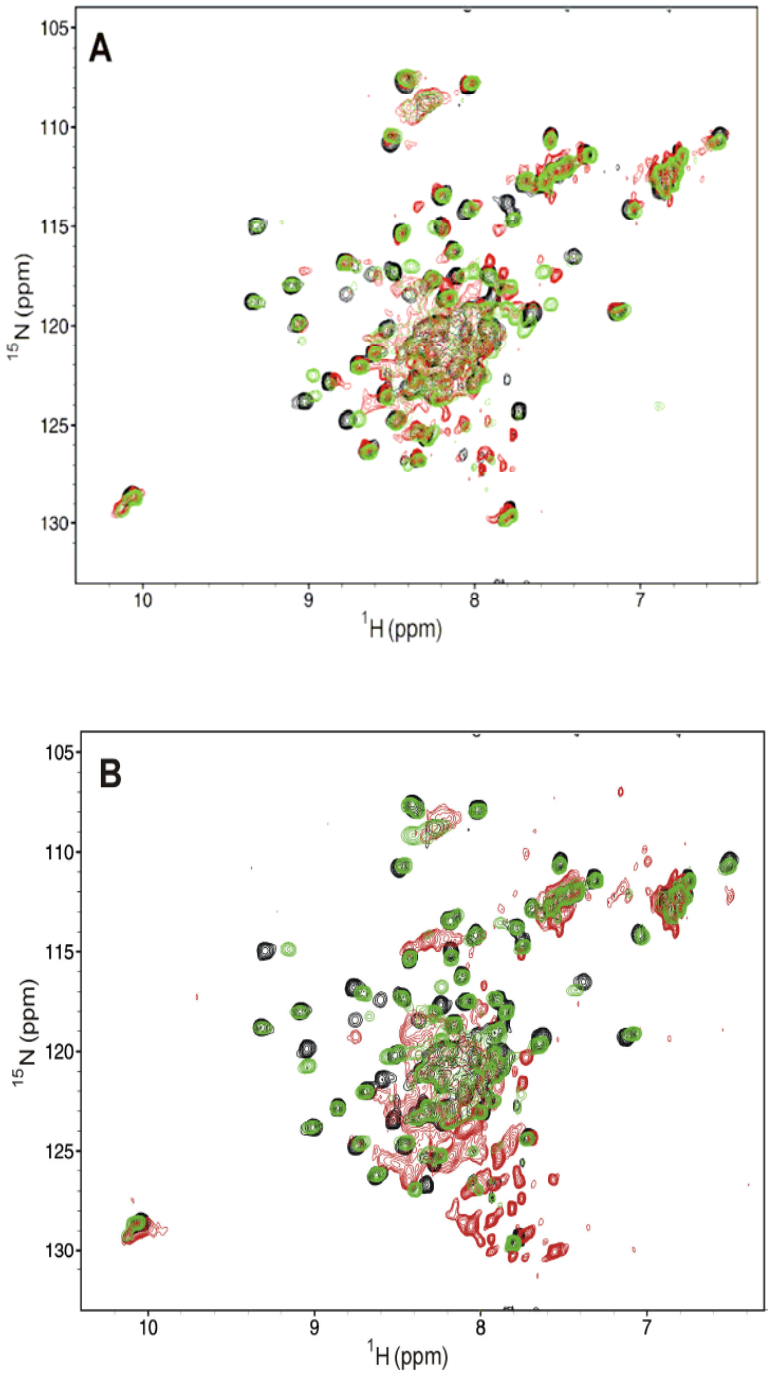

Figure. 1.11: Evaluation of the deletional optimization of CBP-4 by 2D NMR spectroscopy. Superimposed are ^{15}N-HSQC spectra of the ^{15}N-uniformly labeled proteins; **A**: wild-type CBP-4 (black), CBP-4Δ(Gln168-Asp174) (green) and CBP-4Δ(Ser167-Ile178) (red); **B**: wild-type CBP-4 (black), CBP-4Δ(Leu216- Lys223) (green) and CBP-4Δ(Gly213-Glu225) (red).

The inability of these constructs to form stable IGF-I/NBP-4/del-CBP-4 ternary complexes, as demonstrated by analytical gel filtration of the protein mixture (data not shown) indicated that either the global fold was disrupted by these deletions or/and residues important for IGF-I-binding were removed. The former is more likely as the probability of misfolded disulfide pairing in the *E. coli*-expressed recombinant proteins with 3 disulfide bridges is high (Rozhkova et al., 2004).

1.4.2 X-ray crystallography

The crystals of the binary complex (NBP-4 residues 1-92 and IGF-I) were obtained from 23% PEG 1500, 25 mM Tris pH 7.0 after 3 weeks in a form of plates measuring ca. 0.5 x 0.3 x 0.1 mm. The ternary complex (NBP-5 residues 1-83, CBP-5 residues 170-247 and IGF-I) failed to crystallize.

Prior to plunge freezing, the crystals from the binary complex were soaked for ca. 30 s in a drop of a reservoir solution containing 20% v/v glycerol as cryoprotectant. The crystals belong to the space group P21 and contained one complex per an asymmetric unit. The data was collected from a plunge frozen crystal at a rotating anode laboratory source. The structure was determined by molecular replacement using the Molrep program from the CCP4 suite (CCP4 suite, 1994). The structure of the complex of IGF-I and a fragment of the N-terminal domain of IGFBP-4 (residues 3-82) (PDB entry 1WQJ) was used as a probe structure (Siwanowicz et al., 2005). Rotation search in Patterson space yielded one peak of height 12.11σ over the highest noise peak of 4.21σ. Translation search gave a 14.47σ peak over the noise height of 4.49σ. The initial R-factor of the model was 0.47. Model was completed and revised manually using Xfit software

(McRee, 1998). Arp/wArp was used to add solvent atoms (Lamzin and Wilson, 1993). The structure was finally refined by the Refmac5 program (CCP4 suite, 1994). Final electron density maps were of good quality; there were however no interpretable densities for residue Pro63 and side chains of residues Glu11, Glu12, Lys13, Arg16, Try37, Leu42, Glu66, His70, Gln76, Met80, Glu81 and Leu82 in NBP-4 (1-92) model. The IGF-I model had no interpretable electron density for region Gly30-Pro39 and side chains of Arg50 and Glu58. These parts were removed from the model. The final R crystallographic factor was 0.24 and Rfree 0.27. Data collection and refinement statistics are summarized in Table 1.1.

It is evident from the structure of the NBP-4(1-92)/IGF-I binary complex (Figure 1.12) that the sequence Ala83-Leu92, of which the fragment Glu84-Glu90 forms a short helix, does not contact IGF directly. In the study of Qin et al. (1998) deletion of Glu90 and Ser91 led to the reduced IGF-I and –II binding activity, suggesting functional importance of these residues. Our crystallographic structure, however, shows no contribution of these two residues in formation of the IGF binding site. The presence of the 10-amino acid-long fragment may, however, have an indirect influence on IGF binding: side chains of Ile85, Ile88, and Gln89 shield Tyr60 side chain from the solvent and constrain its conformation that otherwise would point away from the IGF surface, as can be seen in the NBP-4(3-82)/IGF-I complex structure (Siwanowicz et al., 2005). Tyr60 along with Pro61 forms a small hydrophobic cleft, in which Leu54 of IGF-I is inserted, thus extending the hydrophobic contact area of the two proteins. The position of the His70 side chain in NBP-4(3-82) was rotated ca. 180° relative to the corresponding His71 of miniBP-5. In the structure of NBP-4(1-92), the imidazole ring of histidine is

Table 1.1: Data collection and refinement statistics for the NBP-4(1-92)/IGF-I complex.

Data collection	
Space group	$P2_1$
Cell constants (Å	a=32.33 b=38.99 c=61.33, β=99.89
Resolution range (Å)	2.0-2.5
Wavelength (Å)	1.542
Observed reflections	36728
Unique reflections	5177
Whole resolution range:	
Completeness (%)	99.98
*R*merge	6.0
I/σ(I)	11.8
Last resolution shell:	
Resolution range (Å)	1.6-1.7
Completeness (%)	76.9
*R*merge	17.8
I/σ(I)	20.6
Refinement	
No.of reflections	5086
Resolution (Å)	3.0 – 2.5
R-factor (%)	23.8
Rfree (%)	27.0
Average B (Å2)	36.5
R.m.s bond length (Å)	0.007
R.m.s. angles (°)	1.09
Content of Asymmetric unit	
No. of protein complexes	1
No. of protein residues/atoms	179/1063
No. of solvent atoms	31

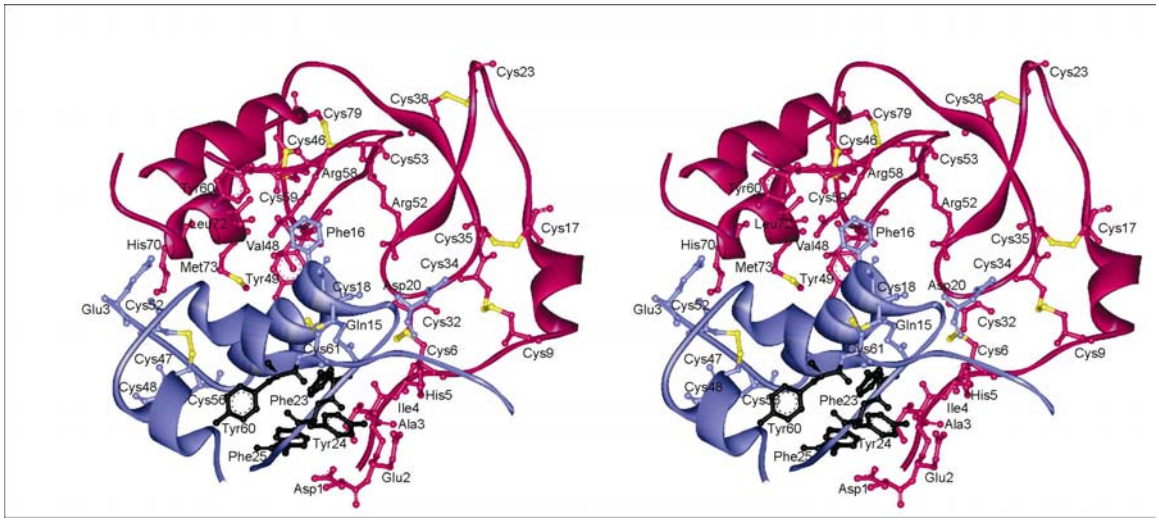

Figure 1.12: Structure of the NBP-4(1-92)/IGF-I complex.

Ribbon plot of the complex; NBP-4 (residues 1-92) is shown in magenta, IGF-I in blue. Residues marked in black are determinants for binding to IGF-IR.

however flipped back to the configuration observed in the mini-NBP-5/IGF-I complex and forms a network of hydrogen bonds with side chains of Glu3 and Glu9 of IGF-I. The amino-terminal part of IGFBP-4 can be further divided into two subdomains: the fragment from residues Asp1-Cys39 and the segment Met44-Glu90, joined by a short, glycine - leucine rich linker. Each of the subdomains has its own system of disulfide bridges reinforcing their folds. Evident from the binary complex structure lack of a extensive contact areas between the subdomains that would impose rigid linkers as well as amino acid composition of the linker, prompted us to examine molecular motions in the uncomplexed NBP-4 using NMR ^{15}N relaxation measurements. The experiment demonstrated that the linker is rigid even in the absence of bound IGF-I.

The N-terminal domain can be viewed as consisting of a globular base, corresponding to the miniBP-5 that contains the primary IGF binding site, and an

extended palm followed by a short hydrophobic thumb (Ala3, Ile4). The thumb interacts with IGF residues Phe23, Tyr24 and Phe25 upon complex formation. The palm is rigid because of four disulfide bonds arranged in a ladder-like manner plane. A number of H bonding inter-subdomain interactions prevent the palm to notably move with respect to the base. The high degree of rigidity of the N-terminal domain of IGFBPs may be of significance when the competition with IGF-IR for IGF binding is concerned. Previous studies revealed that Phe23, Tyr24 and Phe25 of IGF-I and corresponding Phe26, Tyr27 and Phe28 of IGF-II are important for binding to insulin and IGF-type I receptors (56-60). To displace the hydrophobic thumb that covers the primary IGF-IR binding site of IGFs (IGF-I, Phe23-Phe25), the receptor also has to lift the rest of the N-terminal domain, which is bound to the opposite side of the IGF-I molecule, and does not prevent receptor binding on its own (Kalus et al., 1998). Thus, the thumb does not have to significantly contribute to the overall binding affinity of IGFBPs for IGFs. This mechanism is expected to be shared by all IGFBPs given the conserved arrangement of the N-terminal cysteine residues and the consistent presence of two hydrophobic residues at positions -2 and -3 with respect to the first N-terminal Cys residue.

Truncation of the thumb (residues 1-5) reduces the IGF-I binding of NBP-4 to that of miniNBP-4 (residues 39-82), suggesting that the palm (residues 6-39) does not contribute directly to IGF binding. The segment appears therefore to serve solely a mechanical purpose as a rigid linker between primary binding sites-the base and the thumb residues. The central element of the palm consists of a GCGCCXXC consensus motif, around which the polypeptide chain (residues Cys6-Cys23) is bent forming a

disulfide ladder and assuring proper spatial relationship between the base and the thumb (Fig.1.12 and 1.13).

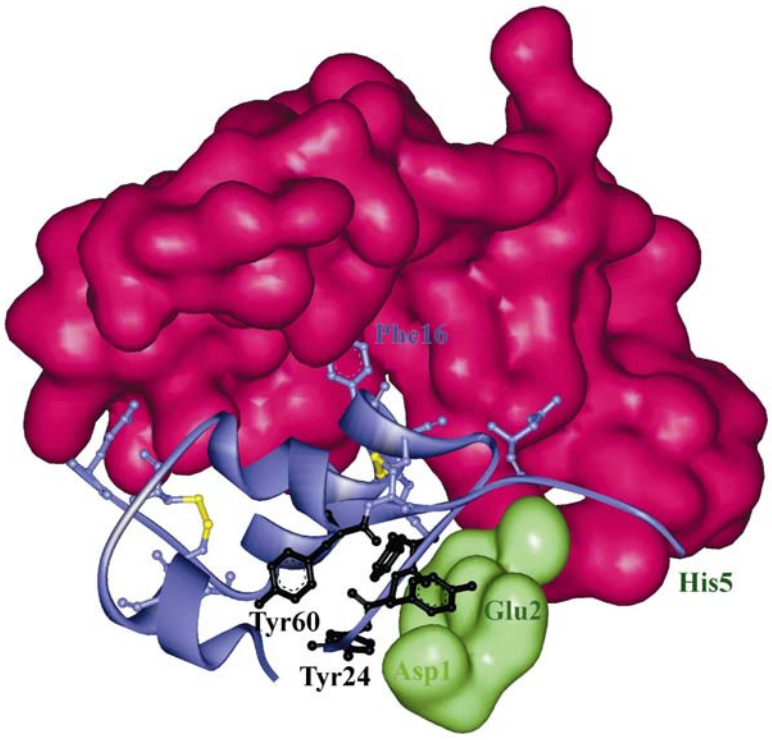

Figure 1.13: Binary complex of NBP-4(residues 1-92)/ IGF-I.
NBP-4 (residues 1-92) is presented as a surface plot: the "base" and "palm" region are colored in magenta, "thumb" in green. IGF-I is shown as a blue ribbon. The key IGF residues responsible for IGF-IR binding are shown in black.

Over the last few years, considerable progress has been made in understanding IGFBPs from a structural point of view. Information on structural determinants of the IGFBP/IGF binding can be used in design of leads that would regulate the actions of IGFs. This can be carried out either by site-directed mutagenesis of IGFBPs and thus generate IGFBPs of modified binding affinity, or by design of novel, low molecular weight ligands. For example, IGF-I and IGF-II exhibit neuroprotective effects in several forms of brain injury and neurodegenerative diseases. This implies that targeted release

of IGF from their binding proteins might have therapeutic value for stroke and other IGF responsive diseases. New approaches are taken in developing antibodies against IGF to block binding to the IGF-IR. Garcia-Echeverria et al. (2004) recently described the use of IGFBPs as agents to block IGF binding to the IGF-IR. Along with biochemical and molecular approaches, structural biology will help us to widen our understanding of the nature of the binding interaction.

2 Expression and interaction studies on integrin linked kinase and parvin

2.1 Introduction

Integrins are a large family of cell surface receptors that mediate cell adhesion and influence migration, signal transduction, and gene expression. The cytoplasmic domains of integrins play a pivotal role in these integrin-mediated cellular functions. Through interaction with the cytoskeleton, signaling molecules, and other cellular proteins, integrin cytoplasmic domains transduce signals from both the outside and inside of the cell and regulate integrin mediated biological functions (Hynes, 1992; Schwartz et al., 1995). Integrin-linked kinase (ILK) was identified during a search for proteins capable of interacting with the cytoplasmic domain of integrin (Hannigan et al., 1996). ILK is an intracellular serine/threonine kinase that interacts with the β1-integrin cytoplasmic domain and functions as a scaffold in forming multiprotein complexes connecting integrins to the actin cytoskeleton and signaling pathways. ILK also plays an important role in cancer progression (overexpression was reported to be associated with cell proliferation, metastasis, and invasion) and has emerged as a valid therapeutic target in cancer (Graff et al., 1991; Jockusch et al., 1995; Giancotti et al., 1999).

2. 1.1 Molecular architecture of ILK

Evolutionarily, ILK has been shown to be highly conserved and ILK homologues have been found in human, mice, *Drosophila* and *C. elegans*. (Hannigan et al., 1997). The

molecular architecture of ILK contains three structurally and functionally distinct domains. The extreme N-terminal domain of ILK is comprised primarily of four ankyrin repeats (Dedhar et al., 2000), followed by a pleckstrin homology (PH)-like domain that binds to phosphatidylinositol triphosphate (Delcommenne et al., 1998; Tu et al., 1999; Huang et al., 1999) as shown in Figure 2.1. The C-terminal domain contains a kinase catalytic site (Hannigan et al., 1996) that also mediates interaction of ILK with actin binding adapter proteins. The integrin binding region is present proximal to the catalytic region (Yamaji et al., 2001; Tu et al., 2001).

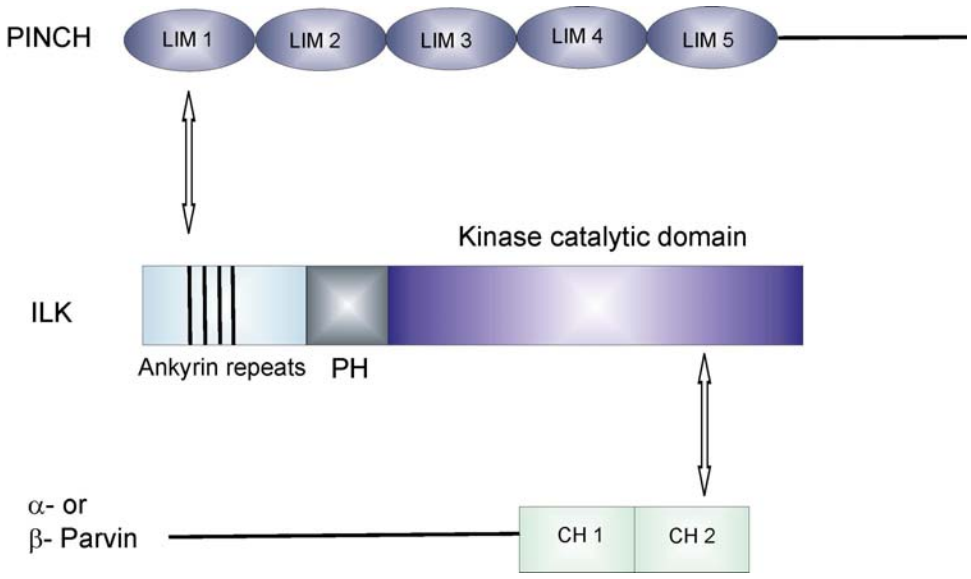

Figure 2.1: Schematic representation of the integrin linked kinase (ILK) and its protein-binding motif.

The N-terminal ankyrin repeats and the C-terminal kinase catalytic domain flank a pleckstrin homology (PH) domain in ILK. PINCH and ILK form a tight complex in cells through the LIM-1 domain of PINCH and the ankyrin repeats of ILK. The C-terminal domain of ILK contains a binding site for the second calponin homology (CH2) domain of α- and β- parvin.

2.1.2 ILK binding proteins

ILK has emerged as a key component of the cell-extracellular matrix (ECM) adhesion structures. Many proteins that interact with ILK are found in sites of integrin connection to the actin cytoskeleton. The C-terminal domain of ILK interacts with three different cytoplasmic adapter proteins: α-parvin, β-parvin and paxillin (Tu et al., 2001). At its N-terminus, ILK ankyrin domains bind to a range of adaptor and signaling molecules, such as PINCH (Tu et al., 1999) and ILK associated proteins (ILKAP) (Leung et al., 2001), which are crucial for ILK localization to focal adhesions and regulation of its function.

2.1.2.1 C-terminal interactions of ILK

α-parvin and β-parvin: Human α- and β- parvin were independently identified through their interactions with ILK (Tu et al., 2001; Yamaji et al., 2001), paxillin (Nikolopoulos et al., 2000) or actin (Olski et al., 2001). Although mammalian α- and β-parvins are encoded by two different genes, they possess identical domain architecture and share a high level of sequence similarity (human α- and β- parvins are 75 % identical and 87 % similar at the amino acid sequence level). α-parvin, also referred as CH-ILKBP or actopaxin, contains two calponin homology (CH) domains and the second calponin (CH2) domain mediates its interaction with ILK (Tu et al., 2001). β-parvin, also referred as affixin, binds via its CH2 domain to the C-terminal domain of ILK. It is a substrate for ILK kinase activity and the phosphorylation of β-parvin by ILK is thought to be involved in enhancing the ability of the β-parvin CH2 domain to inhibit cell spreading (Yamaji et al., 2001).

Paxillin: Paxillin is a multidomain protein that localizes to focal adhesions and functions as a cytoskeletal scaffold protein (Turner et al., 1990; Turner, 2000). The C-terminal domain of paxillin is composed of four LIM domains (originally identified as a cysteine-rich repeat in LIN-11, ISI-1 and Mec3 proteins) that mediate paxillin targeting to focal adhesions (Brown et al., 1996). The N-terminal domain contains five leucine-rich sequences (LDXLLXXL) named LD motifs, which are highly conserved (Brown et al., 1998). Paxillin LD motifs exhibit differential binding to several molecules important in the regulation of actin cytoskeleton such as focal adhesion kinase (FAK) (reviewed by Turner, 1998), vinculin (Brown et al., 1996) and α-parvin (Nikolopoulos and Turner, 2000). LD1 motif of paxillin binds to C-terminal domain of ILK, a region that is near the integrin binding site on ILK (Nikolopoulos and Turner, 2000, 2001). The requirement for paxillin binding in the recruitment of ILK to focal adhesions, coupled with the close physical proximity of the paxillin and integrin binding sites on ILK, may have important implications in the efficient transduction of extracellular cues via these proteins.

2.1.2.2 N-terminal interactions of ILK

PINCH: PINCH (**p**articularly **i**nteresting **n**ew **c**ysteine-**h**istidine-rich protein) is a family of cell–ECM adhesion proteins that consist of five LIM domains and a short C-terminal tail (Wu, 1999). One of the key activities of PINCH is interaction with ILK (Tu et al., 1999; Wu, 1999; Velyvis et al., 2001, Zhang et al., 2002). PINCH and ILK contain multiple protein-binding domains. They form a tight complex in cells by the direct interaction of the N-terminal LIM1 domain of PINCH and the N-terminal ankyrin-repeat

domain of ILK (Wu, 2004; Tu et al., 1999). In mammalian cells, formation of the PINCH–ILK complex occurs before, and is essential for, their localization to cell–ECM adhesions. Furthermore, it stabilizes both proteins and prevents proteasome-mediated degradation. The PINCH-ILK complex, in turn, is coupled to the actin cytoskeleton through several links (Zhang et al., 2002).

2.1.3 Cellular functions of PINCH-ILK-Parvin (PIP) complexes

Based on biochemical and structural analyses of the domains that mediate the interactions between PINCH, ILK and parvin proteins, several dominant-negative inhibitors of the PINCH-ILK-parvin (PIP) complexes have been tested. Expression of the dominant-negative inhibitors (e.g., the ILK binding LIM1 containing PINCH fragments, the PINCH-binding ANK domain-containing ILK fragments) in mammalian cells effectively disrupted the assembly of the PIP complex, which led to impaired cell shape modulation, motility and ECM deposition (Zhang et al., 2002; Guo and Wu, 2002). This points the functional importance of the PIP complexes in cellular processes that require the integrin-actin linkage. ILK and its binding partners are also critically involved in intracellular signaling, which controls cell cycle progression and survival (Persad et al., 2000). There are two general mechanisms by which the PIP complexes (as seen in Figure 2.2) function in ECM control of cell behaviour. Firstly, the PIP complexes provide a crucial linkage between integrins and the actin cytoskeleton, where, the components of the PIP complexes are capable of interacting with both the membrane (e.g. β1 integrins) and cytoskeletal components (actin, Nck-2, paxillin) of the ECM adhesion structures. Secondly, the PIP complexes serve as signaling mediators that transduce signals (e.g

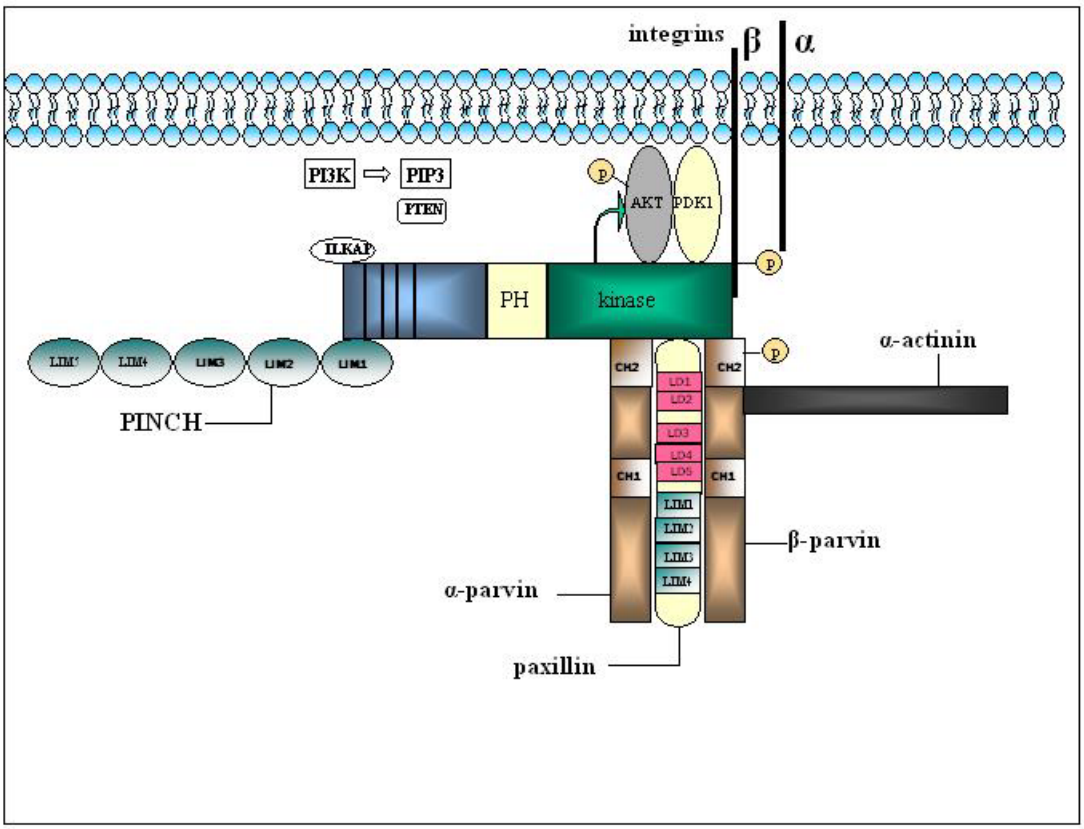

Figure 2.2: Multiprotein ILK complex in focal adhesions.

The integrin-binding region is within the carboxyl terminus of integrin-linked kinase. The ankyrin repeat domain of ILK binds to an adaptor protein, PINCH and ILK-associated phosphatase (ILKAP), which is a serine/threonine phosphatase and has been shown to negatively regulate ILK kinase activity and ILK signalling. The PH-like domain of ILK likely binds and is activated by phosphoinositide phospholipids, such as phosphatidylinositol 3,4,5-triphosphate (PIP3). The tumour suppressor PTEN dephosphorylates PIP3 to phosphatidylinositol 4,5-diphosphate, resulting in the inhibition of ILK activity. Several adaptor proteins with actin-binding properties interact with the C-terminus of ILK. The CH2 domain of β-parvin (affixin) can also bind to α-actinin, another actin-binding protein, and this interaction depends on phosphorylation of the CH2 domain of β-parvin by ILK. Paxillin can also interact with ILK, and inhibiting ILK activity results in the loss of paxillin localization to focal adhesions. The PINCH-ILK-Parvin complexes (PIP) link the integrins to the actin cytoskeleton and mediate bi-directional signaling between the ECM and intracellular compartment.

serine/threonine phosphorylation, interaction induced conformational changes) to downstream effectors and thereby control cytoskeleton organization, spreading, motility, proliferation and survival (reviewed by Wu, 2004).

2.1.4 Role of ILK in tumorigenesis and invasion

ILK expression has been shown to elevate with the increase in prostate tumor grade and this correlates with an increase in proliferation vs. apoptosis that drives the accumulation of prostate cancer progression (Graff et al., 2001). The activation of ILK in correlation to the progression of cancer becomes evident in tumors or cell lines that lack the tumor suppressor PTEN, which negatively regulates ILK activity (Dedhar, 2000; Persad et al., 2000, 2001a). Interestingly ILK plays a major role in the regulation of nuclear activation of β-catenin in PTEN-null prostate cancer cells (Persad et al., 2001a). Loss of PTEN expression occurs in many cancers (Yamada and Araki, 2001), and is especially a prominent feature of prostate cancer and glioblastomas, as 50% of human prostate tumors and 80% glioblastoma multiform contain mutations of PTEN. Besides PTEN, two other potential tumor suppressor proteins, DOC-2 (deletion of ovarian carcinoma 2) and SAP-1 have been shown to negatively regulate ILK activity, which is constitutively upregulated in cells with inactivating mutations in these genes (Wang et al., 2001). SAP-1, a transmembrane protein tyrosine phosphatase, was shown to negatively regulate ILK and PKB/Akt in a PI3 kinase-dependent manner and to induce apoptosis (Takada et al., 2002). These findings suggest that maintenance of low basal activity of ILK is crucial for tumor suppression, and that several negative signals may contribute to the suppression of this activity. Thus, the consequences of ILK over-expression or constitutive activation

leads to anchorage-independent cell survival, oncogenic transformation and increased tumorigenicity.

2.1.5 ILK as a therapeutic target in cancer

We can foresee that the increased expression of ILK in epithelial cells, beyond a certain threshold, leads to activation or inhibition of several signaling pathways. Also the constitutive activation of ILK kinase activity through the inactivation of tumour supressors, such as PTEN or through ILK regulators like β-parvin, can also result in the activation of signaling pathways involved in malignant progression. Currently, there are questions that need to be addressed: Is ILK expression or activity altered in human cancers? What types of cancer would benefit from anti-ILK therapy?

ILK protein levels can be readily inhibited with ILK-specific RNAi in various cell-culture models (Troussard et al., 2003). Small-molecule inhibitors of ILK kinase activity have been identified by high-throughput screening strategies. One class of compounds has been extensively characterized and reported to be highly selective, ATP antagonist inhibitors of ILK activity (Persad et al., 2001b). These compounds, KP-SD-1, KP-392 and QLT0254, have been shown to inhibit a range of signaling pathways activated by ILK and to suppress cancer cell growth in cell culture as well as xenograft in vivo models (Tan et al., 2001; Yau et al., 2005). The inhibitors are highly effective against PTEN-negative cancer cells, and are potent inhibitors of AKT Ser 473 phosphorylation (Tan et al., 2004).

Both antisense and small-molecule inhibitors of ILK result in inhibition of cyclin D1 expression and cell proliferation; inhibition of expression and activation of matrix

metalloproteinase 9 and inhibition of metastasis. They can also result in inhibition of AKT activation, cell survival and tumour angiogenesis. The inhibition of ILK activity in cancer cells can also result in the stimulation of expression of E-cadherin, preventing invasion. This is an obvious strategy for exploitation in the future.

Other approaches for inhibiting ILK function might be to identify inhibitors of phosphatidylinositol 3,4,5-triphosphate binding to ILK, or small molecules that selectively interfere with the interaction of ILK with PINCH or α-parvin and β-parvin. Combination therapy with other agents that inhibit parallel signaling pathways that also control these phenotypes could lead to novel cancer-specific therapies.

2.2 Aim of the study

Our studies were directed to the expression, purification, and determination of the exact boundaries for the kinase domain of ILK. Experiments also involved in studying the interaction of the C-terminal domain of ILK with the cytoplasmic adapter proteins: parvin and paxillin.

2.3 Experiments and method

2.3.1 Expression test-time course

50 ml LB-media containing appropriate antibiotic, was inoculated with a single bacterial colony of kinase A construct from a fresh LB agar plate, and incubated at 37°C in a 100 ml flask with vigorous shaking (280 rpm). OD_{600} was monitored until it reached 0.6-0.7 and was induced with 1 mM IPTG (end concentration). The culture was grown for 3 h and 1 ml sample for electrophoresis was taken before induction (t = 0), 1, 2 and 3 h after induction (t = 1, 2, 3). The samples were centrifuged and pellet was dissolved in 50 µl of 2 x SDS PAGE loading buffer (Sambrook and Russell, 2001) and heated for 5 min. 15 µl from every sample was loaded on gel as represented in Figure 2.3.

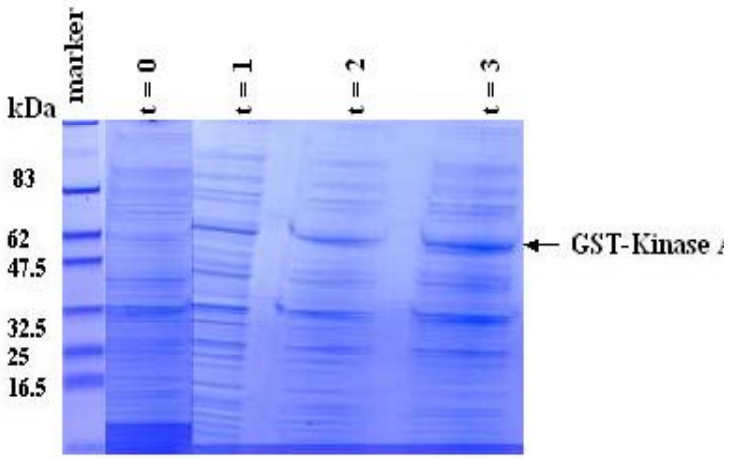

Figure 2.3: Expression test of the GST-tagged kinase A construct (residues 160- 450).

Coomassie stained SDS PAGE. The samples for electrophoresis were taken after every hour. For details refer section 2.3.1.

2.3.2 Solubility test for ILK constructs

A bacterial culture with a tested kinase A construct (Figure 2.4) was grown exactly like

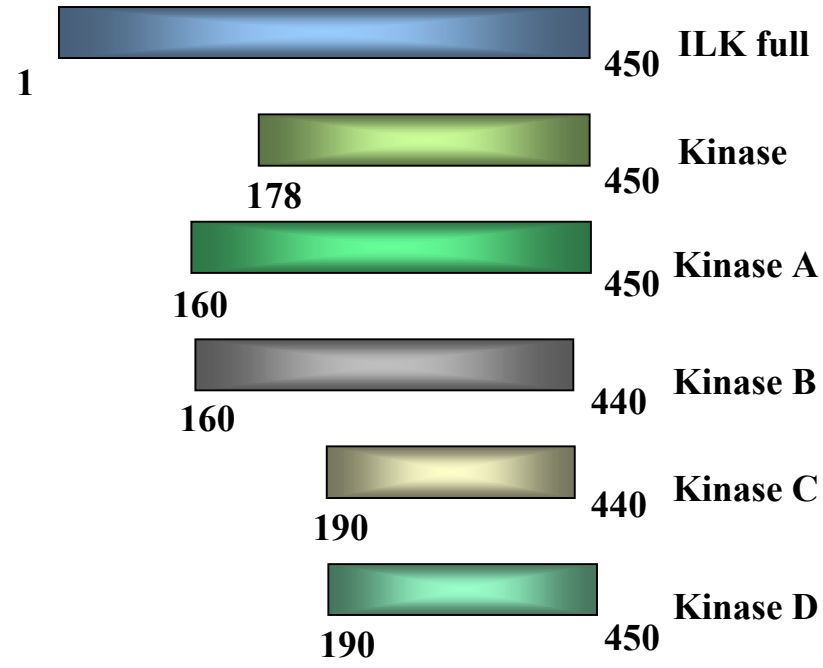

Figure 2.4: The different ILK constructs used for *E. coli* expression studies.

that for the expression test. After 3 h of incubation after induction, culture was centrifuged at 4000 rpm for 30 min at 4°C. The pellet was resuspended in 5 ml PBS buffer and the suspension was then sonicated with a maximum sonicator power for 2 x 10s. The sonicated suspension was then centrifuged for 20 min at 4°C with 23,000 rpm. The pellet was dissolved in 5 ml buffer containing 8 M urea, 0.1 M NaH_2PO_4, 0.01 M Tris-HCl, pH 8.0 with 10 mM β-ME. 20 µl samples for electrophoresis were taken from supernatant as well as from the dissolved pellet. 20 µl samples were mixed with 20 µl of the 2 x SDS PAGE loading buffer (Sambrook & Russell 2001) and heated for 5 min. 15 µl of sample was loaded on the gel as represented in Figure 2.5.

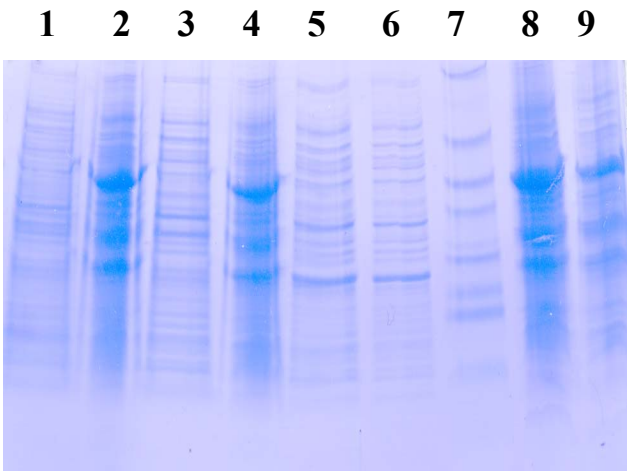

Figure 2.5: Solubility test for ILK constructs.

Kinase A (residues 160-450) and kinase B (residues 160-440) at 37°C. Lane 1: kinase A before induction; lane 2: kinase A 3 h after induction; lane 3: kinase B before induction; lane 4: kinase B 3 h after induction; lane 5: kinase A supernatant; lane 6: kinase B supernatant; lane 7: marker; lane 8: kinase A pellet; lane 9: kinase B pellet.

2.3.3 Solubility optimization test

Eukaryotic proteins that are overexpressed in *E. coli* are very often insoluble creating so-called inclusion bodies. This is connected to the loss of proteins tertiary structure and consequently to the loss of protein activity. There are few factors that can directly influence the solubility of the protein produced in *E. coli*. They include temperature of the culture during the expression (16-37°C); optical density at which the culture was induced (OD_{600} = 0.5-1.0); the inductor (here: IPTG) concentration which was used for induction (0.05-2 mM, end concentration); as well as time after induction after which the culture was harvested (2-16 h). More detailed introduction to the overexpression and purification of eukaryotic proteins in *E. coli* can be found in Marston (1986).

Cultures of bacteria containing tested construct for protein expression were grown similar to the cultures described in the solubility test in section 2.3.2. For every tested construct, two temperatures were tested (25°C and 16°C), along with two different concentrations of IPTG (0.5 mM and 1.0 mM) as well as, the time after induction after which the culture was harvested (8 and 14 h). Altogether for every given construct 16 different expression conditions were tested.

2.3.4 Finding the exact boundaries for the kinase domain of ILK

There is only a limited number of results supporting the domain organization of ILK. In addition to being preliminary, these reports contradict each other. Qin and group (2001) for the first time published the solution structure of the LIM1 domain of the focal adhesion adaptor, PINCH and characterized its interaction with the ankyrin repeat domain of ILK. For their experiments, they used residues 1-189 of ILK. However, according to Dedhar's group the ankyrin repeats constitute residues 33-164 and the residues between 180-212 correspond to PH domain of ILK.

The preliminary expression studies were carried out with the full length ILK fused with an N-terminal His-tag in the department of Reinhard Fässler (Molecular Medicine). Very low amount of protein was found in the soluble fraction. Hence, the future experiments included expression of full length as well as other domains of ILK as a GST fusion protein. In our studies we observed another prominent band on SDS-PAGE apart from the GST fusion protein. It was evident that the protein was undergoing proteolysis at some stage of expression or purification and it was important to determine the exact residues from which a different construct had to be made. 10 residues from the C-

terminus and 10 residues to the N-terminal domain of ILK were deleted (kinase B) and added (kinase A), respectively. These were expressed and purified in *E. coli* as GST fusion proteins.

2.3.4.1 STEP 1: Purification of the GST fusion protein (kinase A and kinase B domain)

The overexpressed polypeptide was purified with glutathione sepharose (Pharmacia, FRG). A bacterial pellet from 1 l culture was resuspended in 30 ml modified buffer (as mentioned in section 1.2.1.6), one protease inhibitor cocktail tablet (Roche) and 10 mM β-ME. It was then subjected to sonication using microtip 4 x 2 min, output control 7, 50%. The mixture was then centrifuged at 23,000 rpm for 1 h at 4°C. The pH of the lysate was adjusted to 7.5 and kept for binding with previously equilibrated glutathione sepharose for 6 h in cold room. The mixture was loaded on a column followed by washings with PBS and the protein was eluted with GEB buffer.

Glutathione elution buffer (GEB):

10 mM reduced glutathione
50 mM tris-HCl, pH 8.0
0.05% NaN_3

2.3.4.2 STEP 2: Gel filtration - superdex S200pg column

After elution, the protein was concentrated to 5.0 ml using a 10 kDa amicon membrane (Millipore). The sample was filtered and loaded on HiLoad 16/60 superdex S200pg. Figure 2.6 shows the elution profile of the purified kinase B construct. The fractions corresponding to the fusion protein were checked on SDS-PAGE (Figure 2.7).

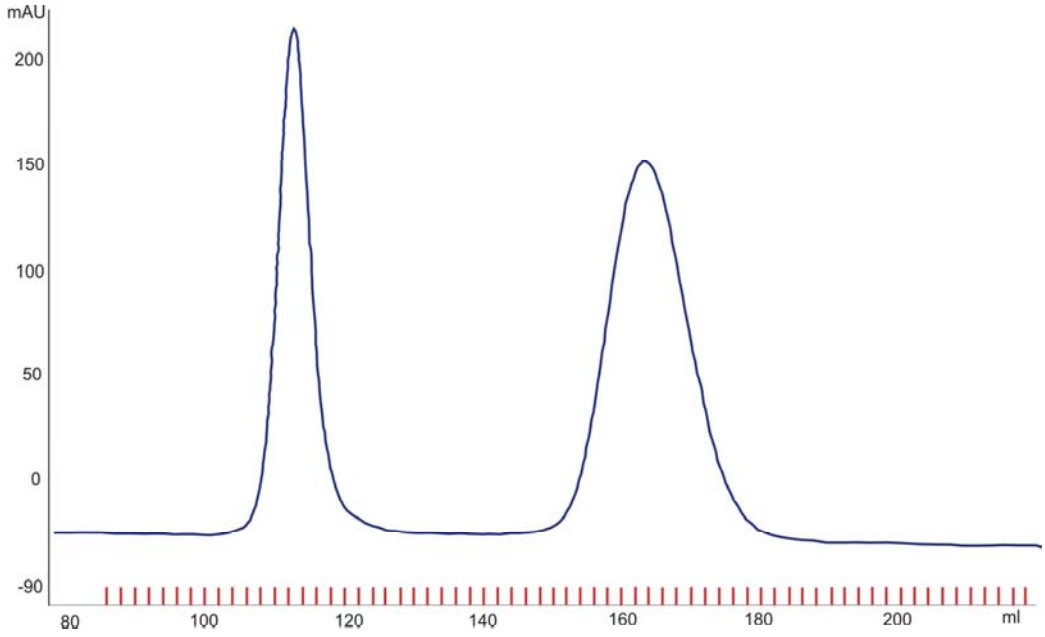

Figure 2.6: A chromatogram of the kinase domain of ILK (construct B) purified on superdex S200pg column.

The first peak corresponds to kinase domain of ILK and the second to the GST and proteolysed product from the kinase domain of ILK.

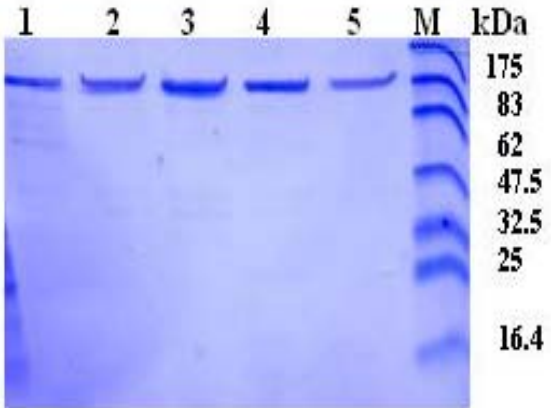

Figure 2.7: SDS-PAGE analysis of fractions of kinase B construct eluted from superdex S200pg column.

Lane 1-5: fractions corresponding to kinase B after gel filteration.

2.3.5 Expression and purification of the kinase C and kinase D constructs

One Shot® BL21 Star™ (DE3) chemically competent cells were transformed with the plasmid DNA according to the protocol described in section 2.3.2. Growth media contained ampicillin as a selective antibiotic. Typically, the cells were induced at OD_{600} = 0.7-0.8 by addition of IPTG (0.5 mM end concentration) and protein expression was performed for 14 h with vigorous shaking at 16°C. The culture was harvested by centrifugation (4000 rpm, 30 min, 4°C) and the purification protocol was similar to that used for kinase B construct in section 2.3.4.1.

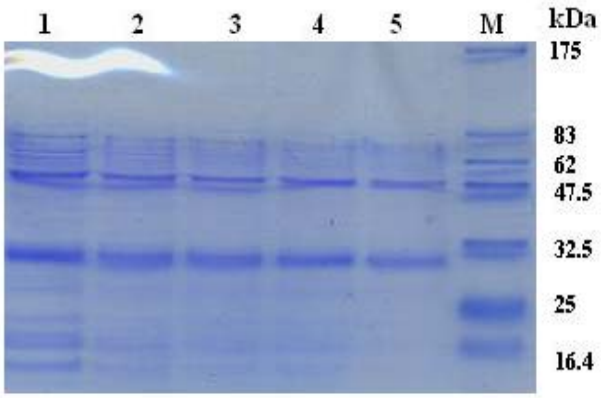

Figure 2.8: SDS-PAGE analysis of the kinase C fractions eluted from glutathione sepharose. Lane 1: kinase C fraction 2; lane 2: kinase C fraction 3; lane 3: kinase C fraction 5; lane 4: kinase C fraction 7; lane 5: kinase C fraction 9.

The kinase fractions after checking on SDS-PAGE (Figure 2.8) were purified on S200pg column. The elution profile is represented in Figure 2.9.

2.3.6 Expression tests for BEVS constructs

Another expression system was used to test the protein solubility. The baculovirus

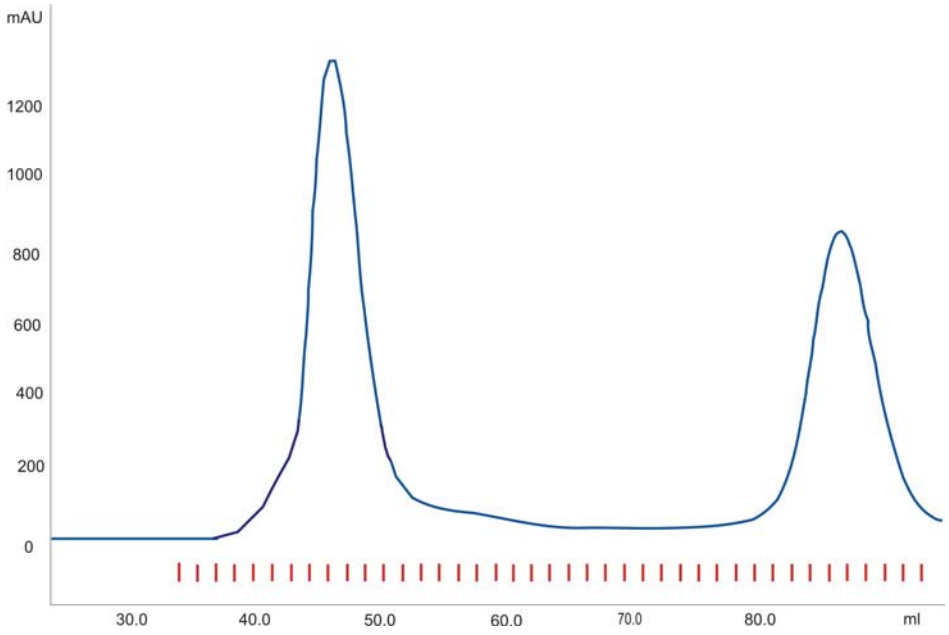

Figure 2.9: A chromatogram of the kinase domain of ILK (construct C) purified on superdex S200pg column.

The first peak corresponds to kinase domain (construct C) of ILK and the second peak shows the GST protein.

expression **v**ector **s**ystem (BEVS) has many advantages in comparison to bacterial system. Baculoviruses (family *Baculoviridae*) belong to a diverse group of large doublestranded DNA viruses that infect many different species of insects as their natural hosts. The baculovirus genome is replicated and transcribed in the nuclei of infected host cells where the large baculovirus DNA (between 80 and 200 kb) is packaged into rod-shaped nucleocapsids. Since the size of these nucleocapsids is flexible, recombinant baculovirus particles can accommodate large amounts of foreign DNA. *Autographa californica* nuclear polyhedrosis virus (AcNPV) is the most extensively studied baculovirus strain. Infectious AcNPV particles enter susceptible insect cells by facilitated endocytosis or fusion, and viral DNA is uncoated in the nucleus. DNA replication starts

about 6 h **p**ost-**i**nfection (pi). In both *in vivo* and *in vitro* conditions, the baculovirus infection cycle can be divided into two different phases, early and late. During the early phase, the infected insect cell releases extracellular virus particles (ECV) by budding off from the cell membrane of infected cells. During the late phase of the infection cycle, occluded virus particles (OV) are assembled inside the nucleus. The OV are embedded in a homogenous matrix made predominantly of a single protein, the polyhedrin protein. OV are released when the infected cells lyse during the last phase of the infection cycle. Whereas the first ECV are detectable 10 h pi, the first viral occlusion bodies of wild-type AcNPV virus develop 3 days pi but continue to accumulate and reach a maximum between 5-6 days pi. Occlusion bodies are visible under light microscope where they appear as dark polygonal-shaped bodies filling up the nucleus of infected cells (Rohrmann, 1986; Summers and Smith, 1978). Additionally this system is capable of performing several post-translational modifications (N- and O-linked glycosylation, phosphorylation, acylation, amidation, carboxymethylation, isoprenylation, signal peptide cleavage and proteolytic cleavage). The sites where these modifications occur are often identical to those of the authentic protein in its native cellular environment. More details about the BEVS, are presented in the manual by O'Reilly et al. (1994).

2.3.6.1 Test expression

The *Sf9* (*Spodoptera frugiperda*) cells were infected at a concentration of 2 mln cells/ml with a high-titer baculovirus stock. 1 ml sample for SDS PAGE was taken after 0, 42, 51 and 67 h pi and prepared like the samples in the expression test in *E. coli* (section 2.3.1)

with the only difference that they were heated for at least 20 min minutes. To further assay the ILK protein, Western blot analysis were carried on the same samples. The samples were resolved by SDS-PAGE (Figure 2.12) and transferred on to a nitrocellulose membrane and were further detected by ILK antibody.

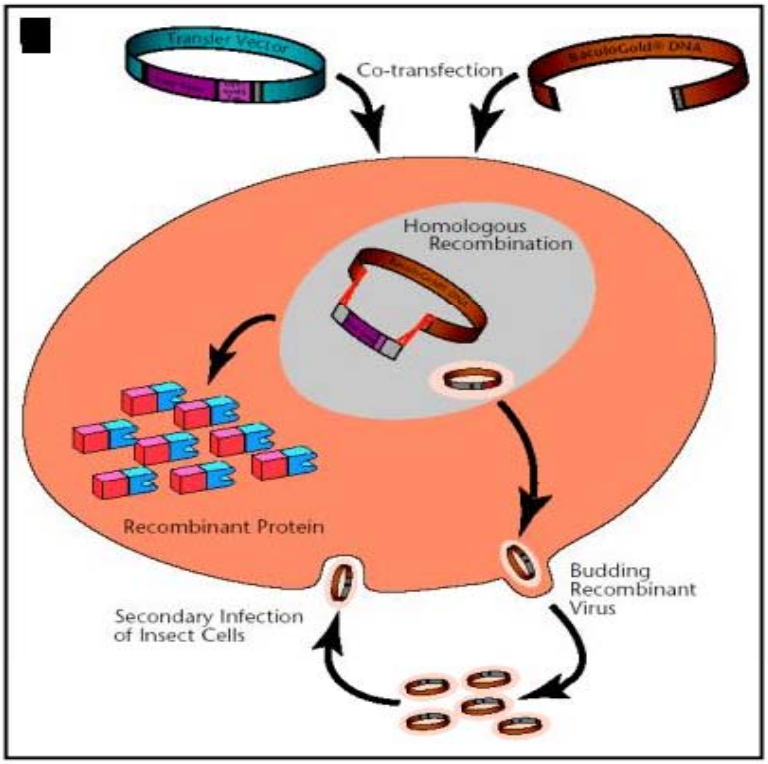

Figure 2.10: The baculovirus life cycle (*in vitro*).

The baculovirus genome is too large to directly insert foreign genes easily. Hence, the foreign gene is cloned into a transfer vector that contains flanking sequences which are homologous (5' and 3' to the insert) to the baculovirus genome. BaculoGold DNA (Pharmingen) and the transfer vector containing cloned gene are co-transfected into *Sf9* insect cells. Recombination takes place within the insect cells between the homologous regions in the transfer vector and the BaculoGold DNA. Recombinant virus produces recombinant protein and also infects additional insect cells thereby resulting in additional recombinant virus.

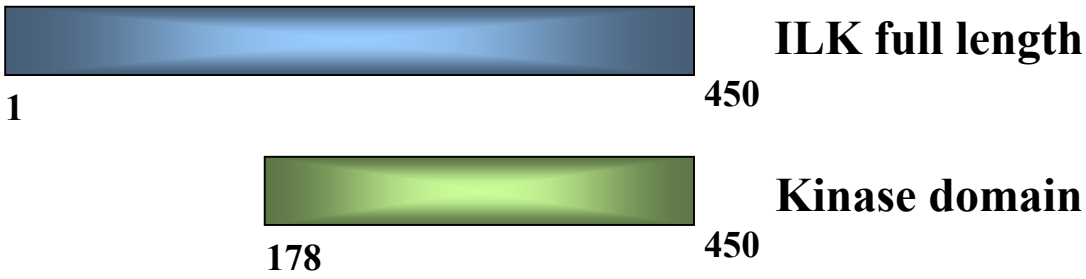

Figure 2.11: The different ILK constructs used for the baculovirus expression studies.

2.3.6.2 Baculovirus ILK expression

After the preliminary identification of ILK protein from Western blot analysis the two baculovirus constructs GST-ILK (residues 1-450) and GST-kin (residues 178-450) as

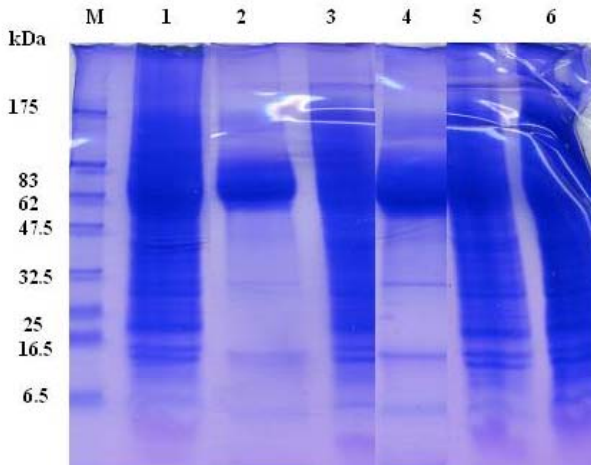

Figure 2.12: Expression test of the GST tagged ILK (residues 1- 450) and kinase construct (residues 178 - 450).

Lane 1: GST-ILK pellet after 67 h; lane 2: GST-ILK supernatant after 67 h; lane 3: GST-ILK pellet after 50 h; lane 4: GST-kinase supernatant after 67 h; lane 5: GST-kinase supernatant after 67 h; lane 6: GST-kinase supernatant after 50 h.

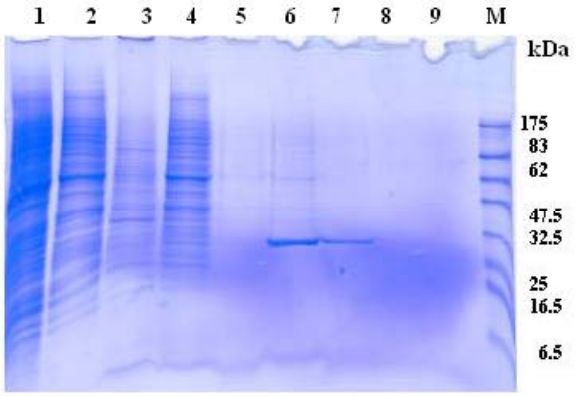

Figure 2.13: SDS-PAGE analysis of the GST-ILK fractions eluted from glutathione sepharose.

Lane 1: GST-ILK pellet; lane 2: GST-ILK supernatant; lane 3: GST-ILK after sonication and centrifugation; lane 4: GST-ILK flowthrough; lane 5: fraction 1; lane 6: fraction 2; lane 7: fraction 3; lane 8: fraction 4; lane 9: fraction 5.

depicted in Figure 2.11 were used for protein overexpression in insect cells. The expression tests were carried out as described in O'Reilly et al. (1994). The viable cells (98 %) with a cell density of 2×10^7 *Sf9* cells/ml were seeded in a spinner flask. The cells were allowed to grow at 27°C and inoculated with a high viral stock of GST-ILK (10 ml to 1l culture). They were harvested 51 h after pi by centrifuging at 6,000 rpm for 30 min at 4°C and purified as mentioned in section 2.3.4.1. Figure 2.13 shows the SDS-PAGE analysis of GST-ILK fractions eluted from glutathione sepharose.

2.3.7 Parvin family of proteins

2.3.7.1 Expression of the GST and His-tagged β-parvin

The CH2 domain of β-parvin (residues 258-364) was expressed in *E. coli* as a GST fusion protein and also as a His-tagged protein. 10 ml LB-media containing appropriate

antibiotic was inoculated with a single bacterial colony from a fresh LB agar plate, and incubated at 37°C overnight with vigorous shaking (280 rpm). Next day, 10 ml of overnight grown culture was inoculated to 1 l LB medium containing appropriate antibiotics and grown at 37°C. The temperature was reduced to 18°C at OD_{600} 0.4 and allowed to grow till it reached 0.8 and was then induced with 0.5 mM IPTG (end concentration). The culture was grown for 14 h and then pelleted at 5000 rpm for 30 min at 4°C.

2.3.7.2 Purification of the GST tagged β-parvin

The overexpressed polypeptide was purified with glutathione sepharose (Pharmacia, FRG). Bacterial pellet from 1 l culture was resuspended in 30 ml of modified buffer (section 1.2.1.6), one protease inhibitor cocktail tablet (Roche) and 10 mM β-ME. It was subjected to sonication using microtip 4 x 2 min, output control 7, 50%. Purification was similar to the protocol mentioned in section 2.3.4.1.

2.3.7.3 Gel filtration - superdex S200pg column

After elution, the protein was concentrated to 5.0 ml using a 3.0 kDa Amicon membrane (Millipore). The sample was filtered and loaded on HiLoad 16/60 Superdex S200pg (Amersham Pharmacia). The fractions corresponding to the fusion protein from the major and small peak were checked on SDS-PAGE (Figure 2.14). The fractions corresponding to the monomeric peak were pooled and the GST tag was cleaved using precession protease. The cleavage of tag was monitored by testing the protein on a SDS- PAGE gel at different intervals (Figure 2.15). Some amount of protein precipitated when the GST-

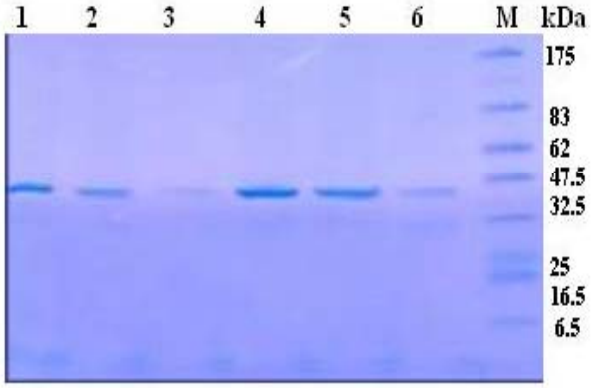

Figure 2.14: SDS-PAGE analysis of the GST tagged β-parvin eluted from superdex S200pg column.

Lane 1-6: GST tagged β-parvin elution.

tag was cleaved, hence glycerol was added to the precession buffer. The protein after cleavage was concentrated using a 3.0 kDa Amicon membrane.

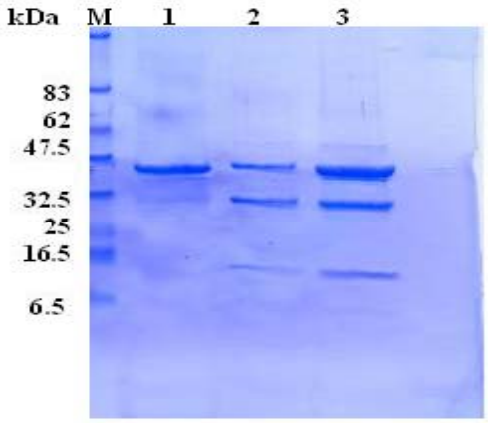

Figure 2. 15: Cleavage of the GST tag of β-parvin by precession protease.

Lane1: uncleaved GST tagged β-parvin; lane 2: partial cleavage of the tag after 8 h; lane 3: partial cleavage of the tag after 24 h.

2.3.7.4 Purification of the His tagged β-parvin

The 1 l culture pellet from His-tag β-parvin was resuspended in modified parvin lysis buffer (section 1.2.1.6). Cells were sonicated by applying 3 x 5 min pulses at a 50% cycle and 80% energy. The sample was centrifuged at 20,000 g for 45 min before applying the supernatant on a Ni-NTA-agarose (Qiagen) and purified with a modified wash buffer and eluted using elution buffer containing 20% glycerol. The protein sample was pooled and for the final purification it was loaded on a superdex S200pg column.

2.3.7.5 Co-purification of the kinase domain of ILK and the CH2 domain of β-parvin

2.3.7.6 Expression of the GST tagged kinase domain and the GST tagged β-parvin

Based on previous co-immunoprecipitation assays it was known that β-parvin interacts with the C-terminus of ILK. In our studies, we tested the binding of these proteins. For

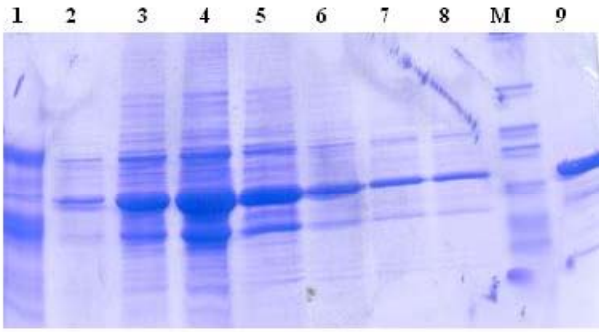

Figure 2.16: SDS PAGE analysis of the co-purification of the GST tagged kinase domain and the GST tagged β-parvin.

Lane 1: GST- kinase B protein; lane 2-lane 8: elution fractions; lane 9: GST β-parvin protein.

the first set of experiments GST-tagged kinase domain (kinase B construct) and GST tagged β-parvin constructs were used. 1 l culture pellet from both the constructs was mixed and purified using glutathione sepharose beads as mentioned in section 2.3.7.2.

2.3.7.7 Co-purification of the GST tagged kinase domain and the His tagged β-parvin

1 l culture pellet of His- tagged β-parvin was carried out as mentioned in section 2.3.7.4. The lysate was incubated with Ni-NTA beads for 1 h before adding the lysate from GST-tagged kinase domain followed by elution using a modified elution buffer.

2.3.7.8 Co-expression of the kinase domain of ILK and β-parvin

The pETDuet and pACYCDuet vectors (Novagen) facilitate the cloning and expression of multiple target proteins in a set of expression host strains. These vectors each contain two expression units, each controlled by a separate T7*lac* promoter. Each T7*lac* promoter

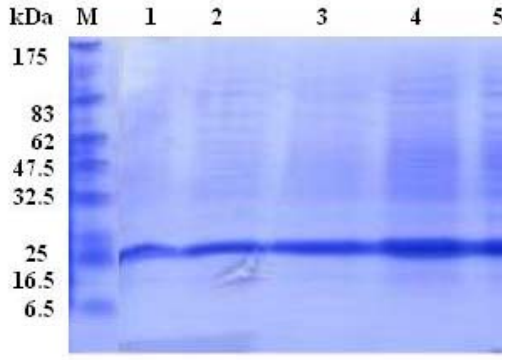

Figure 2.17: SDS PAGE analysis of the co-purification.

Lane 1- 5: eluted fractions from the GST tagged kinase domain and the His-tagged β-parvin.

is followed by an optimal ribosome binding sequence and multiple cloning site (MCS). The pETDuet-1 vector carries the ColE1 replicon and an ampicillin resistance marker; the pACYCDuet-1 vector carries the P15A replicon and chloramphenicol resistance marker. The protein purification was carried out as described in section 2.3.7.4.

2.4 Results

2.4.1 Expression test

All ILK constructs which were tested for expression in *E. coli*, gave moderate to high expression. They were however, insoluble, creating inclusion bodies. At this point, two different approaches for the studies were initiated. Firstly, to either find a different expression condition under which the expressed protein is soluble (see next section); secondly, to increase the solubility of the constructs by expressing it at lower temperature. Attempts for refolding were not made because all constructs were fused with GST.

2.4.2 Solubility optimization

The results from solubility optimization for different ILK constructs are represented in Table 2.1. The best conditions for protein expression were observed by growing at 16°C for 14 h with 0.5 mM IPTG (end concentration). This resulted in partial solubility, but ILK full length (residues 1-450) and kinase full length (residues 178–450) though expressed in high amounts was also prone to very high degree of proteolysis.

2.4.3 Purification of the kinase A and kinase B contructs

Elution of kinase A (residues 160-450) showed two bands of almost equal intensity for the fusion protein (55.0 kDa) as indicated with an arrow in Figure 2.18. Apart from this, another prominent band just above GST around 28 kDa (indicated with an arrow) was observed. In case of kinase B construct the equal intense band with the fusion protein was not observed, but the other prominent band was still present (Figure 2.19).

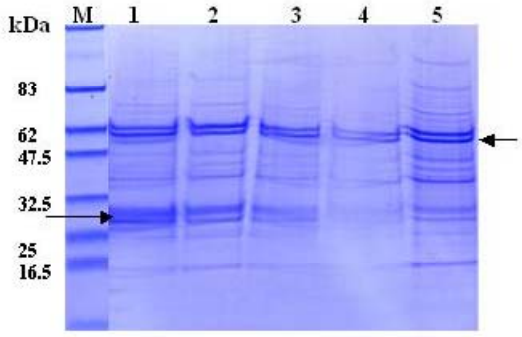

Figure 2.18: SDS-PAGE analysis of the kinase A fractions eluted from glutathione sepharose.

The arrow (right) shows the fusion protein and the cleaved part of the same. The arrow (left) shows the other prominent part of the protein.

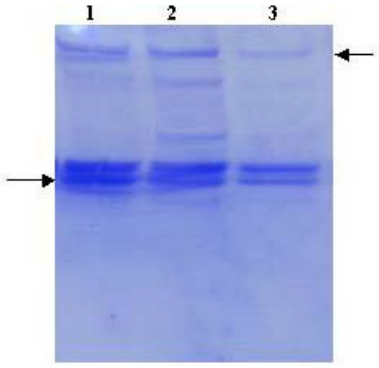

Figure 2.19: SDS-PAGE analysis of the kinase B fractions eluted from glutathione sepharose.

The arrow (right) shows only a single band for the fusion protein. The arrow (left) shows the other prominent part of the protein.

Construct	Expression	Solubility	Proteolysis
ILK full length (1 - 450)	high	~ 40% soluble	very high
Kinase full length (178 - 450)	high	~ 40% soluble	high
Kinase A (160 - 450)	moderate	~ 20% soluble	high
Kinase B (160 - 440)	moderate	~ 20% soluble	high
Kinase C (190 - 440)	low	~ 20% soluble	very low
Kinase D (190 - 450)	low	~ 20% soluble	very low

Table 2.1: Results of the expression and solubility tests of the *E. coli* ILK constructs.

From the purification and MS analysis of kinase A and B constructs, it was evident that the fusion protein was cleaving from the anterior C-terminus of ILK because the kinase A construct (residues 160-450) contains an additional 10 residues in the C-terminus when compared to the kinase B (residues 160-440) construct. The 10 residue (C-terminus) devoid kinase B construct also showed a single band for the fusion protein. It was also evident that a major amount of proteolysis is from the N-terminal region of kinase A construct, which gave rise to the other prominent part of the protein (left arrow in Figure 2.18). Hence, based on these results it was suggested that along with the C-

terminal domain of kinase, the N-terminal region also contributed in proteolytic cleavage. The next set of experiments was designed, by deleting 30 residues from the N-terminus of kinase B construct that gave rise to a new (kinase C, residues 190-440) construct. Also to verify if the last 10 residues of the C-terminal of ILK plays a role in proteolysis a new construct (kinase D, residues 190- 450) was generated.

2.4.4 Purification of the kinase C construct

Kinase C showed no proteolysis, but the expression of this construct was very low and in the final purification step the protein aggregates. The 1D proton spectrum of GST kinase C showed characteristics of a partially folded protein (Rehm et al., 2002). The spectrum was compared to that of GST and the folded part in kinase C was identical to the GST spectra and the rest constituted an unfolded protein.

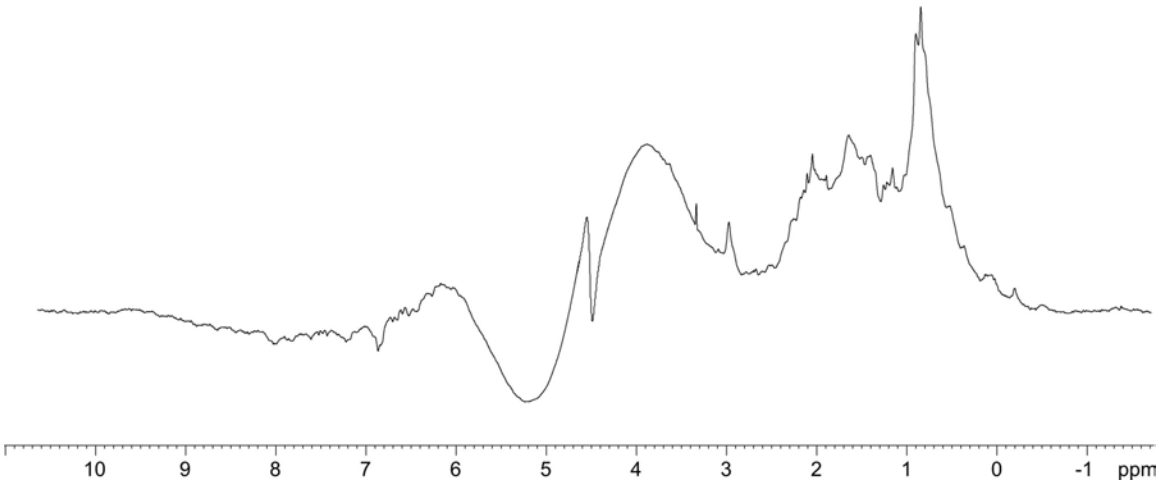

Figure 2.19: 1D ^{1}H NMR spectrum of GST kinase C construct.
The protein was dissolved in PBS buffer (pH 7.0) and the spectrum was recorded at 300 K.

2.4.5 Baculovirus expression of ILK constructs

2.4.5.1 Preliminary identification

The preliminary identification of ILK protein was carried by Western blot analysis. Figure 2.20 shows the identification of ILK from the cell pellet.

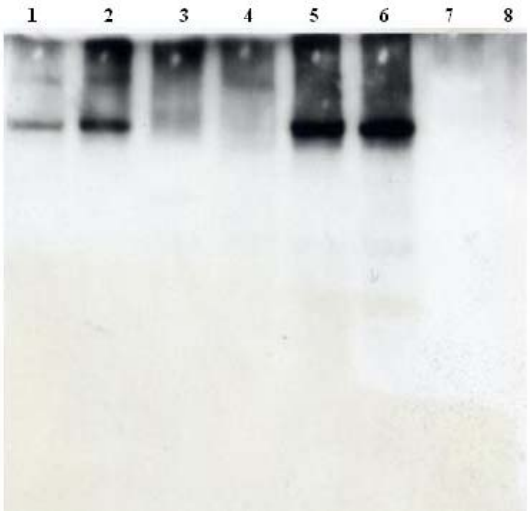

Figure 2.20: Western blot analysis of the GST-ILK and GST-kinase constructs.
Lane 1: GST-ILK pellet after 42 h; lane 2: GST-ILK pellet after 51 h; lane 3: GST-ILK pellet after 67 h; lane 4: GST-ILK supernatant after 67 h; lane 5: GST-kinase pellet after 42 h; lane 6: GST-kinase pellet after 51 h; lane 7: GST-kinase pellet after 67 h; lane 8: GST-kinase supernatant after 67 h.

2.4.5.2 Baculovirus ILK purification

The two baculovirus ILK constructs GST-ILK (residues 1-450) and GST-kin (residues 178 - 450) were overexpressed in *Sf9* cell lines. The ILK protein was then detected using ILK antibodies (Figure 2.21).

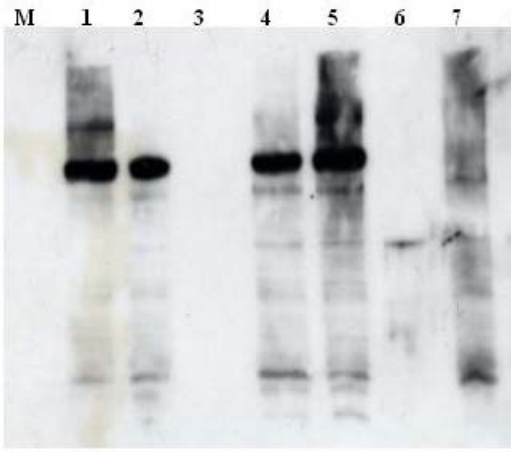

Figure 2.21: Western blot analysis of the GST-ILK fractions from glutathione sepharose elution.

Lane 1: GST-ILK lysate; lane 2: GST- ILK fraction 6 from elution; lane 3: only SDS loading dye; lane 4: GST-ILK fraction 3 from elution; lane 5: GST-ILK pellet after 48 h; lane 6: GST-ILK supernatant after 48 h; lane 7: pellet GST-ILK from negative control; lane 8: supernatant from negative control.

2.4.6 Expression of the GST and His-tagged β-parvin

The elution profile of the purified GST tagged β-parvin is represented in Figure 2.22. The first (small) peak shows the fusion protein as an aggregation. The major peak shows the monomeric form of the fusion protein. Only one single band corresponding to the fusion protein was observed. The GST tag was cleaved using precision protease but it resulted in only partial cleavage of the tag. The protein was then concentrated. The CH2 domains of β-parvins are very hydrophobic and due to this phenomenon majority of the protein stick to the membrane. Different methods were employed to concentrate β-parvin. These included lyophilization, concentrating by centricons and ammonium sulphate precipitation. These methods unfortunately did not result in concentrating the protein.

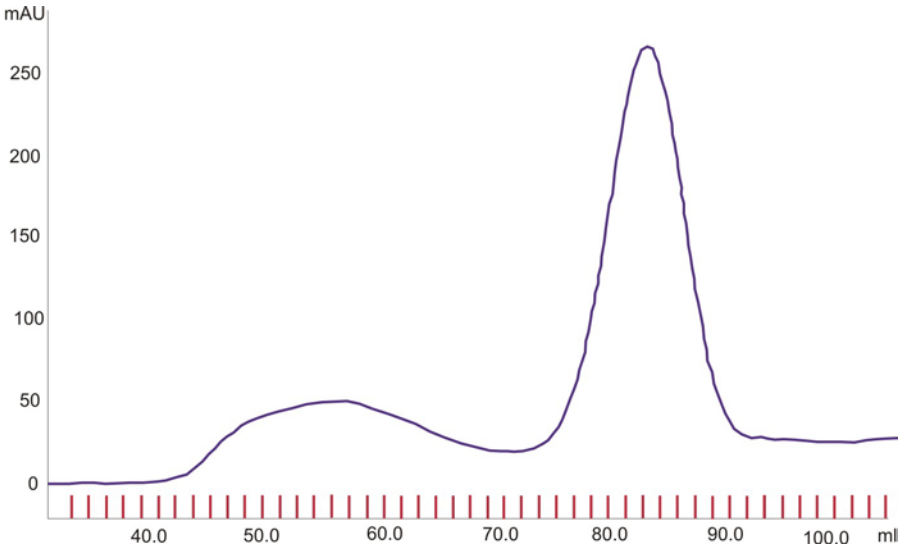

Figure 2.22: **A chromatogram of the GST tagged β-parvin from superdex S200pg column.** The first peak corresponds to an aggregated β-parvin and the second to a monmeric β- parvin protein.

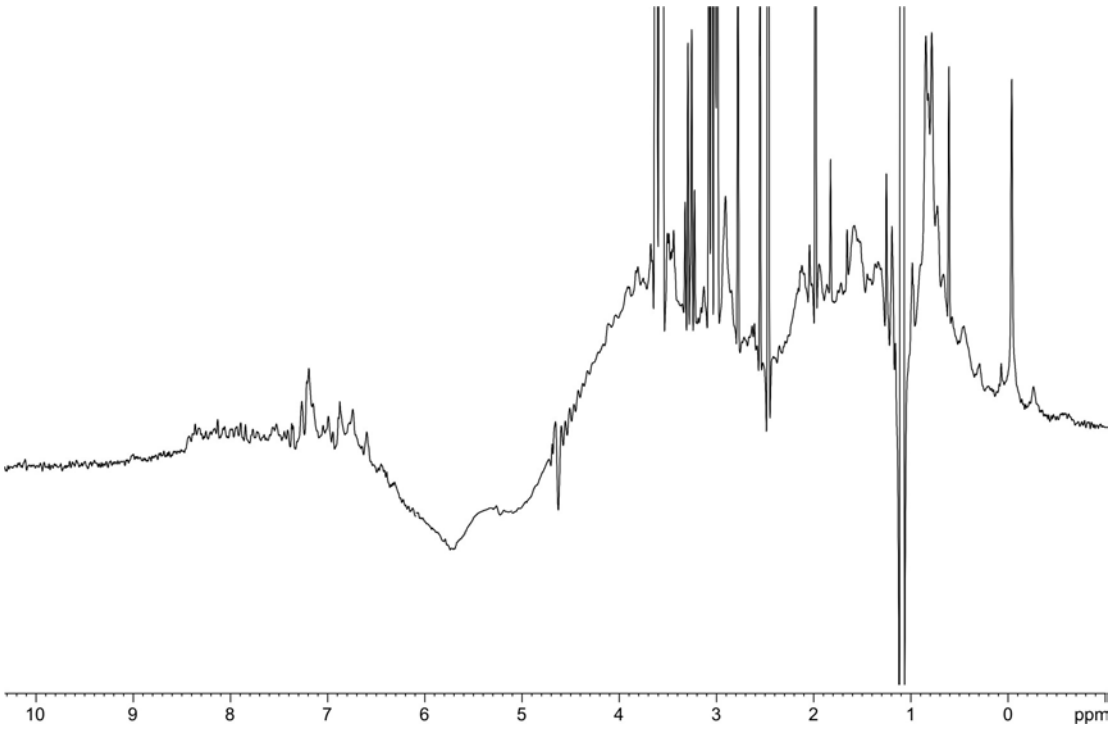

Figure 2.23: 1D spectra of the GST tagged β-parvin.

2.4.7 Co-purification of the kinase domain of ILK and the CH2 domain of β-parvin

During elution the majority of the protein precipitated, the eluted fractions were checked on SDS PAGE. The concentration of β-parvin was high compared to the kinase domain. Both the proteins were tagged with GST, hence it was not possible to determine from this experiment if they were interacting with each other. In the co-purification experiment of GST-tagged kinase domain and His tagged β-parvin, only β-parvin could be detected. In the co-expression studies of kinase domain of ILK and β-parvin, only β-parvin was expressed in both constructs, the ILK kinase domain formed inclusion bodies.

2.5 Discussion

Our studies had a long term aim at finding the three-dimensional structure of the kinase domain of ILK. The kinase domain was expressed based on previous reports, but the expression from these constructs resulted in a high degree of proteolysis. The newly designed constructs, inhibited proteolysis but the expression of the kinase domain was very low and the protein eluted in an oligomeric state. Several methods were tested by modifying the salt concentration and altering the pH of the buffer, but none changed the oligomeric state of the expressed protein. Studies, however, showed a shorter kinase domain without the overlap of the PH (pleckstrin homology) domain. It would be interesting to test if this short domain of ILK functions in cell lines in a similar way that was previously carried out for the full length kinase domain of ILK. In a recent study Tsuruo's group (2005) showed a decrease in ILK expression and cell detachment when cells were treated with Hsp90 inhibitors. Most of the cellular targets (known as clients) of Hsp90, such as Akt, Raf-1, and 3-phosphoinositide-dependent protein kinase-1 (PDK1), were important participants in signaling pathways that drive tumor cell proliferation and survival (Sato et al., 2000; Fujita et al., 2002; Schulte et al., 1995). Hsp90 inhibitors are expected to be potent anti-cancer drugs (Neckers et al., 1999). In their studies, Tsuruo's group found ILK as one of the Hsp90 client protein. Hsp90 inhibitor treatment dissociated ILK from Hsp90 and promoted proteasome-dependent degradation and they concluded that ILK requires the association of Hsp90 for its intracellular stability. Future studies can be directed at expressing ILK in the presence of Hsp 90.

In an attempt to increase the stability of the expressed ILK proteins, different expression systems were tested. The GST-ILK protein overexpression in baculovirus was

low when compared to test expression in *E. coli*. Only by means of Western blots the overexpressed protein could be detected (Figure 2.21). The ILK antibody detected the protein from 42 h pi. At 67 h pi, no traces of protein were detected. This showed that the protein was not toxic to the cell because its presence was observed even at 58 h pi (data not shown). Taking this into account different time points after transfection were set to optimize the protein expression, the cells were spinned 48, 51, 54 and 58 h pi, but none showed an increase in ILK overexpression. This low expression rates could also result from too high or too low multiplicity of infection (MOI). For protein expression, the MOI should be generally between 3-10. Measures were taken to optimize the MOI for GST–ILK and GST-kinase constructs but these did not show any changes in expression of ILK. It is a known fact that some proteins may not be stable in virus infected cells, especially membrane bound glycoproteins and secreted proteins may be produced at lower levels than nuclear or cytoplasmic proteins. ILK is known for its association with integrin domains and its close proximity to the membrane might lead to its low expression rates in insect cells. Hence, further attempts for expression should focus more on a membrane protein expression and purification approach. Increasing the amount of overexpressed protein is another concern in BEVS, which can be carried out by using a different insect cell culture medium that can support maximum cell growth and recombinant gene expression. These factors can be taken into consideration. Further advances can be made by expressing the kinase domain (residues 190-440) in insect cell lines. This kinase C construct was comparatively less prone to proteolysis when compared to all the other ILK constructs that were expressed in *E. coli.*

In our studies both the α- and β- parvin calponin homology domain (CH2) showed high expression when expressed in *E. coli.* The CH domain is a protein module of about 100 residues that was first identified at the N-terminus of calponin, an actin binding protein playing a regulatory role in muscle contraction. Three major groups of CH-domain-containing proteins have been recognized on the basis of sequence analysis (Gimona et al., 2002). Proteins containing a single N-terminal CH domain (1×CH proteins) include calponin itself as well as signaling proteins such as Vav, IQGAP and Cdc24. Proteins with an F-actin-binding domain (ABD) composed of two CH domains in tandem (2×CH proteins) include spectrins, dystrophin, filamins and plakins. Finally, proteins of the fimbrin/plastin family contain two ABDs in a tandem and constitute the 4×CH protein group. Both CH domains of parvin are more closely related to the CH1 domain than to any other class, and yet they diverge from the CH1 domain of the ABD. Sequence analysis suggests that these proteins arose by a duplication of the CH domain that was independent of that which gave rise to the ABD. Parvins are also exceptional in that the CH domains do not appear in combination with other known domains (Korenbaum and Rivero; 2002). The crystal structure of the CH2 domains of spectrin (Carugo et al., 1997) and utrophin (Keep et al., 1999) are known. An essential feature in these structures is the hydrophobic residues that are entirely buried, building the hydrophobic core of the protein. Parvins show more hydrophobic residues in the CH2 domain when compared to the other proteins in this family. This also led to purifying the protein in the presence of buffers containing glycerol. However, no effective method could be employed in concentrating the protein.

Co-expression of proteins is an important objective for biochemical and structural analysis of protein complexes because it often increases authenticity of biological activity and increases solubility of protein partners. This has been experimented by Li et al. (1997). They designed a novel double cistronic vector to co-express retinoid-X receptor (RXR) and its partner ligand-binding domains in the same bacterial cell. This resulted in a dramatic increase in production of soluble and apparently stable heterodimer. More recently, Lunin et al. (2004) crystallized the complex of MAP kinase scaffold protein MP1 with its partner p14 (an adaptor protein). They used a single plasmid containing two ORFs under the control of separate promoters. This is a complex with a critical role in endosomal MAP kinase signaling. Similarly, the kinase domain of ILK and the β-parvin gene were cloned into a dual expression vector, so that it would increase the solubility and stability of the protein. We could only find the expression of β-parvin, whereas kinase domain was found as in inclusion bodies. This was not surprising because the kinase domain could be expressed as a soluble fraction only with the aid of a GST fusion protein. Future studies on ILK can be carried out only by first increasing the solubility of CH2 domains of β-parvin. Using these domains along with LD1 motif of paxillin, an efficient construct may be generated, which could finally be used to stabilize the kinase domain of ILK.

3 Structural studies on the 14-3-3σ protein

3.1 Introduction

The 14-3-3 protein family was originally identified by Moore and Perez (1967) during a systematic classification of brain proteins. The name '14-3-3' denotes the elution fraction containing these proteins following DEAE-cellulose chromatography and their migration position after subsequent scratch gel electrophoresis (Moore and McGregor, 1965).

14-3-3 proteins belong to a family consisting of highly conserved acidic proteins, with molecular weights of 25-30 kDa. It is composed of at least seven mammalian isoforms (β, γ, ε, σ, ζ, τ, and η) that are found in all eukaryotic cells. 14-3-3 proteins are mainly cytoplasmic molecules and they act as an adaptor or "chaperone molecule", which is able to move freely from cytoplasm to nucleus and vise-versa (Muslin et al., 1996). It can form homodimers or heterodimers, and interact with various cellular proteins. 14-3-3 are phosphoserine-binding proteins that bind to the consensus motifs identified as R(S/X)XpSXP and RXXXpSXP, where pS represents phospho-serine or phospho-threonine and X any amino-acid. These consensus motifs are present in almost all of the 14-3-3 binding proteins (Yaffe et al., 1997). Table 3.1 describes some of the proteins that interact with 14-3-3 in a phosphorylation-dependent manner (*Y*affe et al., 1997; Urschel et al., 2005). Recently, using direct proteomic analysis, researchers have identified a large number of polypeptides (>200) that can associate with 14-3-3 proteins. These polypeptides are involved in numerous cell functions (Rubio et al., 2004; Benzinger et al., 2005). A study demonstrated that some of the 14-3-3 binding proteins are involved in the regulation of the cytoskeleton, GTPase function, membrane signaling, and cell fate

determination (Jin et al., 2004). The important consequences of these interactions include alterations of enzymatic activity, inhibition or promotion of protein interactions, and enhanced post-translational modifications such as phosphorylation. However, many other consequences are still unknown. So far, the most common function of 14-3-3 is sequestration of proteins in the cytoplasm, leading to inhibition of their function (Fu et al., 2000).

In epithelial cells, one particular 14-3-3 isoform, 14-3-3σ, appears to play a particularly important role in cell proliferation, cell cycle control, and human tumorigenesis. Given the importance of 14-3-3σ in mitotic regulation, it is paradoxical that many different types of epithelial cancers have recently been found to down-regulate 14-3-3σ expression at the mRNA and protein level, either through promoter methylation and gene silencing (Suzuki et al., 2000; Umbricht et al., 2001) or through up-regulation of a specific E3 ubiquitin ligase that targets 14-3-3σ for destruction (Urano et al., 2001). This may be related to an alternative function of 14-3-3σ in promoting cell senescence, although to date this has only been demonstrated in human keratinocytes (Dellambra et al., 2000).

3.1.1 14-3-3σ protein

14-3-3σ is also known as human epithelial marker (HEM) or as stratifin. By immunohistochemistry, 14-3-3σ was seen in both the cytoplasm and the nucleus of normal tissue. 14-3-3σ protein has been linked to cancer most directly (Hermeking, 2003; Lodygin and Hermeking, 2005). In human keratinocytes 14-3-3σ expression is induced

during differentiation and is necessary for the exit from the stem cell compartment, whereas its loss allows bypass of senescence (Pellegrini et al., 2001).

The major regulator of 14-3-3σ is the tumor suppressor gene, p53. Following cellular DNA damage, p53 is activated. Subsequently, p53 either mediates a cell cycle arrest or apoptosis, ensuring the maintenance of gene stability. p53 regulates the cell cycle by inducing G1/S arrest which is mediated by p21. In addition, p53 regulates the G2/M checkpoint by inducing *14-3-3*σ expression. Upon DNA damage, p53 becomes dephosphorylated and is able to bind the promoter region 1.8 Kb upstream of 14-3-3σ transcription start site. The subsequent activation and increased expression of 14-3-3σ lead to the sequestration of CDK1/cyclin B1 in the cytoplasm, and thereby blocks the interaction of CDC2 with CDK1 and the entry of the cell into mitosis, allowing time for DNA repair (Lakin et al., 1999; Hermeking et al., 1997; Taylor and Stark, 2001). Furthermore, 14-3-3σ may directly increase the transcriptional activity of p53, suggesting a positive feedback loop. In cancer, mutated p53 results in a decrease in 14-3-3σ expression. Therefore, 14-3-3σ will not be able to arrest the cancerous cell in the G2 phase, thus allowing the occurrence of mutations and aberrant chromosome structures.

3. 1. 2 14-3-3σ and cancer

14-3-3σ methylation and its aberrations expression are seen in preneoplastic lesions and in morphologically normal tissue adjacent to cancer (Gasco et al., 2002; Cheng et al., 2004; Umbricht et al., 2001). Epigenetic modification of the *14-3-3*σ gene is a very early event in carcinogensis and can precede many morphologic change in tissue. Therefore, evaluation of *14-3-3*σ methylation in body fluids may be useful in monitoring recurrence

Physical properties	**•28-33 kDa acidic proteins** **•conserved structure** **•forms hetero- and homodimers** **•at least 7 isoforms in mammals, 15 in plants, 2 in yeast,** *Drosophila*, **and** *C.elegans*
Phosphorylation-dependent interactions	**•protein kinases** (*murine leukemia viral oncogene homologue - RAF1, MEK kinase, PI3 kinase and Grb10)* **•receptor proteins** *(insulin-like growth factor 1 and glucocorticoid receptors*) **•enzymes** *(serotonin N-acetyltransferase, tyrosine and tryptophane hydroxylase)* **•structural and cytoskeletal proteins** *(vimentins and keratins)* **•cell cycle control proteins** *(cdc25, p53, p27 and wee1)* **•proteins involved in transcriptional control** (*histone acetyltransferase and TATA box binding proteins)* **•proteins involved in apoptosis** *(BAD)*
Binding properties	**•pS/pT binding proteins** **•consensus: RSXpSXP (mode 1) RXXXpSXP (mode 2)** **•non-consensus: pS/pT-binding phosphorylation-independent binding**
Functional properties	**•modulate enzymatic activity** **•alter localization** **•prevent dephosphorylaton** **•promote protein stability** **•mediate and inhibit protein interactions**

Table 3.1: Characteristics of the 14-3-3 family of proteins.

in cancer patients and/or detecting early disease. However, 14-3-3σ methylation was detected in normal lymphocytes, and lymphoid malignancies (Bhatia et al., 2003). This may give false positive results when using body fluid as a source to detect 14-3-3σ methylation. Secondly, when analyzing 14-3-3σ methylation in human tissues for research purposes, strong inflammatory reactions accompanying epithelial tumors could give false positive results. In lung cancer, inactivation of *14-3-3*σ by DNA methylation appears to be type specific where it is more frequent in small cell carcinoma cell lines (57%) than in non-small cell carcinoma cell lines (6%) (Osada et al., 2002). In breast cancer, using a proteomic approach, Vercoutter-Edouart et al. (2001) showed that 14-3-3σ is strongly downregulated in breast cancer in comparison to normal breast tissue, whereas, the levels of other isoforms (α, β, ζ, δ) were the same in both normal and breast cancer. Therefore, 14-3-3σ may play an important role in breast cancer carcinogenesis. No association between p53 mutations and 14-3-3σ expression in human tissues was seen, suggesting that the constitutive expression of 14-3-3σ may be dependent on other factors rather than p53 (Yatabe et al., 2002; Mhawech et al., 2005).

3.1.3 14-3-3 proteins as therapeutic targets

With the growing emergence of RNAi and targeted gene delivery, there exists the possibility of modulating the expression levels of individual 14-3-3 isoforms for therapeutic purposes. Inhibition of 14-3-3 protein expression may prove detrimental to the cells. Alternatively, specific isoforms or specific functions of these isoforms may be targeted.

One isoform that could be a potential target for therapeutic agents is 14-3-3σ (Kawabe, 2005). However, no inhibitor of 14-3-3σ has been designed. Difopein is a competitive inhibitor of BAD (*bcl-xL/bcl-2-associated* death promoter homolog) binding to 14-3-3σ. Treatment of cells with difopein might cause BAD to dissociate from 14-3-3σ and to bind to Bcl2. This will cause the cells to enter apoptosis. Difopein could be used in conjunction of conventional chemotherapy to trigger apoptosis. Another approach could be through phosphorylation of 14-3-3 substrates, such as Cdc25C, which leads to cell cycle progression. Thereby, cells with DNA damage will undergo mitotic catastrophe and apoptosis (Hermeking, 2004). However, the most appealing therapeutic approach is by using methylation inhibitors. 14-3-3σ is frequently silenced by CpG methylation in numerous types of cancer. Reversal of this hypermethylation can be achieved by administration of the metyltransferase inhibitor 5-aza-2-deoxycytidine (5-Aza) and histone deacetylase inhibitors (Esteller, 2005). *In vitro* studies revealed that treatment of the cell lines with 5-Aza triggered the re-expression of 14-3-3σ in the cells, and 14-3-3σ mRNA expression level was increased in a dose-dependent manner. 14-3-3σ expression is lost in numerous carcinomas. This loss may lead to mitotic catastrophe and sensitize epithelial cells to DNA-damaging agents (Dhar et al., 2000). More recently, other 14-3-3 (β, γ, ε, ζ, τ,) isoforms have been identified in cancer (Qi et al., 2005). Alternatively, investigation into the posttranslational modifications and regulation of individual 14-3-3 isoforms may provide alternative approaches to isoform specific 14-3-3 directed therapies.

3.2 Aim of the project

This project was aimed at structural studies on 14-3-3σ. So far the structures of 14-3-3τ and 14-3-3ζ have been solved. In order to identify structural differences between the 14-3-3 isoforms, which may determine biological specificity, the crystal structure of 14-3-3σ was determined and compared to the structures of 14-3-3τ and 14-3-3ζ. In this study, the 14-3-3σ was successfully crystallized that allowed determining a high resolution X-ray structure of the protein. The results provide a basis for the experimental validation of determinants of ligand and dimerization specificity.

3. 3 Experiments and methods

3.3.1 Expression and purification of 14-3-3σ

14-3-3σ was amplified by PCR using the primers 5'-ggtaattgagggtcgcatggagagaga gccagtctgatc-3' and 5'-agaggagagttagagcctcagctctggggctcctgggg-3' with an adenoviral expression vector as a template and subcloned into pET30XaLic (Novagen). *E. coli* BL21 cells transformed with this plasmid were grown at 37°C to an OD_{600} of 0.6–0.8. To induce protein expression, IPTG was added to a final concentration of 1 mM and cells were further incubated at 28°C for 4 h. Cells were lysed in lysis buffer (section 1.2.1.6) and the native 6×His-tagged 14-3-3σ protein was purified using Ni-NTA-agarose according to the manufacturers' protocol. For removal of the 6×His-tag, the protein was incubated with 10 U of Factor Xa per 1 mg of protein for 72 h at room temperature (Figure 3.1).

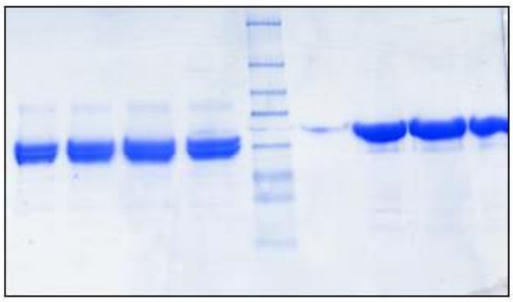

Figure 3.1: SDS PAGE of the 14-3-3σ protein.
Lanes on left side of the protein marker represent 14-3-3σ without His-tag and lanes on right side of the protein marker represent 14-3-3σ with His-tag.

Further purification was performed using size exclusion chromatography with S75pg (Figure 3.2).

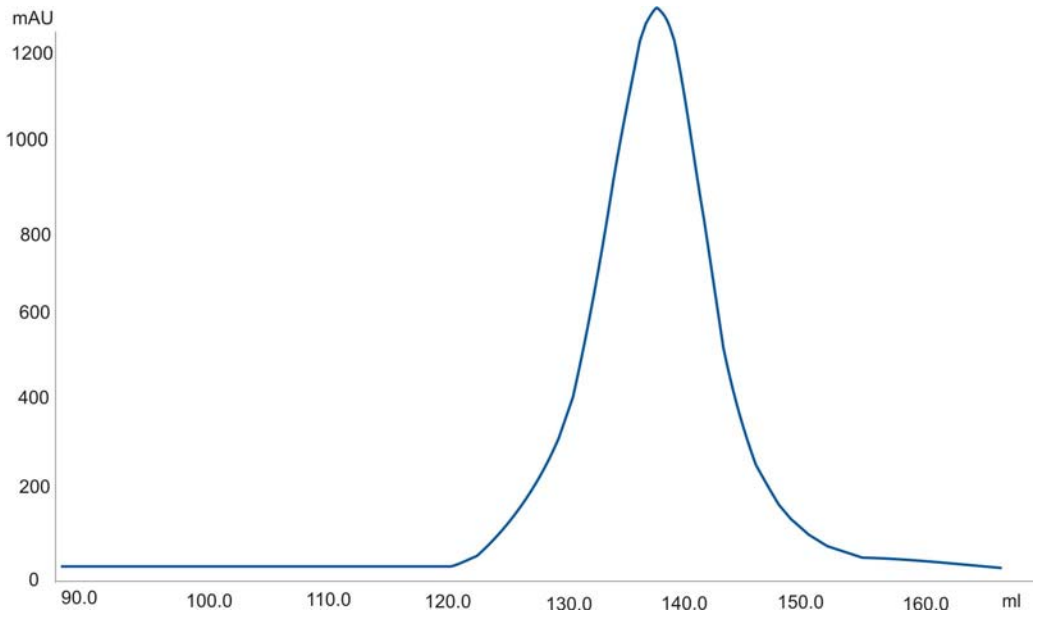

Figure 3.2: A chromatogram of the 14-3-3σ protein purified on S75pg column.
The 14-3-3σ eluted as a dimer.

3.3.2 Crystallization of the 14-3-3σ protein

Initial screening for crystals were performed with crystal screen I and II (Hampton Research). Crystallization of the protein was carried out with the sitting drop vapor diffusion method.

3.3.3 Data collection

A 2.8 Å dataset was collected on the MPG/GBF beamline BW6 at DESY, Hamburg, Germany. Diffraction data for the structure refinement was collected at 90K. Diffraction images were acquired with MARCCD detectors.

3.4 Results and Discussion

3.4.1 Purification and folding

The 14-3-3σ protein expressed in large amount (10 mg/ l) in *E. coli.* The correct folding of the purified protein was confirmed by NMR (1D spectra represented in Figure 3.3).

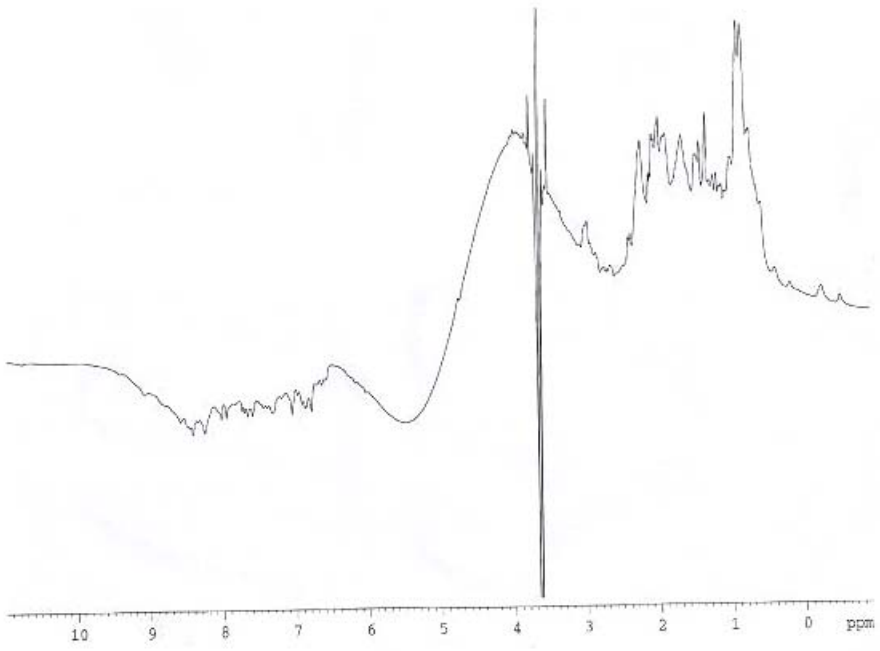

Figure 3.3: 1D ^{1}H NMR spectrum of the 14-3-3σ without His-tag.
The spectrum shows characteristics of a folded protein.

3.4.2 Crystallization and data refinement

The best crystals were obtained from 40% PEG 4000, 0.6 M ammonium sulfate and 0.1M Tris pH 9.0. They appeared after several weeks and grew to a final size of ca. 0.3 × 0.2 × 0.1 mm. Crystals were flash frozen after soaking for ca. 30 s in a drop of reservoir solution containing 30% (v/v) glycerol as a cryoprotectant. The crystals belong to the

Table 3.2: Data collection and refinement statistics

Data collection	
Space group	*P*212121
Cell constants (Å	a=71.650 b=80.850 c=99.130
Resolution range (Å)	3.0-2.8
Wavelength (Å)	1.05
Observed reflections	124574
Unique reflections	19297
Whole resolution range:	
Completeness (%)	99.4
*R*merge	4.5
I/σ(I)	11.8
Last resolution shell:	
Resolution range (Å)	2.85-2.8
Completeness (%)	95.9
*R*merge	27.4
I/σ(I)	
4.9	
Refinement	
No.of reflections	18756
Resolution (Å)	3.0 – 2.8
R-factor (%)	22.1
Rfree (%)	31.2
Average B (Å2)	41.8
R.m.s bond length (Å)	0.021
R.m.s. angles (°)	1.95
Content of Asymmetric unit	
RMSD of monomers (Å)	1.07
No. of protein molecules	2
No. of protein residues/atoms	452/6874
No. of solvent atoms	73

space group P212121 with unit cell dimensions a =71.65 Å, b = 80.85 Å, c = 99.13 Å and contained one dimer molecule per asymmetric unit. The summary of the data collection and refinement statistics are presented in Table 3.2.

The collected data were integrated, scaled and merged by XDS and XSCALE programs (Kabsch, 1993). The structure of the 14-3-3σ dimer was solved by molecular replacement at a resolution of 2.8 Å by using the Molrep program from the CCP4 suite (1994). The structure of the 14-3-3ζ isoform taken from the PDB entry 1QJB (Rittinger et al., 1999) was used as a probe structure after removing the phosphopeptide part. The initial R-factor of the model was 0.46. The model was then refined by Refmac5 (CCP4 suite, 1994) and rebuilt by XtalViev/Xfit (McRee, 1999). Waters were added by Arp/warp (Lamzin, 1993). The final R crystallographic factor was 0.22 and R free 0.31. Most of the model had clear interpretable electron density, however, the loop regions of Glu71A-Lys77A, Ser210A-Asp212A and Glu72B-Gly73B had no interpretable density as well as certain solvent exposed side-chains, and those parts were omitted in the model.

3.4.3 Crystal structure of the 14-3-3σ dimer

The 14-3-3σ protein crystallized as a homodimer. Each monomer consists of nine anti-parallel helices forming an elongated bundle. The first four helices participate in the formation of the homodimer. The remaining five helices form a deep groove providing the phosphopeptide-binding site. The overall root-mean-square-deviation (RMSD) between monomers calculated for the backbone atom is small (1.07 Å), but a clear difference is observed in the position of the ninth helix. This helix is shifted about 1.7 Å

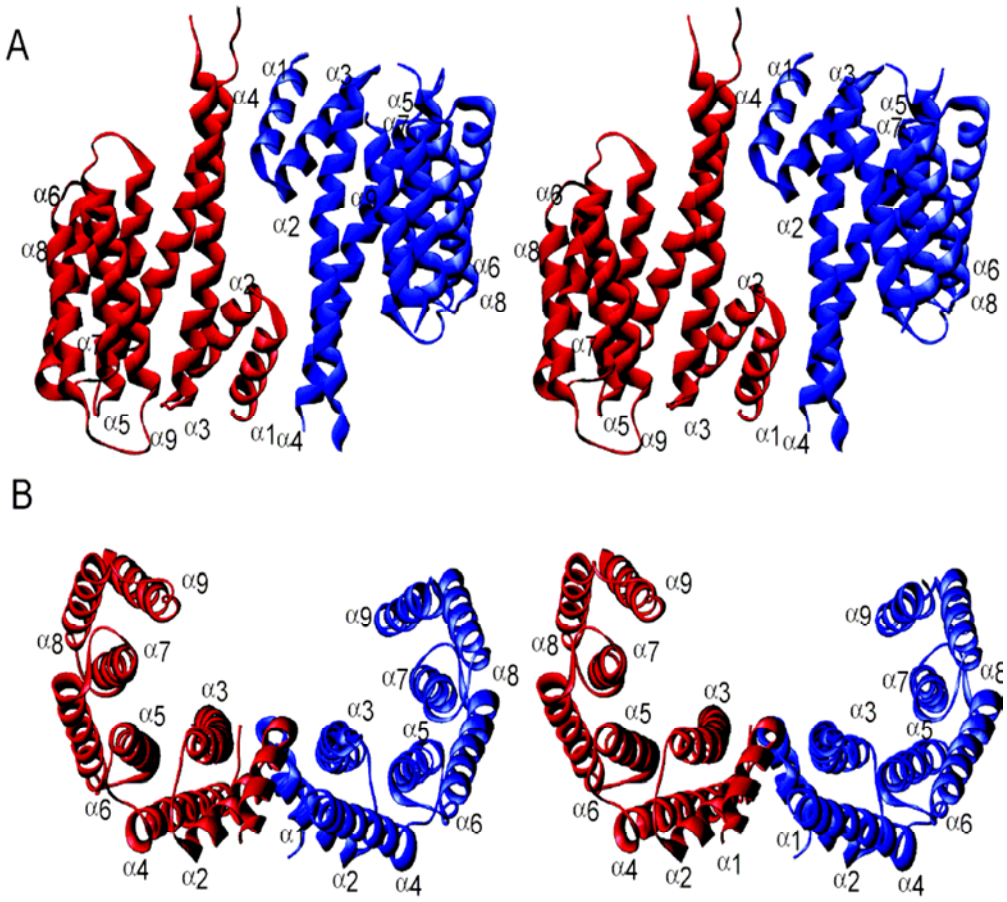

Figure 3.4: An overall ribbon plot of the 14-3-3σ homodimer.

Each monomer consists of nine antiparallel helices and the protein dimerizes in a perfect 2-fold symmetry. The dimer forms a large cup-shaped space between monomers with two phosphopeptide binding sites at it sides. The C-terminal helix of the monomer A (blue) is significantly shifted toward the binding site, chain B is shown in dark-red (**A**) a view perpendicular to the helices axis is presented. (**B**) A view parallel to this axis.

towards the ligand binding cleft in one monomer (chain A) compared to the second (chain B). As crystal packing probably causes this shift, it may indicate flexibility and adaptability of this region to structural changes that accompany ligand binding. A ribbon plot of the 14-3-3σ structure is shown in Figure 3.4.

3.4.4 Structural comparison of 14-3-3σ, τ, and ζ

We compared our structure of 14-3-3σ to the previously published structures of 14-3-3ζ and 14-3-3τ (Yaffe et al., 19975; Obsil et al., 2001; Liu et al., 1995; Xiao et al., 1995). Only the structure of 14-3-3ζ solved by Liu et al. was determined in an unliganded form, i.e. in the same state as 14-3-3σ determined here. The two additional structures of 14-3-3ζ and 14-3-3τ were determined bound to a phosphopeptide or a sulfate group, respectively. In addition, the structure of 14-3-3ζ has the same overall fold compared to the published structures of the ζ and τ isoforms (Obsil et al., 2001).

It was found that the structure of 14-3-3σ has the same overall fold as the known fold of the ζ and τ isoforms. The interface mechanism responsible for dimerization is identical for the three 14-3-3 isoforms. Most residues not conserved between isoforms are localized on the outer surface of the molecule, while the phosphopeptide-binding cleft is highly conserved (Fig.3.5). The dimerization surfaces of the 14-3-3σ, ζ, and τ isoforms display several differences, which may alter the binding constant of different isoform combinations and result in limited heterodimerization. Among the isoforms (Fig. 3.5) the most significant changes between the σ isoform and the two other isoforms are Ser5 (σ)-Glu5(ζ,τ), Glu20(σ)-Asp20(ζ,τ), Phe25(σ)-Cys25(ζ,τ), Gln55(σ)-Arg55(ζ,τ) and Gln80(σ)-Met78(ζ)- Leu(τ). In the 14-3-3τ isoform the loop Glu131-Thr141 has adopted a different main chain conformation than in 14-3-3σ and ζ, however, these loop residues have the same character and it is unlikely that they affect 14-3-3 dimerization.

The most significant difference between the structures of 14-3-3 isoforms solved so far and our structure of 14-3-3σ is seen in the configuration of the loop located between Ala203 and Asp215 (Fig. 3.5). This component of the structures is in “an open

conformation" relative to the ligand-binding site in 14-3-3σ and has a different position when compared to the peptide/small molecule bound 14-3-3ζ and τ isoforms and also a different fold in the 14-3- 3ζ/serotonin N-acetyltransferase complex. The movement of this fragment is large between the 14-3-3σ and the peptide bound 14-3-3ζ structures (about 4.2 Å between Cα of Ser207ζ and Ser209σ). In the structures of the 14-3- 3ζ and τ isoforms this loop partly folds upon itself producing "a closed conformation". In the structure of 14-3- 3ζ bound to serotonin N-acetyltransferase, the C-terminal portion of the loop is pushed away from the phosphopeptide binding cleft by the intruding serotonin N-

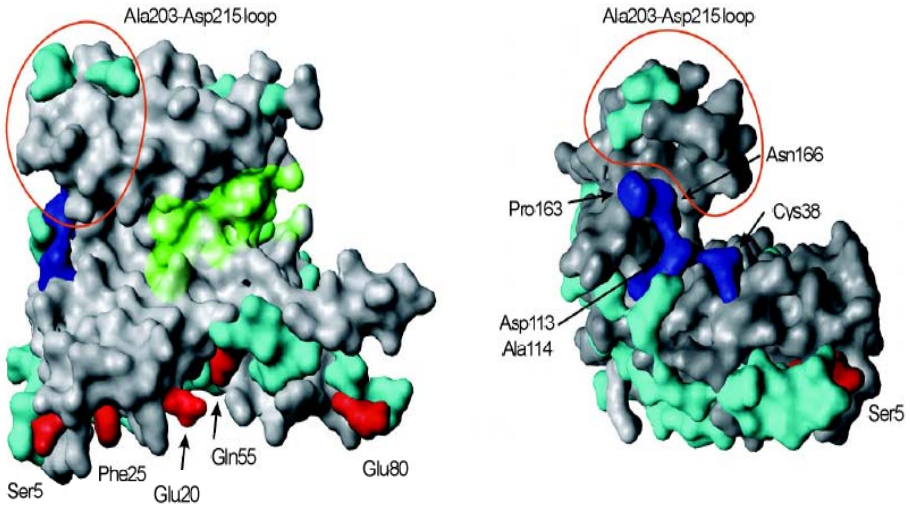

Figure 3.5: Comparative structural analysis of phosphopeptide binding and dimerization interfaces in 14-3-3 proteins.

Surface plot of the 14-3-3σ monomer. Residues belonging to the dimerization surface that differ significantly from other isoforms are shown in red. Residues forming the edge of the peptide binding site, which differ, from the 14-3-3τ and ζ isoforms are shown in dark blue. Other non-conserved residues are shown in green whereas conserved parts are in gray. The Ala203-Asp215 loop has been marked by a circle (in red line). The phosphopeptide binding region is highlighted in light green.

acetyltransferase molecule (Obsil et al., 2001, PDB 1IB1). The long axis of the loop, which runs from Ala203 to Asp215, is rotated 90º relative to the position of this axis in 14-3-3σ. Taken together, the leading difference among the 14-3-3 isoforms is seen in the position of loop 203-215 relative to the phosphopeptide binding site in 14-3-3 structures. These differences suggest that this area is the major ligand-specificity region. In the 14-3-3σ structure this loop is well determined in one monomer (chain B), and partially defined in the other (chain A, no electron density was seen for tip residues Glu210-Ser212). However, in the parts of the chain A loop with interpretable electron densities the fold of the loop is identical in both monomers, indicating that this difference is not caused by crystal packing as each monomer is in a different environment. In the only other structure of a completely free 14-3-3, the ζ isoform presented by Liu et al, this segment of the structure is missing. Our data and the structure determined by Liu et al indicate that this loop might be flexible. This feature however would not interfere with its proposed function of a major ligandspecificity region, which utilizes both sequential and structural di-versities of this region to select for isoform-specific binding partners.

The most significant divergence in amino acid types towards other 14-3-3 isoforms is seen in the same area: at the edge of the phosphopeptide-binding groove at the 14-3-3-residues marked in blue in Figure 3.6. This part has a strictly preserved backbone structure among the 14-3-3 proteins and is in a significant distance (ca. 20 Å) from the primary phosphoserine binding site. Since structural properties of the binding site are analogous for the isoforms for which structures have been determined, the specific amino acids in this part are also prime candidates for determining the isoform specificity towards ligands. The most important changes in amino acid character in this

region are: Asn166(σ)-His164(ζ,τ), Pro163(σ)-Gln161(ζ,τ), Cys38(σ)-Asn38(ζ,τ), Asp209/211(σ,τ)-Glu209(ζ), and Asp113(σ)-Asn111(τ)-Gln111(ζ).

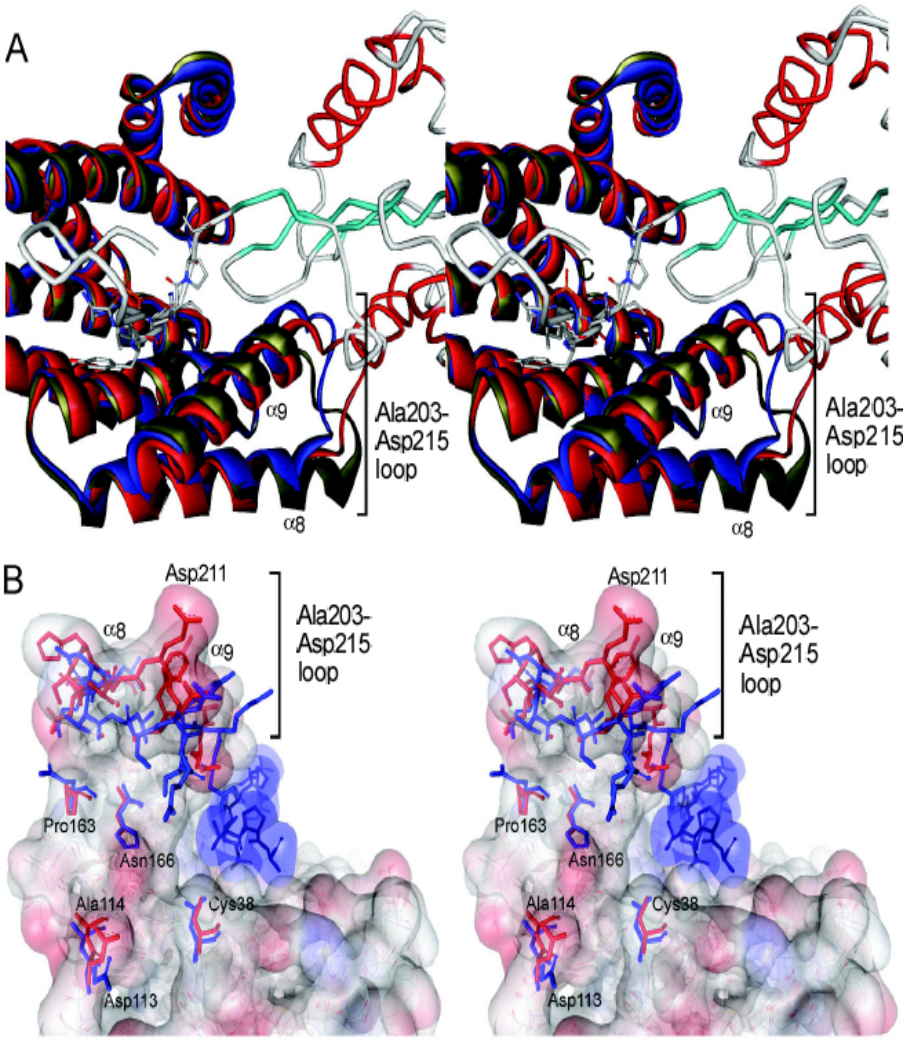

Figure 3.6: Ligand recognition by 14-3-3 proteins.

(**A**) Unbound σ (red) and ζ (blue) are superimposed with the structure of the ζ isoform (green) bound to serotonin N-acetyltransferase (Cα trace) to indicate the structural diversity of the Ala203 and Asp215 loop area. (**B**) Structures of ζ (blue) and σ (red) are overlaid. The molecular surface of the σ isoform is shown half-transparent. The structure and surface of the phosphopeptide from the 1QJA model is shown in light blue. Non-conserved residues in this area are labeled for the σ isoform. Significant difference in the Ala203 and Asp215 loop are evident.

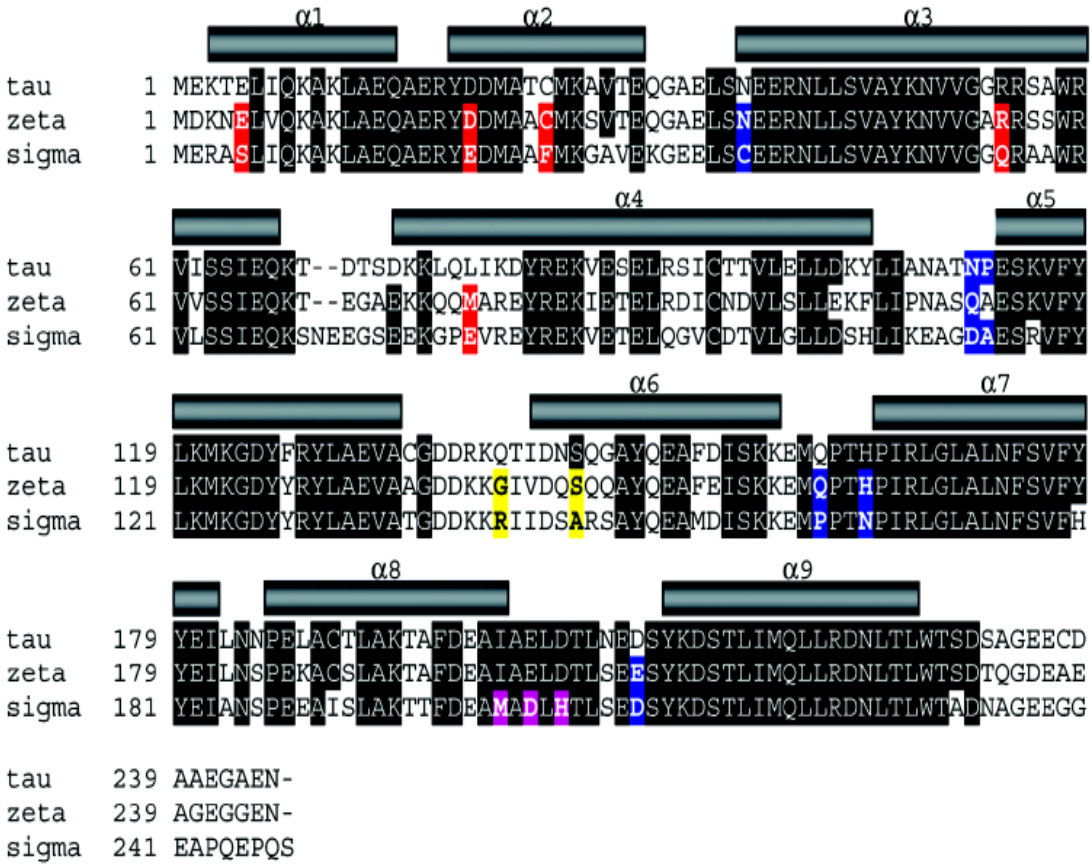

Figure 3.7: Alignments of the primary sequences of 14-3-3σ, ζ and τ.

Differences in the structures identified here are highlighted in colors. Amino acid residues shown with a black background are conserved in at least 6 of the 7 human 14-3-3 isoforms according to reference 14. The positions of α-helices (α1 to α9) are indicated by rods above the alignment. Residues in red presumably determine 14-3-3 dimerization specificity. For 14-3-3σ and 14-3-3ζ these residues are Ser5-Glu5, Glu20-Asp20, Phe25-Cys25, Gln55-Arg55 and Glu80-Met78, respectively. Residues constituting the ligand-specificity region proposed here are shown in blue for 14-3-3σ and ζ, respectively: Cys38-Asn38, Asp113-Gln111, Pro163-Gln161, Asn166-His164 and Asp211-Glu209. For comparison between 14-3-3σ and τ Asp113-Asn111 and Ala114-Pro112 are marked in blue. The yellow residues (Arg142-Gly140, Ala147-Ser145) may be of minor importance for ligand-specificity of 14-3-3σ and ζ. Three 14-3-3σ-specific residues present in the potential ligand-specificity region Ala203-Asp215 are shown in magenta (Met202, Asp204, His206).

In conclusion, the periphery of the phosphopeptide-binding cleft accumulates significant differences both in the fold (residues 203-215 in σ) and residue properties (the σ residues 38, 113, 163, 166, 209). Based on comparison of all mentioned structures, we propose that the Ala203 and Asp215 loop and its neighborhood represent the major ligand specificity region (Figs. 3.6 and 3.8). On the primary sequence level this loop is highly conserved between the seven isoforms, but contains 3 unique amino acids (Met202, Asp204, His206) in 14-3-3σ, which are not found in any other 14-3-3 isoforms (Fig. 3.7). The structure of the phosphopeptide binding site of the 14-3-3σ molecule is

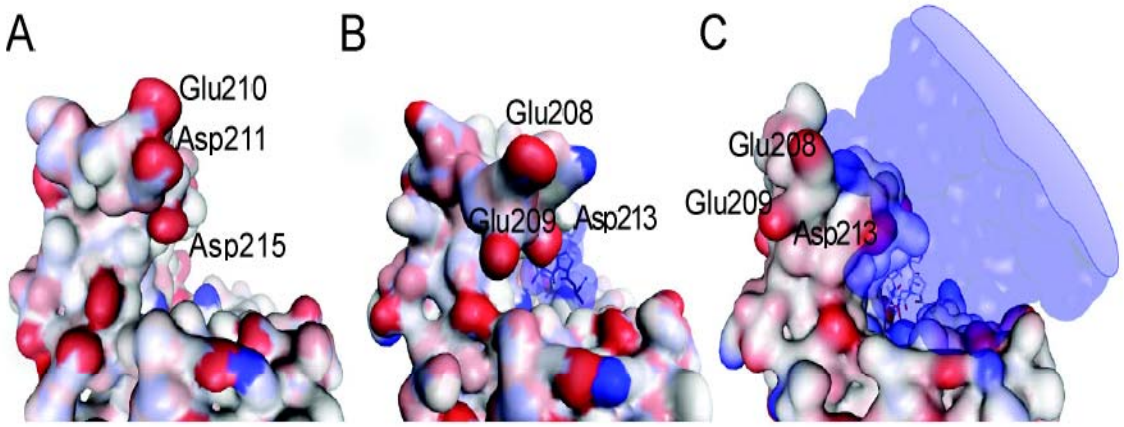

Figure 3.8: Proposed major ligand specificity region of 14-3-3σ.
The figure shows the edge of the phosphopeptide binding groove, from the Cterminal side of a phosphopeptide. (**A**) The molecular surface of the 14-3-3σ isoform colored by atom charge. The structure presents an "open" conformation of the cleft edge. (**B**) The same area of the 14-3-3ζ isoform has a "closed" conformation. (**C**) Serotonin N- acetyltransferase in complex with 14-3-3ζ shown as a semi-transparent surface plot; the phosphoserine region is shown as a stick model. Except for the phosphopeptide cleft, the only possible contact area is localized at the edge of the 14-3-3ζ molecule, thus indicating that this part may be responsible for selective ligand binding.

identical to the ζ and τ isoforms with bound ligands (structures 1QJA and 1QJB) (Fig. 3.9 A), but not to the ζ isoform in its free form (1A4O). This difference is especially pronounced in the conformations of Trp230 and Tyr181, which form an aromatic environment at the N-terminus of a potential 14-3-3-binding peptide. As shown in Figure 3.9 B, the aromatic rings of Trp230 and Tyr181 in 14-3-3σ are oriented in the same plane as in the ζ isoform with a bound phosphopeptide, while in the free form of the ζ isoform they adopt a different orientation. The conformation of additional side chains of the phosphopeptide binding site in 14-3-3σ also resembles the ζ isoform complexed with a peptide more than the uncomplexed 14-3-3ζ. This conformation of 14-3-3σ could result

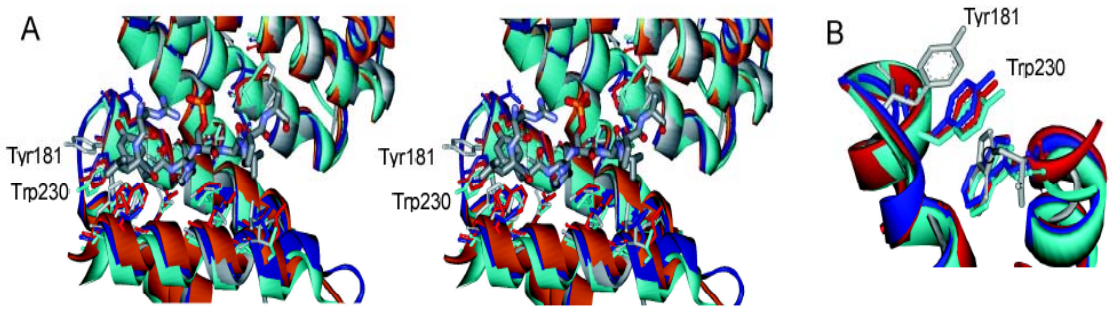

Figure 3.9: Details of the phosphopeptide binding pockets in the 14-3-3ζ and σ isoforms. (**A**) Comparison of the spatial organization of phosphopeptide binding sites in different 14-3-3 structures. ζ isoforms 1QJA (dark blue; bound to a peptide) and 1A4O (gray; without a bound peptide) were superimposed onto the solved 14-3-3σ monomers (chains A and B presented in brown and green, respectively). The phosphopeptide from the 1QJA structure is shown as a bold stick model with the phosphogroup in orange. (**B**) The two aromatic residues that complete the binding site are shown. ζ isoforms 1QJA (dark blue) and 1A4O (gray) are compared to the σ chains A and B presented in red and green, respectively. Positions of side chains in the free σ isoform resemble those of bound ζ isoforms. The free ζ form 1A4O differs significantly from the two other models.

in an increased stability of 14-3-3σ-ligand interactions when compared to 14-3-3ζ interactions. As expression of 14-3-3σ is rapidly induced after DNA damage, a displacement of other 14-3-3 isoforms or preferential binding to ligands by 14-3-3σ may therefore be possible.

Multiple examples of selective ligand binding by different 14-3-3 isoforms exist. Researchers have recently used a targeted proteomics approach (Benzinger et al., 2005) to identify 14-3-3σ-associated proteins *in vivo*. Interestingly, they found that in colorectal cancer cells 14-3-3σ was only present as a homo-dimer or as a hetero-dimer with 14-3-3γ indicating selective dimerization, which may be due to the putative dimerization determinants identified here. The data presented here provides a basis for the experimental validation of determinants of ligand and dimerization specificity by mutational analysis.

4 Summary

The work presented in this thesis was carried out in the Department of Structural Biology at the Max Planck Institute for Biochemistry. The work involved the investigation of three human proteins (ILK, IGF-I, 14-3-3σ) that play a role in the regulation of signal transduction and consequently in cancer. The proteins create a complex network of interacting factors. ILK is a critical component in the integrin pathway. The activity of ILK is stimulated by growth factors/mitogens (IGF-I). The downstream targets of ILK include many signalling molecules, among which are the 14-3-3 family of proteins, which, in turn, play a role in the regulation of mitogenesis.

The first part of the thesis employed techniques of nuclear magnetic resonance spectroscopy and X-ray crystallography to gain a detailed understanding of the Insulin-like growth factor binding proteins (IGFBPs) domain organization and their structural requirements in binding to insulin-like growth factor (IGFs). IGFBPs function as carriers and regulators of the IGF-I and IGF-II. IGFBPs are referred as pleotropic molecules as they regulate cell activity through IGF dependent and IGF independent actions. The IGF independent interactions play a role in modulating cell cycle and apoptosis. The crystal structure of the complex of IGF-I bound to the N-terminal domain of IGFBP-4 (residues 1-92) was determined at 2.5 Å. Further studies showed the “thumb” residues (1-6) of IGFBPs prevent access of the IGF-I receptor to IGF-I through steric hindrance. With the advent of high resolution complex structures of IGF with their high affinity binding proteins, new insights are provided into IGFBP modulation of IGF actions.

The second part of the thesis involved the interaction studies between integrin linked kinase (ILK) and the cytoplasmic adapter protein-parvin. ILK is an ankyrin repeat

containing serine/threonine protein kinase, which has been determined to be a β1-integrin subunit interactor. It forms a multiprotein complex in focal adhesions by interacting with the parvin family of proteins and plays important role in cell spreading and actin organization. ILK has emerged as an attractive target for cancer therapeutics because increased levels of ILK is found in various cancers and inhibiting ILK expression and activity is antitumorigenic. My studies concentrated on protein expression and purification of the kinase domain of ILK. The trials to optimize solubility of a GST-fused ILK kinase domain in *E. coli* were successful. The protein was, however, highly prone to proteolysis and further studies involved in determining the correct boundaries of the kinase domain. Studies showed a shorter kinase domain without the overlap of the PH (pleckstrin homology) domain. These results thus offer a starting basis for future interaction studies of the kinase domain of ILK with adaptor proteins like parvin.

The final part of the thesis involved the investigation of structural differences between the 14-3-3 isoforms. The 14-3-3 proteins are involved in diverse signaling pathways in human cells. In epithelial cells, one particular 14-3-3 isoform, 14-3-3σ, appears to play a particularly important role in cell proliferation, cell cycle control, and human tumorigenesis. We determined the crystal structure of the human 14-3-3σ. Small but significant differences between 14-3-3 isoforms were detected adjacent to the amphipathic groove, which mediates the binding to phosphorylated consensus motifs in 14-3-3-ligands. In addition, a specificity-determining region was found in the structure. The structural differences found in this study will contribute to our understanding of the interaction with specific ligands and may lead to the explanation of different biological functions for these isoforms.

5 Zusammenfassung

Die vorliegende Arbeit wurde in der Abteilung Strukturbiologie am Max-Planck-Institut für Biochemie in Martinsried angefertigt. Die Arbeit umfasst Untersuchungen dreier humaner Proteine (ILK, IGF-I, 14-3-3σ) die eine Rolle in der Signaltransduktion und darausresultierent bei der Krebsentstehung spielen. Die Proteine bilden ein komplexes Netzwerk aus interagierenden Faktoren. ILK ist eine wichtige Komponente im Integrin Signalweg. Die Aktivität von ILK wird durch Wachstumsfaktoren und Mitogene (IGF-I) stimuliert. Unter den nachgeschalteten Zieleproteinen von ILK sind eine Vielzahl von Signalmolekülen, darunter die 14-3-3 Familie, die eine Rolle in der Regulation der Mitogenese spielt.

Der Erste Teil der Arbeit handelt von den Techniken der Kernspinresonanz Spektroskopie und der Röntgenkristallographie um ein detailiertes Verständnis über die Domänen Organisation der Insulin-ähnlichen Wachstumsfaktor bindenden Proteine (IGFBPs) und deren strukturellen Voraussetzungen für die Bindung von der Insulin-ähnlichen Wachstumsfaktor (IGF). IGFBP fungiert als ein Transporter und Regulator für IGF-I und IGF-II. IGFBPs werden als pleotropische Moleküle bezeichnet. Sie können die Zellaktivität über IGF abhängige und IGF unabhängige Mechanismen steuern. Die IGF unabhängigen Interaktionen spielen eine Rolle in der Modulation des Zellzyklus und der Apoptose. Die Kristallstruktur von IGF-I, die an die N-terminale Domäne von IGFBP-4 (AS 1-92) bindet wurde bis 2.5 Å gelöst. Weiterführende Studien zeigten, dass die „Thump“ Reste (1-6) von IGFBP über eine sterische Hinderung die Bindung des IGF-Rezeptors an IGF verhindert. Mit dem Aufkommen von hoch aufgelösten

Komplexstrukturen von IGF mit ihren hoch affinen Bindungspartnern konnten neue Aspekte der Modulation der Aktivität von IGF durch IGFBP erhalten werden.

Der zweite Teil der Arbeit behandelt Interaktionsstudien zwischen der Integrin linked Kinase (ILK) und dem zytoplasmatischen Adaptorprotein Parvin. ILK ist ein Ankyrin Repeat, die eine Serin/Threonin Protein Kinase enthält, welche als ein β1-Integrin Untereinheit Interaktor bestimmt wurde. Sie bildet einen Multiprotein Komplex in *focal adhesions* durch Wechselwirkung mit der Proteinen der Parvin Familie und spielt eine wichtige Rolle in der Zellausbreitung und der Aktinorganisation. ILK hat sich als ein attraktives Ziel in der Krebstherapie herausgestellt, da zum einen erhöhte Werte für ILK in vielen Krebsarten gefunden wurde, und die Hemmung der ILK Expression antitumorgen wirkt. Meine Studien konzentrierten sich auf die Proteinexpression und Reinigung der Kinasedomäne von ILK. Die Versuche die Löslichkeit des GST-Fusionsproteins der ILK Kinase Domäne zu optimieren waren erfolgreich. Das Protein war jedoch sehr anfällig für Proteolyse und weitere Studien zur Bestimmung der korrekten Grenzen der Kinase Domäne sind durchzuführen. Untersuchungen zeigten eine mögliche kürzere Kinase Domäne ohne der Überlappung mit der PH (*pleckstrin homology*) Domäne. Die gewonnenen Ergebnisse bieten eine Grundlage für weiterführende Studien der Interaktion der ILK Kinase Domäne mit Adapterproteinen wie beispielsweise Parvin.

Der letzte Teil der Arbeit zeigt Untersuchungen der strukturellen Unterschiede verschiedener 14-3-3 Isoformen. Die 14-3-3 Proteine kommen in einer Reihe von Signalwegen in humanen Zellen vor. In Epithelzellen spiel eine besondere Isoform von 14-3-3 nämlich 14-3-3σ eine besonders wichtige Rolle in der Zellproliferation, der

Kontrolle des Zellzyklus und der Tumorgenese. Wir haben die Kristallstruktur von 14-3-3σ bestimmt. Kleine aber signifikante Unterschiede zwischen den 14-3-3 Isoformen wurden entlang einer amphipathischen Furche gefunden, die die Bindung von phosphorylierten Konsensusmotifen in 14-3-3 Liganden steuert. Zusätzlich wurde eine spezifitätbestimmende Region in der Struktur identifiziert. Die strukturellen Unterschiede die in dieser Arbeit gefunden wurden werden zu einem genaueren Verständnis der Interaktion mit spezifischen Liganden beitragen, was letztendlich zu einer Erklärung der unterschiedlichen biologischen Funktion der Isoformen führen wird.

6 References

Adams TE, Epa VC, Garrett TP, Ward CW. (2000). Structure and function of the type I insulin like growth factor receptor. Cell. Mol. Life Sci. **57:** 1050-1093.

Aoyagi Y, Fujita N, Tsuruo T. (2005). Stabilization of integrin-linked kinase by binding to Hsp90. Biochem. Biophys. Res Commun. **4:**1061-8.

Bach LA, Rechler MM. (1995). Insulin like-growth factor binding proteins. Diabetes Rev. **3:** 38-61.

Bach LA, Headey SJ, Norton RS. (2005). IGF-binding proteins- the pieces are falling into place. Trends Endocrinol. Metab. **5:** 228-34.

Baxter RC. (2000). Insulin-like growth factor (IGF)-binding proteins: interactions with IGFs and intrinsic bioactivities. Am. J. Physiol. **278:** E967-E976.

Baxter RC, Bayne ML, Cascieri MA. (1992). Structural determinants for binary and ternary complex formation between insulin-like growth factor-I (IGF-I) and IGF binding protein-3. J. Biol. Chem. **267:** 60-65.

Bhatia K, Siraj AK, Hussain A, Bu R, Gutierrez MI. (2003). The tumor suppressor gene *14-3-3*σ is commonly methylated in normal and malignant lymphoid cells. Cancer Epidemiol. Biomarkers Prev. **12:** 165-9.

Benzinger A, Muster N, Koch HB, Yates JR 3rd, Hermeking H. (2005). Targeted proteomic analysis of 14-3-3σ, a p53 effector commonly silenced in cancer**.** Mol. Cell Proteomics **6:** 785-95.

Brakebusch C, Fassler R. (2003). The integrin–actin connection, an eternal love affair. EMBO J. **22:** 2324–2333.

Bramani S, Song H, Beattie J, Tonner E, Flint DJ, Allan GJ. (1999). Amino acids within the extracellular matrix (ECM) binding region (201–218) of rat insulin-like growth factor binding protein (IGFBP)-5 are important determinants in binding IGF-I. J. Mol. Endocrinol. **23:** 117-123.

Brown MC, Perrotta JA, and Turner CE. (1996). Identification of LIM3 as the principal determinant of paxillin focal adhesion localization and characterization of a novel motif on paxillin directing vinculin and focal adhesion kinase binding. J. Cell Biol. **135:** 1109-1123.

Brown MC, Curtis MS, Turner CE. (1998). Paxillin LD motifs may define a new family of protein recognition domains. Nat. Struct. Biol. **5:** 677-678.

Brzozowski AM, Dodson EJ, Dodson GG, Murshudov GN, Verma C, Turkenburg JP, De Bree FM, Dauter Z. (2002). Structural origins of the functional divergence of human insulin-like growth factor-I and insulin. Biochemistry **41:** 9389-9397.

Buckway CK, Wilson EM, Ahlsen M, Bang P, Oh Y, Rosenfeld RG. (2001). Mutation of three critical amino acids of the N- terminal domain of IGF-binding protein-3 essential for high affinity IGF binding. J. Clin. Endocrinol. Metab. **86:** 4943-4950.

Carrick FE, Forbes BE, Wallace JC. (2001). BIAcore analysis of bovine insulin-like growth factor (IGF)-binding protein-2 identifies major IGF binding site determinants in both the amino- and carboxyl-terminal domains. J. Biol. Chem. **276:** 27120-27128.

Carrick FE, Hinds MG, McNeil KA, Wallace JC, Forbes BE, Norton RS. (2005). Interaction of insulin-like growth factor (IGF-I) and –II with IGF binding protein-2: mapping the binding surfaces by nuclear magnetic resonance. J. Mol. Endocrinol. **34:** 685-698.

CCP4, Collaborative Computational Project, Number 4. (1994). The CCP4 Suite: Programs forProtein Crystallography. Acta Cryst. **D50:** 760-763.

Cheng L, Pan CX, Zhang S, Zhang JL, Kinch MS, Li L, Baldridge LA, Wade C, Hu Z, Koch MO, Ulbright TM, Eble JN. (2004). Loss of 14-3-3σ in prostate cancer and its precursors. Clin. Cancer Res. **10:** 3064-8.

Chernausek SD, Smith CE, Duffin KL, Busby WH, Wright G, Clemmons DR. (1995). Proteolytic cleavage of insulin-like growth factor binding protein 4 (IGFBP-4). Localization of cleavage site to non-homologous region of native IGFBP-4. J. Biol. Chem. **270:** 11377-11382.

Clemmons DR. (2001). Use of mutagenesis to probe IGF-binding protein structure/ function relationships. Endocr. Rev. **22:** 800-817.

Cooke RM, Harvey TS, Campbell ID. (1991). Solution structure of human insulin-like growth factor 1: a nuclear magnetic resonance and restrained molecular dynamics study. Biochemistry **30:** 5484-5491.

Carugo KD, Banuelos S, Saraste M. (1997). Crystal structure of a calponin homology domain. Nat. Struct. Biol. **3:** 175-179.

Daughaday WH, Rotwein P. (1989). Insulin-like growth factors I and II. Peptide, messenger ribonucleic acid and gene structures, serum, and tissue concentrations. Endocr. Rev. **10:** 68-91.

Dedhar S. (2000). Cell-substrate interactions and signaling through ILK. Curr. Opin. Cell Biol. **12:** 250–256.

Delcommenne M, Tan C, Gray V, Rue L, Woodgett J, Dedhar S. (1998). Phosphoinositide-3-OH kinase-dependent regulation of glycogen synthase kinase 3 and

protein kinase B/ AKT by the integrin-linked kinase. Proc. Natl. Acad. Sci. USA. **95:** 11211–11216.

De Meyts P, Whittaker J. (2002). Structural biology of insulin and IGF1 receptors: implications for drug design. Nat. Rev. Drug Discov. **1:** 769-783.

Denley A, Cosgrove LJ, Booker GW, Wallace JC, Forbes BE. (2005). Molecular interactions of the IGF system. Cytokine Growth Factor Rev. **16:** 421-439.

Deshayes K, Schaer ML, Skelton NJ, Nakamura GR, Kadkhodayan S, Sidhu SS. (2002). Rapid identification of small binding motifs with high-throughput phage display: discovery of peptidic antagonists of IGF-I function. Chem. Biol. **9:** 495-505.

Dhar S, Squire JA, Hande MP, Wellinger RJ, Pandita TK. (2000). Inactivation of 14-3-3σ influences telomere behavior and ionizing radiation-induced chromosomal instability. Mol. Cell Biol. **20:** 7764-72.

Duan C. (2002). Specifying the cellular responses to IGF signals: roles of IGF binding proteins. J. Endocrinol. **175:** 41-54.

Esteller M. (2005). DNA methylation and cancer therapy: new developments and expectations. Curr. Opin. Oncol. **17:** 55-60.

Firth SM, Baxter RC. (2002). Cellular actions of the insulin–like growth factor binding proteins. Endocr. Rev. **23:** 824-854.

Firth SM, Ganeshprasad U, Baxter RC. (1998). Structural determinants of ligand and cell surface binding of insulin-like growth factor binding protein-3. J. Biol. Chem. **273:** 2631-2638.

Forbes BE, Turner D, Hodge SJ, McNeil KA, Forsberg G, Wallace JC. (1998). Localization of an insulin-like growth factor (IGF) binding site of bovine IGF binding protein-2 using disulfide mapping and deletion mutation analysis of the C-terminal domain. J. Biol. Chem. **273:** 4647-4652.

Fu H, Subramanian RR, Masters SC. (2000). 14-3-3 proteins: structure, function, regulation. Ann. Rev. Pharmacol. Toxicol. **40:** 617-47.

Galanis M, Firth SM, Bond J, Nathanielsz A, Kortt AA, Hudson PJ, Baxter RC. (2001). Ligand-binding characteristics of recombinant amino- and carboxyl-terminal fragments of human insulin-like growth factor-binding protein-3. J. Endocrinol. **169:** 123-133.

García-Echeverría, C, Pearson MA, Marti A, Meyer T, Mestan J, Zimmermann J, Gao J, Brueggen J, Capraro HG, Cozens R, Evans DB, Fabbro D, Furet P, Porta DG, Liebetanz J, Martiny-Baron G, Ruetz S, Hofmann F. (2004). In vivo antitumor activity of NVP-AEW541-a novel, potent, and selective inhibitor of the IGF-1R kinase. Cancer Cell. 5: 231-239.

Gasco M, Sullivan A, Repellin C, Brooks L, Farrell PJ, Tidy JA, Dunne B, Gusterson B, Evans DJ, Crook T. (2002). Coincident inactivation of 14-3-3σ and p16INK4a is an early event in vulval squamous cell neoplasia. Oncogene **21:**1876-81.

Giancotti FG, and Ruislahti E. (1999). Integrin signaling. Science **285:** 1028-1032.

Gimona M, Djinovic-Carugo K, Kranewitter W, Winder SJ**.** (2002). Functional plasticity of CH domains. FEBS Lett. **513:** 98 –106.

Graff JR, Deddens JA, Konicek BW, Colligan BM, Hurst BM, Carter HW, Carter JH. (2001). Integrin-linked kinase expression increases with prostate tumor grade. Clin. Cancer Res. 7: 1987–1991.

Guo L, Wu C. (2002). Regulation of fibronectin matrix deposition and cell proliferation by the PINCH-ILK-CH-ILKBP complex. FASEB J. **16:** 1298-1300.

Hannigan GE, Leung-Hagesteijn C, Fitz-Gibbon L, Coppolino MG, Radeva G, Filmus J, Bell JC, Dedhar S. (1996). Regulation of cell adhesion and anchorage-dependent growth by a new beta 1-integrin-linked protein kinase. Nature **379:** 91–96.

Hannigan GE, Bayani J, Weksberg R, Beatty B, Pandita A, Dedhar S, Squire J. (1997). Mapping of the gene encoding the integrin-linked kinase, ILK, to human chromosome 11p15.5-p15.4. Genomics. **42:** 177–179.

Hannigan GE, Troussard AA, Dedhar S. (2005). Integrin-linked kinase: a cancer therapeutic target unique among its ILK. Nat. Rev. Cancer **5:** 51–63.

Hashimoto R, Ono M. Fujiwara H, Higashihashi N, Yoshida M, Enjohkimura T, Sakano K. (1997). Binding sites and binding properties of binary and ternary complexes of insulin like growth factor–II (IGF-II), IGF- binding protein-3, and acid-labile subunit. J. Biol. Chem. **272:** 27936-27942.

Headey SJ, Keizer DW, Yao S, Wallace JC, Bach LA, Norton RS. (2004a). Binding site for the C-domain of insulin-like growth factor (IGF) binding protein-6 on IGF-II; implications for inhibition of IGF actions. FEBS Lett. **568:** 19-22.

Headey SJ, Leeding KS, Norton RS, Bach LA. (2004b). Contributions of the N- and C terminal domains of insulin-like growth factor (IGF) binding protein-6 to IGF binding. J. Mol. Endocrinol. **33:** 377-386.

Headey SJ, Keizer DW, Yao S, et al., (2004c). C terminal doman of insulin like growth factor IGF binding protein-6: structure and interaction with IGF-II, Mol. Endocrinol. **18:** 2740-2750.

Hermeking H. (2003). The 14-3-3 cancer connection. Nat. Rev. Cancer **3:** 931-43.

Hermeking H, Lengauer C, Polyak K, He TC, Zhang L, Thiagalingam S, Kinzler KW, Vogelstein B. (1997). 14-3-3σ is a p53- regulated inhibitor of G2/M progression. Mol. Cell **1:** 3-11.

Hobba GF, Lothgren A, Holmberg E, Forbes BE, Francis GL, Wallace JC. (1998). Alanine scanning mutagenesis binding tyrosine 60 of bovine insulin like growth factor binding protein-2 is a determinant of insulin like growth factor binding. J. Biol. Chem. **273:** 16691-16698.

Huang Y, Wu C. (1999). Integrin-linked kinase and associated proteins (review). Int. J. Mol. Med. **3:** 563–572.

Hwa V, Oh Y, Rosenfeld RG. (1999). Insulin-like growth factor binding proteins: a proposed superfamily. Acta Paediatr. Suppl. **428:** 37-45.

Hynes RO. (1992). Integrins: Versatility, modulation, and signalling in cell adhesion. Cell **69:** 11-25.

Imai Y, Moralez A, Andag U, Clarke JB, Busby Jr. WH, Clemmons DR. (2000). Substitutions for hydrophobic amino acids in the N-terminal domains of IGFBP-3 and -5 markedly reduce IGF-I binding and alter their biological actions. J. Biol. Chem. **275:** 18188-18194

Isaksson OG, Lindahl A, Nilsson A, Isgaard J. (1987). Mechanism of the stimulatory effect of growth hormone on longitudinal bone growth. Endocr. Rev. **8:** 426-438.

Jansson M, Andersson G, Uhlen M, Nilsson B, Kordel J. (1998). The insulin like growth factor (IGF)–binding protein 1 binding epitope on IGF-I probed by heteronuclear NMR spectroscopy and mutational analysis. J. Biol. Chem. **273:** 24701-24707.

Jin J, Smith D, Stark C. (2004). Proteomic, functional, and domainbased analysis of *in vivo* 14-3-3 binding proteins involved in cytoskeletal regulation and cellular organization. Current Biol. **14:**1436-50.

Jockusch BM, Bubeck P, Giehl K, Kroemker M, Moschner J, Rothkegel M, Rudiger M, Schluter K, Stanke G and Winkler J. (1995). The molecular architecture of focal adhesions. Annu. Rev. Cell Dev. Biol. **11:** 379-416.

Jones JI, Clemmons DR. (1995). Insulin-like growth factors and their binding proteins: biological actions. Endocr. Rev. **16:** 3-34.

Kabsch W. (1993). Automatic processing of rotation diffraction data from crystals of initially unknown symmetry and cell constants. J. Appl. Crystallogr. **26:** 795-800.

Kalus W, Zweckstetter M, Renner C, Sanchez Y, Georgescu J, Grol M, Demuth D, Schumacher R, Dony C, Lang K, Tad Holak. (1998). Structure of the IGF- binding domain of the insulin-like growth factor-binding protein-5 (IGFBP- 5): implications for IGF and IGF-I receptor interactions. EMBO J. **17:** 6558-6572.

Kawabe T. (2004). G2 checkpoint abrogators as anticancer drugs. Mol. Cancer Ther. **3:** 513-519.

Keep NH, Norwood FL, Moores CA, Winder SJ, Kendrick-Jones J. (1999). The 2.0 A structure of the second calponin homology domain from the actin-binding region of the dystrophin homologue utrophin. J. Mol Biol. **3:**1257-1264.

Kelly KM, Oh Y, Gargosky SE, Gucev Z, Matsumoto T, Hwa V, Ng L, Simpson DM, Rosenfeld RG. (1996). Insulin-like growth factor-binding proteins (IGFBPs) and their regulatory dynamics. Int. J. Biochem. Cell. Biol. **28:** 619-637.

Korenbaum E, Rivero F. (2002). Calponin homology domains at a glance (Review). J. Cell Sci. **18:** 3543-5.

Lakin ND, Jackson SP. (1999). Regulation of p53 in response to DNA damage. Oncogene **18:** 7644-55.

Lamzin VS, Wilson KS. (1993). Automated refinement of protein models. Acta Cryst. **D49:** 129-147.

LeRoith D, Werner H, Beitner-Johnson D, Roberts Jr. CT. (1995). Molecular and cellular aspects of the insulin-like growth factor I receptor. Endocr. Rev. **16**: 143-163.

LeRoith D. (2000b). Insulin-like growth factor I receptor signaling-overlapping or redundant pathways. Endocrinology **141:** 1287-1288.

Leung-Hagesteijn C, Mahendra A, Naruszewicz I, Hannigan GE. (2001). Modulation of integrin signal transduction by ILKAP, a protein phosphatase 2C associating with the integrin-linked kinase, ILK1. EMBO J. **20:** 2160–2170.

Li C, Schwabe JR, Banayo E, Evans RM. (1997). Coexpression of nuclear receptor partners increases their solubility and biological activities. PNAS **94:** 2278-2283.

Liu D, Bienkowska J, Petosa C. (1995). Crystal structure of the ζ isoform of the 14-3-3 protein. Nature **376:** 191-4.

Loddick SA, Liu XJ, Lu ZX, Liu C, Behan DP, Chalmers DC, Foster AC, Vale WW, Ling N, De Souza EB. (1998). Displacement of insulin like growth factors from their binding proteins as a potential treatment for stroke. Proc. Natl. Acad. Sci. USA **95:** 1894-1898.

Lodygin D, Hermeking H. (2005). The role of epigenetic silencing of 14- 3-3σ in human cancer. Cell Research **15:** 237-46.

Lowman HB, Chen YM, Skelton NJ, Mortensen DL, Tomlinson EE, Sadick MD, Robinson ICAF, Clark RG. (1998). Molecular Mimics of Insulin-like Growth Factor 1 (IGF-1) for Inhibiting IGF-1: IGF-Binding Protein Interactions. Biochemistry **37:** 8870-8878.

Lunin VV, Munger C, Wagner J, Ye Z, Cygler M, Sacher M. (2004). The structure of the MAPK scaffold, MP1, bound to its partner, p14. A complex with a critical role in endosomal map kinase signaling. J. Biol. Chem. **22:** 23422-30.

Marston, FAO. (1986). The purification of eukaryotic polypeptides synthesized in Escherichia coli. Biochem. J. **240:** 1-12.

McRee DE. (1999). XtalView/Xfit--A versatile program for manipulating atomic coordinates and electron density. J. Struc. Biol. **125:** 156-16.

Mhawech P, Benz A, Cerato C, Gerloz V, Assaly M, Desmond JC, Koeffler HP, Lodygin D, Hermeking H, Hermann F, Schwaller J. (2005). Downregulation of the14-3-3σ in ovary, prostate and endometrial carcinomas is associated with CpG island methylation. Mod. Pathol. **18:**340-8.

Mohan S, Baylink DJ. (2002). IGF-binding proteins are multifunctional and act in a IGF dependent and independent mechanisms. J. Endocrinol. **175:** 19-31.

Moore BW, Perez VJ. (1967a). Specific Acid Proteins in the Nervous System. Englewood Cliffs, New Jersey: Prentice-Hall.

Moore BW, McGregor D. (1965). Chromatographic and electrophoretic fractionation of soluble proteins of brain and liver. J. Biol. Chem. **240:** 1647-53.

Murray-Rust J, McLeod AN, Blundell TL, Wood SP. (1992). Structure and evolution of insulins: implications for receptor binding. Bioessays **14:** 325-331.

Muslin AJ, Tanner JW, Allen PM, Shaw AS. (1996). Interaction of 14-3-3 with signaling proteins is mediated by the recognition of phosphoserine. Cell **84:** 889-97.

Obsil T, Ghirlando R, Klein DC, Ganguly S, Dyda F. (2001). Crystal structure of the 14-3-3ζ : serotonin N-acetyltransferase complex: a role for scaffolding in enzyme regulation. Cell **105:** 257-67.

Olski TM, Noegel AA, Korenbaum E. (2001). Parvin, a 42 kDa focal adhesion protein, related to the alpha-actinin superfamily. Cell. Biol. **114:** 525-538.

O'Reilly DR, Miller L, Luckow VA. (1994). Baculovirus Expression Vectors: A laboratory manual. Oxford University Press, Oxford.

Osada H, Tatematsu Y, Yatabe Y, Nakagawa T, Konishi H, harano T, Tezel E, Takada M, Takahashi T. (2002). Frequent and histological type-specific inactivation of 14-3-3σ in human lung cancers. Oncogene **21:** 2418-24.

Neckers L, Mimnaugh E, Schulte T. (1999). Hsp90 as an anti-cancer target. Drug Resist. Updates **2:** 165–172.

Nikolopoulos SN, Turner CE. (2000). Actopaxin, a new focal adhesion protein that binds paxillin LD motifs and actin and regulates cell adhesion. J. Cell. Biol **151:** 1435-1448.

Nikolopoulos SN, Turner CE. (2001). Integrin-linked kinase (ILK) binding to paxillin LD1 motif regulates ILK localization to focal adhesions. J. Biol. Chem. **276:** 23499-23505.

Pellegrini G, Dellambra E, Golisano O, martinelli E, Fantozzi I, Bondanza S, Ponzin D, McKeon F, De Luca M. (2001). p63 identifies keratinocyte stem cells. Proc. Natl. Acad. Sci. U.S.A **98:** 3156-61.

Persad S, Attwell S, Gray V, Delcommenne M, Troussard A, Sanghera J, Dedhar. (2000). Inhibition of integrin-linked kinase (ILK) suppresses activation of protein kinase B/Akt and induces cell cycle arrest and apoptosis of PTEN-mutant prostate cancer cells. Proc. Natl. Acad. Sci. USA. **97:** 3207–1322.

Persad S, Troussard AA, McPhee TR, Mulholland DJ, Dedhar S. (2001a). Tumor suppressor PTEN inhibits nuclear accumulation of beta-catenin and T cell/lymphoid enhancer factor 1-mediated transcriptional activation. J. Cell Biol. **153:** 1161–1174.

Persad S, Attwell S, Gray V, Mawji N, Deng JT, Leung D, Yan J, Sanghera J, Walsh MP, Dedhar S. (2001b). Regulation of protein kinase B/Akt-serine 473 phosphorylation by integrin-linked kinase: critical roles for kinase activity and amino acids arginine 211 and serine 343. J. Biol. Chem. **276:** 27462–27469.

Pollak MN, Schernhammer ES, Hankinson SE. (2004). Insulin-like growth factors and neoplasia. Nat. Rev Cancer **4:** 505-518.

Qi W, Liu X, Qiao D, Martinez JD. (2005). Isoform-specific expression of 14-3-3 proteins in human lung cancer tissues. Int. J. Cancer **113:** 359-63.

Qin, XZ, Strong DD, Baylink DJ, Mohan S. (1998). Structure- function analysis of the human insulin-like growth factor binding protein-4. J. Biol. Chem. **273:** 23509-23516.

Rechler MM. (1993). Insulin-like growth factor binding proteins.Vitam.Horm.**47:** 1 -114.
Rinderknecht E, Humble RE. (1978). The amino acid sequence of human insulin-like gowth factor I and its structural homology with proinsulin. J. Biol. Chem.**253:** 2769-2776.

Rehm T, Huber R, Holak TA. (2002). Application of NMR in structural proteomics: screening for proteins amenable to structural analysis. Structure (Camb). **12:** 1613-1618.

Rittinger K, Budman J, Xu J, Volinia S, Cantley LC, Smerdoon Sj, Gamblin SJ, Yaffe MB. (1999). Structural analysis of 14-3-3 phosphopeptide complexes identifies a dual role for the nuclear export signal of 14-3-3 in ligand binding. Mol. Cell **4:** 153- 66.

Rohrmann GF. (1986). Polyhedrin structure. J. Gen. Virol. **67:** 1499-1513.

Rosen CJ, Donahue LR. (1998). Insulin-like growth factors and bone: the osteoporosis connection revisited. Proc. Soc. Exp. Biol. Med. **219**: 1-7.

Rozhkova A, Stirnimann CU, Frei P, Grauschopf U, Brunisholz R, Grutter MG, Capitani G, Glockshuber R. (2004). Structural basis and kinetics of inter- and intramolecular disulfide exchange in the redox catalyst DsbD. EMBO J. **23:** 1709-1719.

Rubio MP, Geraghty KM, Wong BH. (2004). 14-3-3-affinity purification of over 200 human phosphoproteins reveals new links to regulation of cellular metabolism, proliferation, and trafficking. Biochem. J. **379:** 395-408.

Sala A, Capaldi S, Campagnoli M, Faggion B, Labo S, Perduca M, Romano A, Carrizo ME, Valli M, Visai L, Minchiotti L, Galliano M, Monaco HL. (2005). Structure and properties of the C-terminal domain of insulin-like growth factor-binding protein-1. isolated from human amniotic fluid. J. Biol. Chem. **280:** 29812-29819.

Sambrook J, Russell DW. (2001). Molecular Cloning. A laboratory manual. Cold Spring Harbor Laboratory Press, New York.

Sato S, Fujita N, Tsuruo T. (2000). Modulation of Akt kinase activity by binding to Hsp90. Proc. Natl. Acad. Sci. USA. **97:** 10832– 10837.

Sato A, Nishimura S, Ohkubo T, Kyogoku Y, Koyama S, Kobayashi M, Yasuda T, Kobayashi Y. (1993). Three-dimensional structure of human insulin like growthfactor-I (IGF-I) determined by 1H –NMR and distance geometry. Int. J. Pept. Protein. Res. **41:** 433-440.

Schulte TW, Blagosklonny MV, Ingui C, Neckers L. (1995). Disruption of the Raf-1-Hsp90 molecular complex results in destabilization of Raf-1 and loss of Raf-1-Ras association. J. Biol. Chem. **270:** 24585–24588.

Schwartz MA, Schaller MD, Ginsberg MH. (1995). Integrins: emerging paradigms of signal transduction. Annu. Rev. Cell Dev. Biol. **11:** 549-599.

Shaffer ML, Deshayes K, Nakamura G, Sidhu S, Skelton NJ. (2003). Complex with a phage- display derived peptide provides insight into the function of insulin-like growth factor-I. Biochemistry **42:** 9324-9334.

Siwanowicz I, Popowicz GM, Wisniewska M, Huber R, Kuenkele KP, Lang K, et al. (2005). Structural basis for the regulation of insulin like growth factors by IGF binding proteins. Structure **13:**155-167

Ständker L, Braulke T, Mark S, Mostafavi H, Meyer M, Honing S, Gimenez-Gallego G, Forssmann WG. (2000). Partial IGF affinity of circulating N- and C-terminal fragments of human insulin like growth factor binding protein-4 (IGFBP-4) and the disulfide bonding pattern of the C-terminal IGFBP-4 domain. Biochemistry **39:** 5082-5088.

Summers MD, Smith GE. (1978). Baculovirus structural polypeptides. J. Virol. **84:** 390-402.

Takada T, Noguchi T, Inagaki K, Hosooka T, Fukunaga K, Yamao T, Ogawa W, Matozaki T, Kasuga M. (2002). Induction of apoptosis by stomach cancer-associated protein-tyrosine phosphatase-1 (SAP-1). J. Biol Chem. **277:** 34359–34366.

Tan C, Cruet-Hennequart S, Troussard A. (2004). Regulation of tumor angiogenesis by integrinlinked kinase (ILK). Cancer Cell **5:** 79–90.

Tan C, Costello P, Sanghera J. (2001). Inhibition of integrin linked kinase (ILK) suppresses β-catenin–Lef/Tcf-dependent transcription and expression of the E-cadherin repressor, snail, in APC–/–human colon carcinoma cells. Oncogene **20:** 133–140.

Taylor WR, Stark GR. (2001). Regulation of the G2/M transition by p53. Oncogene **20:** 1803-15.

Troussard AA, Mawji NM, Ong C, mui A, St- Arnaud R, Dedhar S. (2003). Conditional knock-out of integrin linked kinase demonstrates an essential role in protein kinase B/Akt activation. J. Biol. Chem. **278:** 22374–22378.

Tu Y, Li F, Goicoechea S, Wu C. (1999). The LIM-only protein PINCH directly interacts with integrin-linked kinase and is recruited to integrin-rich sites in spreading cells. Mol. Cell Biol. **19:** 2425–2434.

Tu Y, Huang Y, Zhang Y, Hua Y, Wu C. (2001). A new focal adhesion protein that interacts with integrin-linked kinase and regulates cell adhesion and spreading. J. Cell Biol. **153:** 585–598.

Turner CE, Glenney JR, Burridge K. (1990). Paxillin: a new vinculin-binding protein present in focal adhesions. J. Cell Biol. **111:** 1059-1068.

Turner CE. (1998). Paxillin. Int. J. Biochem. Cell Biol. **30:** 955-959.

Turner CE, Burridge K. (1991). Transmembrane molecular assemblies in cell-extracellular matrix interactions. Curr. Opin. Cell Biol. **3:** 849-853.

Turner CE. (2000). Paxillin and focal adhesion signalling. Nat. Cell Biol. **2:** E231-E236.

Umbricht CB, Evron E, Gabrielson E, Ferguson A, Marks J, Sukumar S. (2001). Hypermethylation of 14-3-3σ (stratifin) is an early event in breast cancer. Oncogene **20:** 3348-53.

Urschel S, Bassermann F, Bai RY, Munch S, Peschel C, Duyster J. (2005). Phosphorylation of Grb10 regulates its interaction with 14-3-3. J. Biol. Chem. **17:** 16987-93.

Vajdos FF, Ultsch M, Schaffer ML, Deshayes KD, Liu J, Skelton NJ, de Vos, AM. (2001). Crystal structure of human insulin like growth factor-1: detergent binding inhibits binding protein interactions. Biochemistry **40:** 11022-11029.

Velyvis A, Yang Y, Wu C, Qin J. (2001). Solution Structure of the Focal Adhesion Adaptor PINCH LIM1 domain and Characterization of its Interaction with Integrin Linked Kinase Ankyrin Repeat Domain. J. Biol. Chem. **276:** 4932–4939.

Vercoutter-Edouart A-S, Lemoine J, Le Bourhis X, Louis H, Boilly B, Nurcombe V, Revillion F, Peyrat JP, Hondermarck H. (2001). Proteomic analysis reveals that 14-3-3s is down-regulated in human breast cancer cells. Cancer Res. **61:** 76-80.

Vorwerk P, Hohmann B, Oh Y, Rosenfeld RG, Shymko RM. (2002). Binding properties of insulin-like growth factor binding protein-3 (IGFBP-3), IGFBP-3 N- and C-terminal fragments, and structurally related proteins mac25 and connective tissue growth factor measured using a biosensor. Endocrinology **143**: 1677-1685.

Yao S, Headey SJ, Keizer DW, Bach LA, Norton RS. (2004). C-terminal domain of insulin - like growth factor (IGF) binding protein 6. Conformational exchange and its correlation with IGF-II binding. Biochemistry **43:** 11187-11195.

Walsh G. (1995). Nervous excitement over neuotrophic factors. Biotechnology **13:** 1167-1171.

Wang SC, Makino K, Xia W, Kim JS, Im SA, Peng H, Mok SC, Singletary SE, Hung MC. (2001). DOC-2/hDab-2 inhibits ILK activity and induces anoikis in breast cancer cells through an Akt-independent pathway. Oncogene **20:** 6960–6964.

Wetterau LA, Moore MG, Lee KW, Shim ML, Cohen P. (1999). Novel aspects of the insulin-like growth factor binding proteins. Mol. Genet. Metab. **68:**161-181.

Wu C. (2004). The PINCH–ILK–parvin complexes: assembly, functions and regulation. Biochimica et Biophysica Acta. **1692:** 55-62.

Wu C. (1999). Integrin-linked kinase and PINCH: partners in regulation of cell-extracellular matrix interaction and signal transduction. J. Cell Sci. **112:** 4485–4489.

Xiao B, Smerdon SJ, Jones DH, Dodson GG, Soneji Y, Aitken A, Gamblin SJ. (1995). Structure of a 14-3-3 protein and implications for coordination of multiple signaling pathways. Nature **376:** 188-91.

Yaffe MB, Rittinger K, Volinia S, Caron PR, Aitken A, Leffers H, Gamblin SJ, Smerdon SJ, Cantley LC. (1997). The structural basis for 14-3-3: phosphopeptide binding specificity. Cell **91:** 961- 71.

Yamaji S, Suzuki A, Sugiyama Y, Koide Y, Yoshida M, Kanamori H, Mohri H, Ohno S, Ishigatsubo Y. (2001). A novel integrin-linked kinase-binding protein, affixin, is involved in the early stage of cell-substrate interaction. J. Cell Biol. **153:** 1251–1264.

Yamada KM, Araki M. (2001). Tumor suppressor PTEN: Modulator of cell signaling, growth, migration and apoptosis. J. Cell Sci. **114:** 2375–2382.

Yatabe Y, Osada H, Tatemasu Y, Mitsudomi T, Takahashi T. (2002). Decreased expression of 14-3-3σ in neuroendocrine tumors is independent of origin and malignant potential. Oncogene **54:** 8310-9.

Yau C, Wheeler JJ, Sutton KL, Hedley DW. (2005). Inhibition of integrin-linked kinase (ILK) by a selective small molecule inhibitor, QLT054 inhibits the PI3K/PKB/mTOR, STAT-3 and FKHR pathways, tumour growth and enhances gemcitabine-induced apoptosis in human primary pancreatic cancer xenografts. Cancer Res. **65:** 1497-1504.

Zeslawski W, Beisel HG, Kamionka M, Kalus W, Engh RA, Huber R, Lang K, Holak TA. (2001). The interaction of insulin like growth factor –I with the N-terminal domain of IGFBP-5. EMBO J. **20:** 3638-3644.

Zhang Y, Guo L, Chen K, Wu C. (2002). A critical role of the PINCH-integrin-linked kinase interaction in the regulation of cell shape change and migration. J. Biol. Chem. **277:** 318-326.

Zhang Y, Chen K, Tu Y, Velyvis A, Yang Y, Qin J, Wu C. (2002). Assembly of the PINCH–ILK–CH-ILKBP complex precedes and is essential for localization of each component to cell–matrix adhesion sites. J. Cell Sci. **115:** 4777-4786.